Microwave Frequency Discriminators

N.D. Geldenhuys

Thesis presented in partial fulfillment of the requirements
for the degree of **Master of Science in Engineering (Electronic)**
at the Department of Electrical and Electronic Engineering
of the University of Stellenbosch.

Supervisor: Dr. J.B. de Swardt

March 2001

Declaration

I, the undersigned, hereby declare that the work contained in this thesis is my own original work, unless stated otherwise, and that I have not previously, in its entirety or in part, submitted it at any university for a degree.

Nicolaas Daniël Geldenhuys December 2000

Summary

The topic of microwave frequency discriminators is introduced. Various applications and implementation techniques of these devices are given and discussed. This thesis may serve as reference foundation for future research on this topic.

Discriminators are developed at both S- and X-band, with high linearity and good sensitivity. The systems used to implement these devices are developed as well. The S-band discriminator is used in a direct FM demodulation system, which works well.

Opsomming

Hierdie is 'n inleiding tot die onderwerp van mikrogolf frekwensie diskrimineerders. Verskeie toepassings en implementeringstegnieke van hierdie toestelle word genoem en bespreek. Hierdie tesis kan dien as verwysings-raamwerk vir toekomstige navorsing oor hierdie onderwerp.

Diskrimineerders is ontwikkel by beide S- en X-band, met 'n goeie lineariteit en sensitiwiteit. Die stelsels wat gebruik word om hulle te implementeer, is ook ontwikkel. Die S-band diskrimineerder is gebruik in 'n direkte FM demodulasie sisteem en werk goed.

Contents

Acknowledgements

I firstly would like to thank Johann de Swardt, my supervisor, for his constant support during this research. Though you shared this journey of discovery with me, your ideas and guidance were invaluable.

I also want to thank Wessel Croucamp and Ashley Cupido from SED for the construction of my discriminators. It was done with high accuracy, and the boxes look really nice.

Then it is a big thank you to Anton, Marius and Willem. They shared the office with me during this dreary year, with computers being stolen and data being lost. Thanks for listening to my findings and developments. Thanks also for your ideas and contributions. Thanks also to my other friends and colleagues for their interest and encouragement.

A special thanks goes to Anton for his VCO. Our systems would have worked nicely together – if only yours were finished in time. It was a pleasure working with you.

A special thanks also goes to my family for their constant support, interest and encouragement. Dankie Mamma vir die konstante gebede hier aan die einde. Dit het maar woes gegaan, maar ek het dit klaar gekry. Prys die Here!

Thank you Lord for giving me the ability and endurance to finish this thesis. May it serve to praise your Name.

Introduction

When this topic was proposed, very little was known at this faculty about techniques of implementing a frequency discriminator at microwave frequencies. It was quite difficult at first to find any information on these higher frequency devices, since the discriminators found in books only cover the low frequency techniques. In the end, a whole world of discriminators was found in numerous articles, which will be introduced in this thesis.

This research project had two main goals. Firstly possible techniques of implementing a discriminator at RF or microwave frequencies had to be researched. Secondly such a device had to be implemented at both S- and X-band, and employed in the direct demodulation of a wide-band FM signal.

As an extension of this introduction, a background will be sketched in Chapter 1 on the world of discriminators. A definition of this device will be followed by the techniques described in books, and an overview of techniques and their applications at RF and microwave frequencies.

A personal goal was set to create a reference foundation for the development of any type of microwave frequency discriminator. Therefore, a broad spectrum of techniques will be discussed in Chapter 2. Most techniques will be described in only a little detail, but some will have design examples as well.

Two discriminators were developed using a technique which was named the 'Mohr Discriminator'. They have center frequencies at 2.45 GHz and 10.5 GHz. Their development will be discussed in detail in Chapter 3. The system used with a discriminator, and specifically the two systems used to test with the S- and X-band discriminators, will be discussed in Chapter 4. Finally, the S-band system will be used to test a direct modulation/demodulation system in Chapter 5.

Chapter 1

Background on Discriminators

In this chapter the discriminator's function will be defined, and some basic concepts surrounding them will be introduced. A brief overview of applications for and ways of implementing high and low frequency discriminators will be given. Some of the techniques which normally appear in books will be discussed. There will also be an illustration of the time-domain activity, which will give a better understanding of the discriminator's working.

1.1 Definition and basic concepts

A frequency discriminator is simply defined as

> A converter of frequency changes into amplitude changes;
> or in other words, an FM to AM converter.

A discriminator normally has some frequency or phase dependency which cause an amplitude variation over frequency. This dependency can either be a tuned circuit at lower frequencies, or some transmission line structure at higher frequencies. The transfer function is in the form of an S. Therefore the element used in block diagrams show such an S-curve, as can be seen in Figure 1.1.

A general discriminator system (see Figure 1.1) consist of

the discriminator – either has two parts or two outputs;
– is the focus of this research project;
two diode detectors – will detect the amplitude modulation for both outputs; and
a differential amplifier – produce the output to the system.

Many of the discriminator techniques have the detectors as part of the proposed discriminator circuit. The circuit can be analyzed without the detectors and differential amplifier present. The output of the system is then similar to the difference of the absolute values

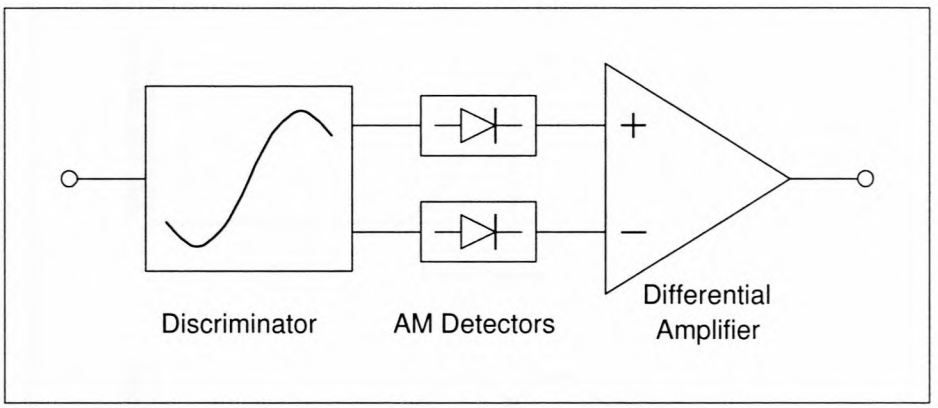

Figure 1.1: A general Discriminator system.

of the transmission coefficients of the discriminator ($V_{out} = |S_{21}| - |S_{31}|$). This can only be done if it is assumed that the detectors are linear over the operating range of the discriminator. The actual output will be a scaled version, due to losses in the detectors, as well as other contributing factors. The detectors do form an important part of the system, but is the topic of another research project, and will therefore not be discussed in great detail.

1.2 Lower frequency discriminators

Discriminators are discussed in textbooks under topics such as 'FM Receivers' [1] and 'Angle Modulation and Demodulation' [2][3]. Their designs are aimed at the demodulation of narrow-band FM signals at a system's IF. Other applications include the creation of error-signals in the stabilization of oscillators [1] or in an automatic frequency control (AFC) system [4].

There exist many circuits that can be used to implement the FM to AM conversion. The simplest circuit is a differentiator, which can be made with an RC-network. Its transfer function is given by

$$|H(f)| = j2\pi fRC. \tag{1.1}$$

1.2.1 Slope detector and Balanced discriminator

The rising half of the frequency characteristic of a tuned circuit is partially linear (see Figure 1.2 (a)). The linear region is usually not wide enough. To obtain a linear characteristic over a wider band, two circuits tuned at frequencies f_1 and f_2 are connected

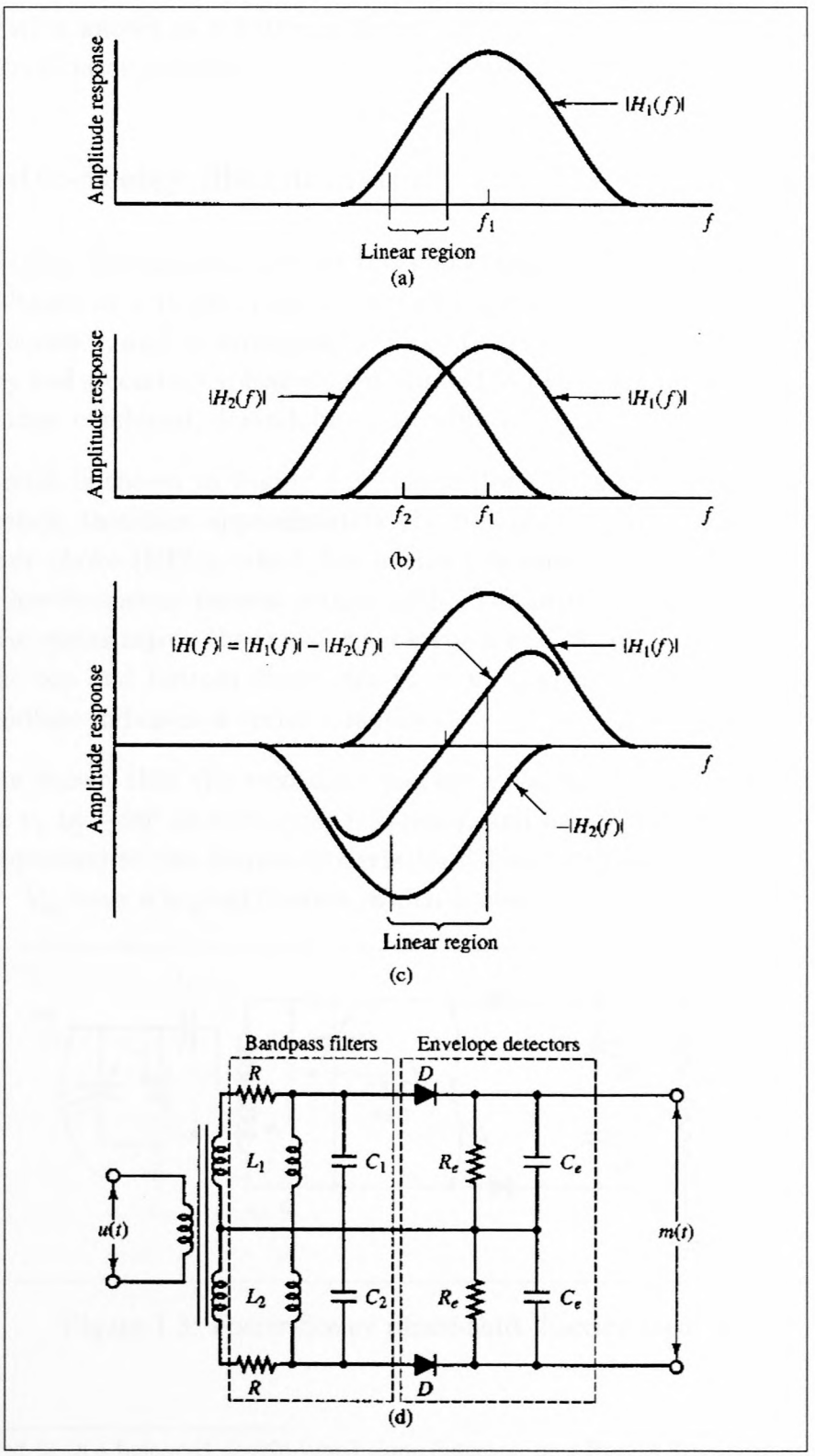

Figure 1.2: Derivation of a balanced discriminator. (a) Bandpass filter. (b) Stagger-tuned band-pass filters. (c) Amplitude response $H(f)$ of balanced discriminator. (d) Balanced discriminator. [2]

in a configuration known as a balanced discriminator[1]. The schematic derivation of the balanced discriminator response and a typical circuit is shown in Figure 1.2.

1.2.2 Foster-Seeley discriminator

The Foster-Seeley discriminator utilize the phase-angle shift between the primary and secondary voltages of a tuned transformer to change FM to AM. The phase angle is a function of frequency, and by arranging for phasor-sum and phasor-difference components of the primary and secondary voltages to be applied to two envelope detectors, the outputs of which are then combined, demodulation is achieved.

The basic circuit is shown in Figure 1.3. Capacitor C_c has negligible reactance at the carrier frequency, therefore approximately the full primary voltage appears across the radio-frequency choke (RFC), which has a high reactance at the carrier frequency, and provides the low frequency current return path. The primary voltage is connected from the RFC to the center tap on the transformer secondary. The result is that the RF voltages applied to the top and bottom diodes are $\mathbf{v}_a = \mathbf{v}_p + \mathbf{v}_1$ and $\mathbf{v}_b = \mathbf{v}_p - \mathbf{v}_2$ respectively, where the boldface indicates a vector quantity.

It can also be shown that the secondary voltage $\mathbf{v}_s = \mathbf{v}_1 + \mathbf{v}_2$ is shifted from the primary voltage $\mathbf{v}_p$ by $-90°$ at the center frequency, and has a further phase shift which is directly proportional to the frequency deviation. The resulting output voltage given by $V_o = V_{ao} - V_{bo}$ have a typical S-curve, which is zero at the carrier frequency.

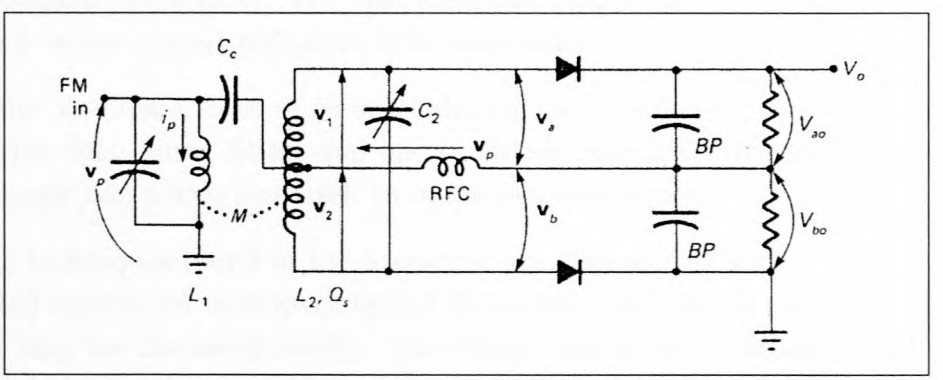

Figure 1.3: Foster-Seeley phase-shift discriminator. [1]

[1] Also referred to as a balanced double-tuned slope detector, or a Round-Travis detector.

1.3 Applications at microwave frequencies

There are several applications for frequency discriminators. As for lower frequency discriminators, the techniques at microwave frequencies are implemented in the demodulation of FM signals [5][6]. The advantage is that the signal does not need to be mixed down to an IF, it can be demodulated directly from the microwave FM signal to a baseband signal containing the wanted information. This makes the implementation of broadband FM communication more feasible.

Discriminators are also useful in stabilizing oscillators. Resonator-discriminators are often used as part of a feedback loop used for controlling the frequency of oscillation [7]–[13]. Apart from stabilizing, it is also used for noise degeneration in oscillators [14][15].

Another major application is in the measurement of noise in FM sources [16]–[21]. It is even used at mm-wave frequencies to measure and reduce the oscillator chirp in radar systems [22]. Other useful applications are in instantaneous frequency-measuring receivers (IFR) [23]–[25], as well as in AFC systems [31].

1.4 Overview of implementation techniques

Discrete components are not practically viable for use at microwave frequencies. There are however, numerous implementation techniques which employ various types of transmission line and waveguide structures. The operating bandwidth vary from high-Q resonator-like circuits, to a bridge circuit with over 50% bandwidth.

Most circuits use some form of power splitting and combining. Hybrids are used extensively with delay lines, filters and open- and/or short-circuited stubs. These hybrids include a magic tee, which lent itself to numerous techniques.

Most of the techniques found in the literature are discussed in some detail in Chapter 2. Only selected techniques were investigated thoroughly, and design examples will be given; others will only be discussed briefly. The Mohr discriminator formed the focus of this research, and the development thereof will be discussed in great detail in Chapter 3.

1.5 Illustration of Time-domain activity

To understand the working of the discriminator, it can be helpful to take a look at a time-domain analysis of a simple discriminator (this was done in PSpice [60]). A discriminator which employs a simple two-branch hybrid and phase delay lines, will be used in this demonstration. It forms part of the development of the S-band Mohr discriminator (Section 3.3).

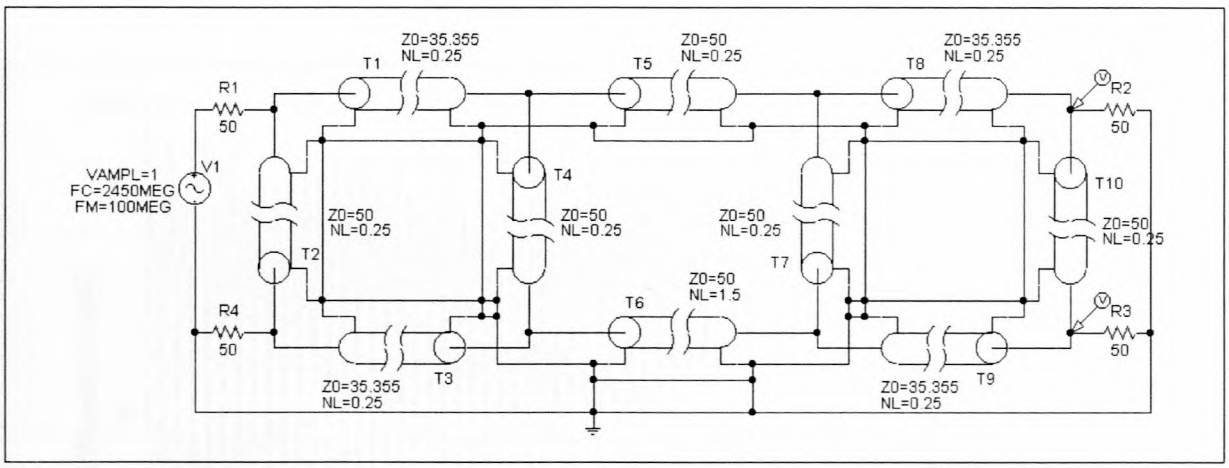

Figure 1.4: Discriminator circuit used for time-domain illustration.

The circuit which is used for this illustration is shown in Figure 1.4. All the transmission lines are a quarter wavelength at 2.45GHz, except for T6 which is one-and-a-half wavelengths long. The voltage source is a single frequency FM source, with a center frequency of 2.45 GHz. The modulating frequency is set to 100 MHz, which gives a ± 100 MHz frequency deviation at a rate of 100 MHz. The two output waveforms are taken at the terminating resistances R2 and R3.

The output RF signals have an amplitude modulation which is related to the frequency of the input signal. In an actual discriminator system, the difference of the AM-detected RF signals at ports 2 and 3 (at R2 and R3), would be taken as the output to the system. As an illustration of the system's behaviour, the difference of the absolute values of the RF signals is shown in Figure 1.5, together with the RF signals. If this difference signal is negative, the frequency is below 2.45 GHz, and if it is positive, it is above 2.45 GHz. The amplitude of the (detected) output signal is directly related to the frequency, and can be used in various applications as mentioned.

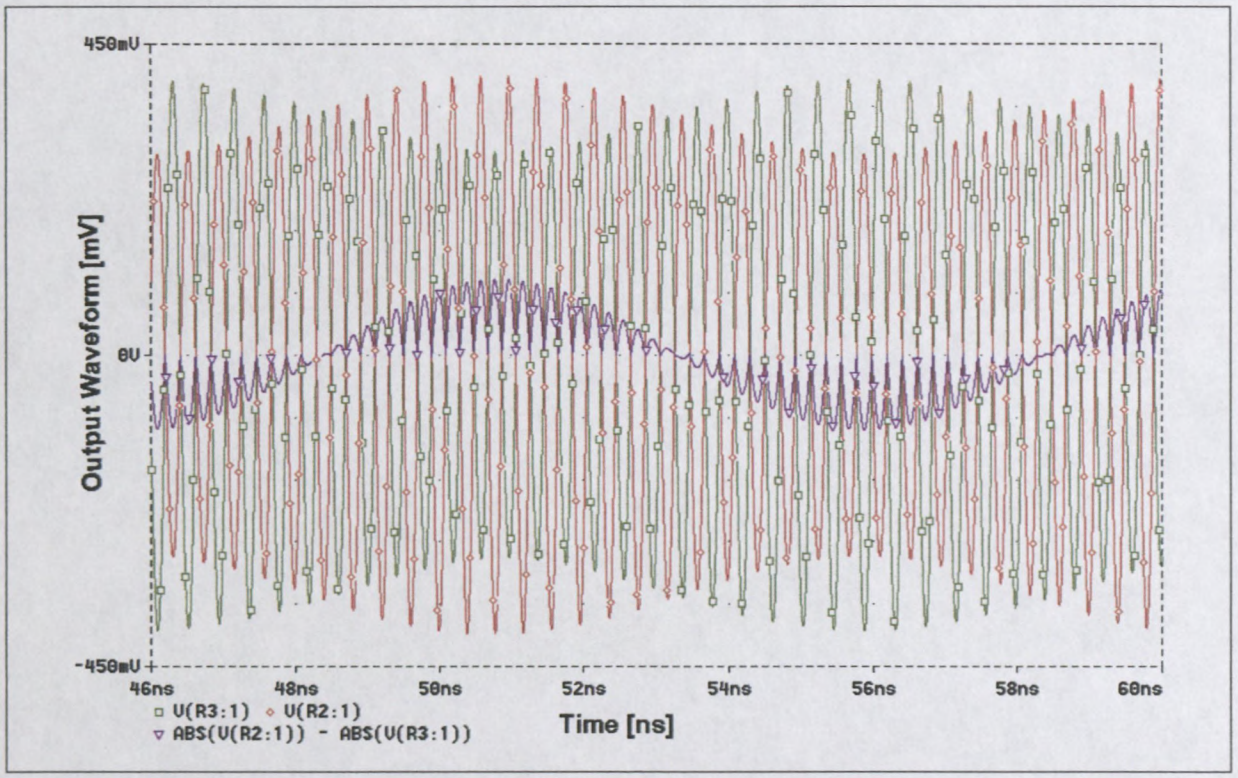

Figure 1.5: Time-domain waveforms at the output of the discriminator. (The difference is taken only as an illustration.)

Chapter 2

Implementation Techniques at Microwave Frequencies

In this chapter some of the techniques used for implementing frequency discriminators at RF and microwave frequencies will be discussed. A thorough discussion will be given for selected techniques, for which design examples will be given as well. Other techniques which have constructional or other complexities, will only be discussed briefly.

Some basic properties which may influence the choice of the implementation technique, include the bandwidth, the linearity over the required band, and the sensitivity of the complete system. The bandwidth is seen as the band over which the transfer function of the discriminator is linear. The linearity is of great importance, since a conversion of frequency to amplitude is more easily interpreted if it is linear. The sensitivity is expressed as the change in amplitude for a change in frequency, and has a unit in the form of mV/MHz. It depends on the input power of the system. In some systems the sensitivity is used for calculations regarding the gain of a loop.

2.1 Slope discriminator

This technique uses hybrids and the attenuating slope of two indentical low-pass filters to achieve its discrimination. It is one of two techniques described in an article which develops direct modulating and demodulating techniques at microwave frequencies [5].

2.1.1 Article discussion (from [5])

The balanced slope discriminator consist of two 90° 3 dB hybrids, two low-pass filters (LPF) having identical characteristics and two differential detective diodes. The circuit model of this discriminator is shown in Figure 2.1.

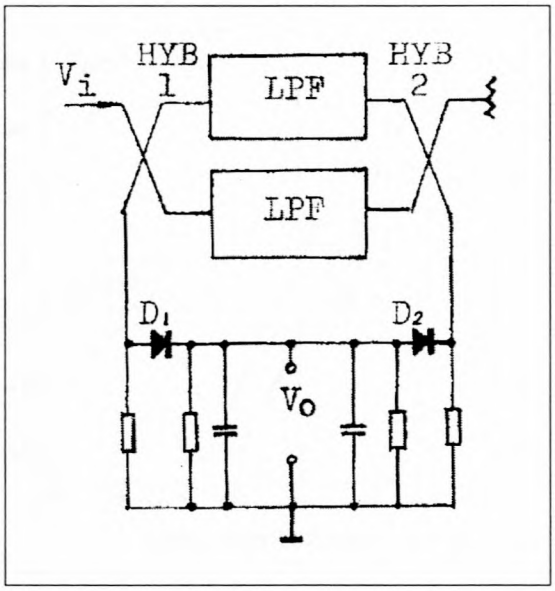

Figure 2.1: Circuit model for slope discriminator. [5]

The ratio of output voltage V_o to the peak input voltage V_m is given by the equation:

$$\frac{V_o}{V_m} = K_d \left(1 - \left(1 + \frac{1}{A}\right) \cdot H(\omega)\right) \tag{2.1}$$

where

$H(\omega)$ is the transmission function of the LPF,
A is the attenuation of the LPF, and
K_d is a coefficient of additional attenuation related to the insertion loss of two hybrids, as well as the detective efficiency of the detectors.

If the LPF were lossless: $A = 1$, and the center frequency ω_o of the discriminator could be obtained by letting $H(\omega) = 0.5$. Practically $A > 1$, so the center frequency ω_o' can be solved from the equation $H(\omega') = A/(1 + A)$. Therefore, $\omega_o' < \omega_o$. In oder to raise the slope of the discriminator, the Cauer response LPF must be adopted.

The discriminator has been built on alumina substrate. The measured S-type characteristic is shown in Figure 2.2 (dotted line). About 8 mV/MHz discrimination sensitivity can be obtained at the center frequency when the input level is 10 mW. The non-linear distortion is less than 5% within ±4 MHz.

2.1.2 Practical working

The input signal is split equally to the two filters, with a 90° phase difference. The reflected signals from the filters, are added in phase at port 2 (see Figure 2.3) due to

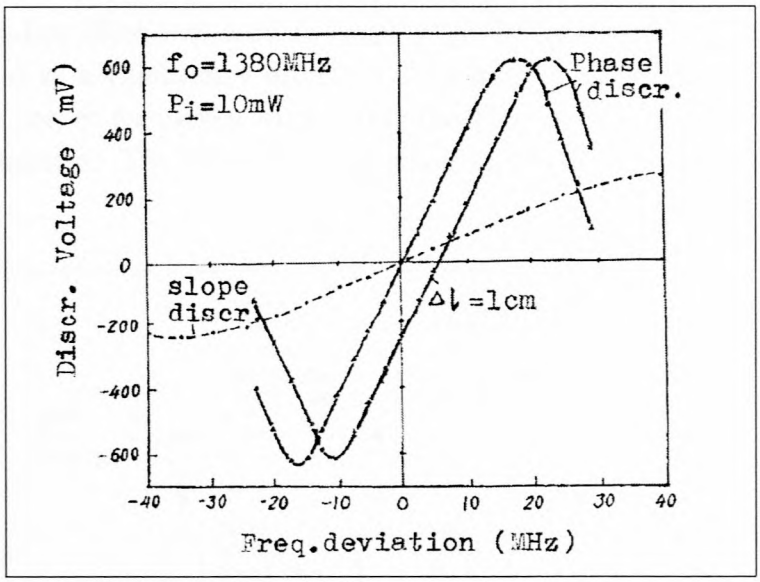

Figure 2.2: Characteristics of the slope and phase discriminators. [5]

another 90° phase difference. The filtered signals are also added in phase at port 3.

The signals at ports 2 and 3 are then similar to the reflection and transmission coefficients of the filter. The discrimination sensitivity is thus dependent on the slope of the filter's transmission coefficient.

2.1.3 Design example

The design consist of two ideal hybrids and two identical transmission line filters, at a center frequency of 2 GHz. Only the hybrids and filters were used in this design, with the circuit shown in Figure 2.3. It was analyzed in Microwave Office 2000 [61].

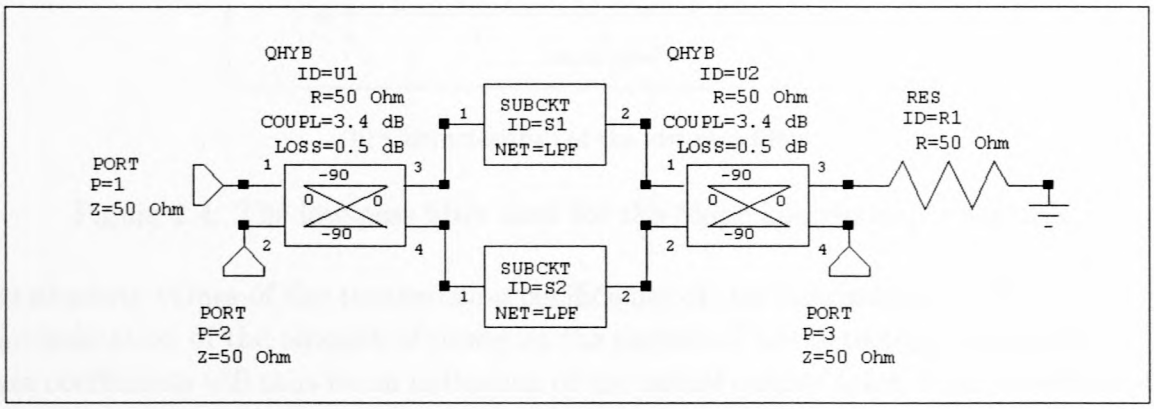

Figure 2.3: Circuit used for analysis of slope discriminator.

A fifth order stub-line filter was used to employ the low-pass filter (Figure 2.4 (a)). The filter was designed as a Chebyshev filter with the help of ZSyn [62]. To achieve a good sensitivity and a center frequency at 2 GHz, the filter was optimized – the values are given on the schematic. The filter's transmission and reflection coefficients is shown in Figure 2.4 (b).

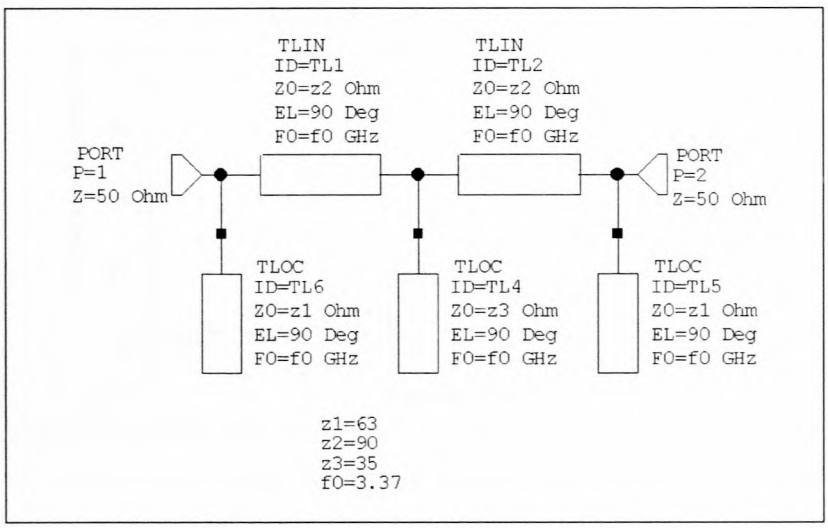

(a) Stub-line low-pass filter.

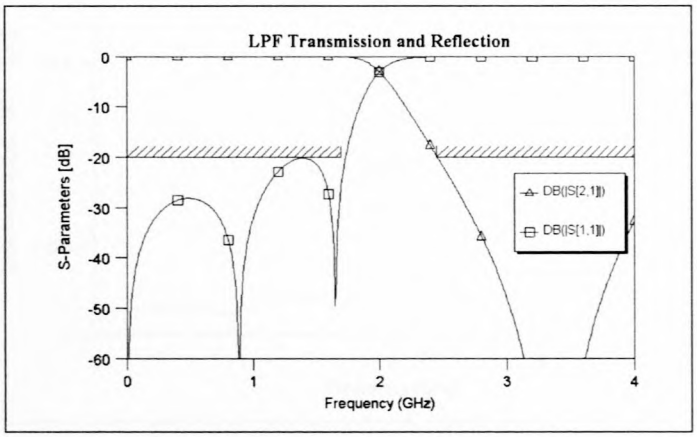

(b) Characteristics of the low-pass filter.

Figure 2.4: The low-pass filter used for the Slope Discriminator example.

The absolute values of the transmission coefficients of the discriminator ($|S_{21}|$ and $|S_{31}|$), is an indication of the amount of power at the output of the detectors. The difference of these coefficients will thus be an indication of the actual output taken from the differential detector circuit. The transmission coefficients and their difference is shown in Figure 2.5.

This discriminator does seem easy to develop, but does not have a good linearity over a

large part of its S-curve. Furthermore, when a more practical transmission line hybrid was employed, the slopes were not nearly as smooth, and only a very small part was still linear.

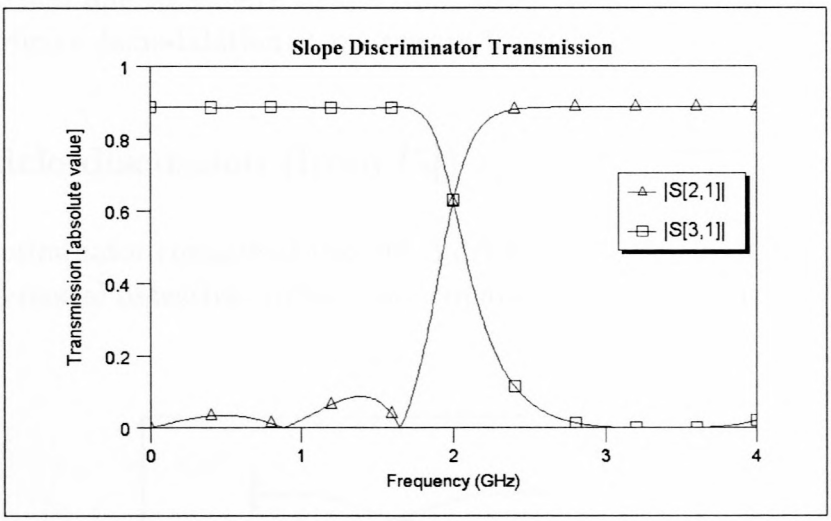

(a) Transmission coefficients.

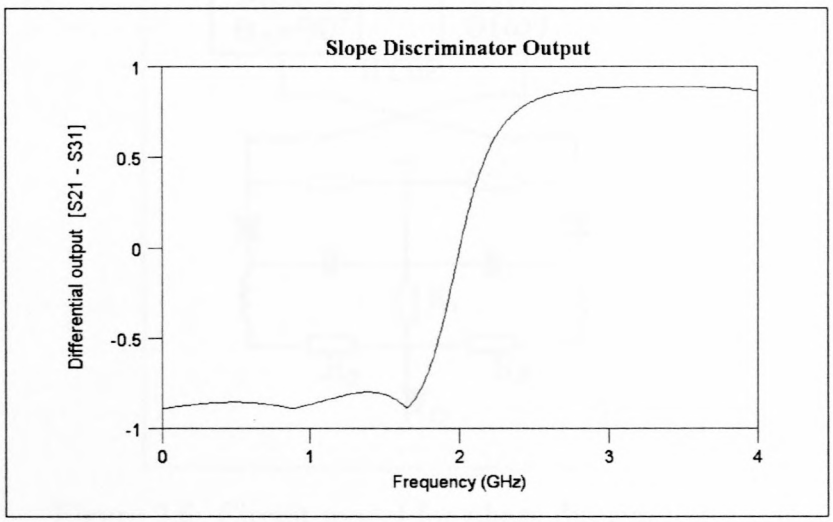

(b) Differential output ($V_{out} = |S_{21}| - |S_{31}|$).

Figure 2.5: Analysis of the Slope Discriminator.

2.2 Phase Discriminator

This technique uses hybrids and the phase difference between a band-pass filter (BPF) and a transmission line to achieve its discrimination. It is the second of two techniques developed for direct demodulation at microwave frequencies [5].

2.2.1 Article discussion (from [5])

The phase discriminator consists of two 90° 3 dB hybrids, a BPF, a compensative delay line and a differential detective circuit. The circuit model of this discriminator is shown in Figure 2.6.

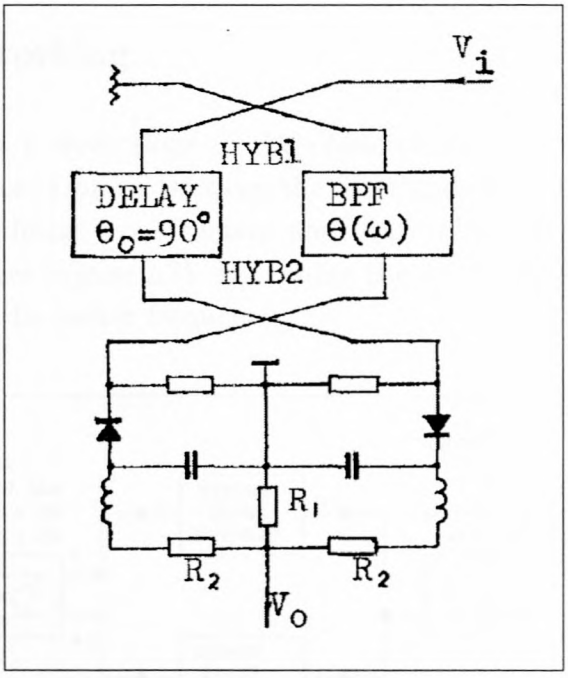

Figure 2.6: Circuit model for phase discriminator. [5]

The ratio of output voltage V_o to the peak input voltage V_m is given as follows:

$$\frac{V_o}{V_m} = K_d \frac{a}{\sqrt{1+a^2}} \cos(\theta - \theta_o) \tag{2.2}$$

where $a = A_d/A_f$ and it is assumed that $a < 0.5$. A_d is the insertion attenuation of the delay line. A_f is the insertion attenuation of the BPF. K_d is a coefficient related to the loss of the hybrids and the detective efficiency of the detector. The phase shift of the delay line is $\theta_o = 90°$, when the length of the line is $\lambda_g/4$ (λ_g – wavelength in the substrate).

Moreover, if the BPF has a Chebyshev response, the phase-frequency characteristics is approximately $\theta = Ka \cdot \sin^{-1}(\omega - \omega_o)$. When $f < f_s$, Equation 2.2 can be expressed in the following formula:

$$\frac{V_o}{V_m} = K(f - f_o) \tag{2.3}$$

where f_o is the center frequency of the BPF.

The phase discriminator has been made on alumina substrate. This discrimination sensitivity is better than the sensitivity of the slope discriminator. Experimental discrimination characteristics of the phase discriminator is also shown in Figure 2.2 (solid line). The sensitivity of the discriminator of 25 mV/MHz can be obtained when the input level is 10 mW. The center working frequency of the discriminator can be changed if the length of the compensation delay line is varied.

2.2.2 Practical working

The band-pass filter has a steep slope in the phase of its transmission coefficient in the pass-band. The difference in phase between the filter and the delay line, then produce an in- and out-of-phase addition (constructive and destructive interference) for the amplitudes at ports 2 and 3 (see Figure 2.7). By tuning the delay line's length, the phase-offset is changed, and with it the center frequency.

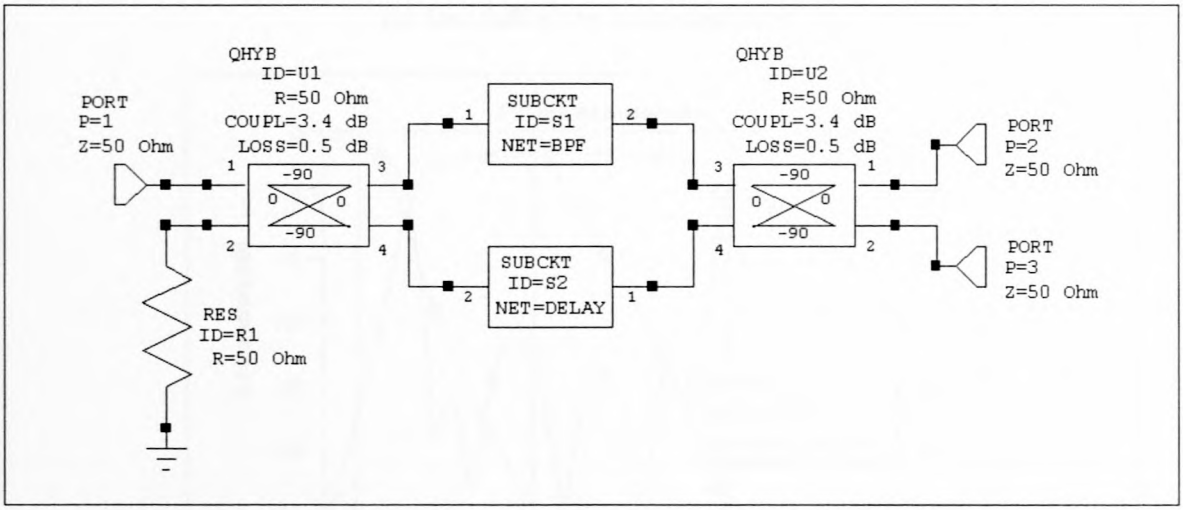

Figure 2.7: Circuit used for the Phase Discriminator example.

2.2.3 Design example

A design was done with two ideal hybrids, a coupled-line band-pass filter and a transmission line (the delay line). The circuit diagram shown in Figure 2.7 was analyzed in Microwave Office [61]. The center frequency was tuned to 2.3 GHz by changing the delay-line length. The output is again taken as the difference between $|S_{21}|$ and $|S_{31}|$.

A fifth order coupled-line filter, which was developed as part of a *Skripsie* project [26], was used to employ the band-pass filter. The filter consist of six coupled-line sections, and is symmetric. One half of this circuit is given in Figure 2.8 (a). The characteristics of this filter is shown in Figure 2.8 (b).

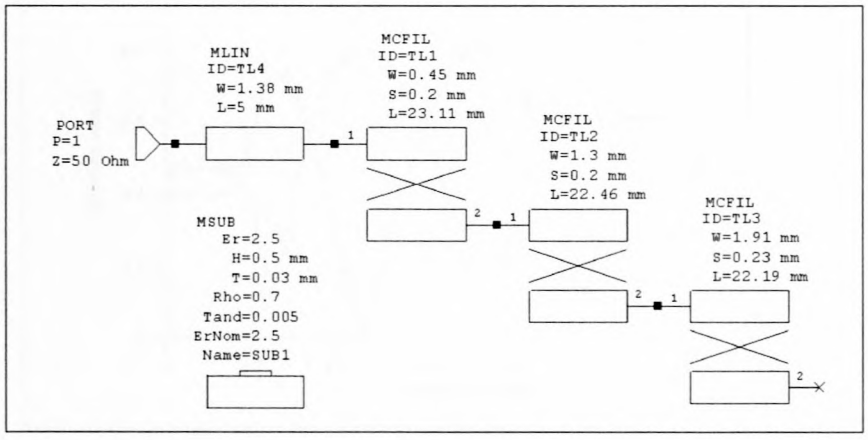

(a) One half of the band-pass filter.

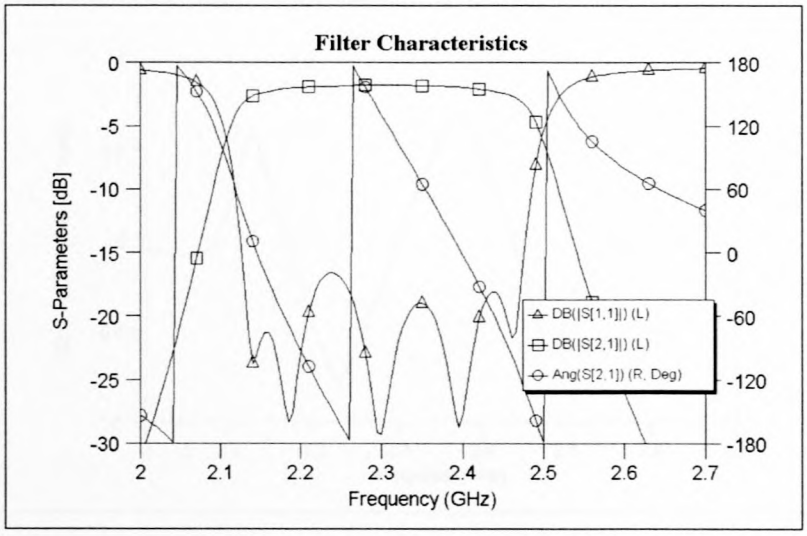

(b) Characteristics of the filter.

Figure 2.8: The band-pass filter used for the Phase Discriminator example.

The phase difference between the steep linearly sloped deviation of phase of the filter in the pass-band, and the much flatter linear slope for the transmission line, leads to the frequency-dependent constructive and destructive interference of the signals at the second hybrid. The amplitude deviation of these signals at the output of this hybrid, as well as their difference, is shown in Figure 2.9.

The bandwidth of this technique depends on that of the filter. Its linearity depends on the quality of the phase-transmissions through the filter and the hybrids. It is a simple technique and seem to work sufficiently.

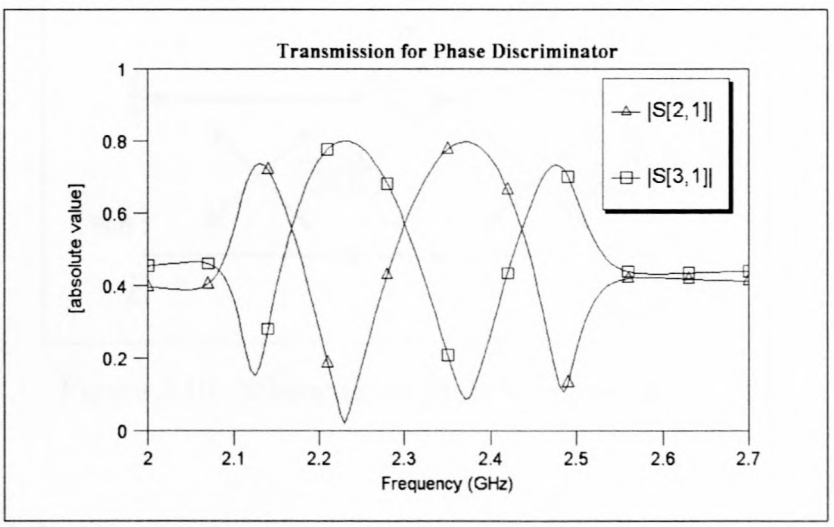

(a) Transmission coefficients.

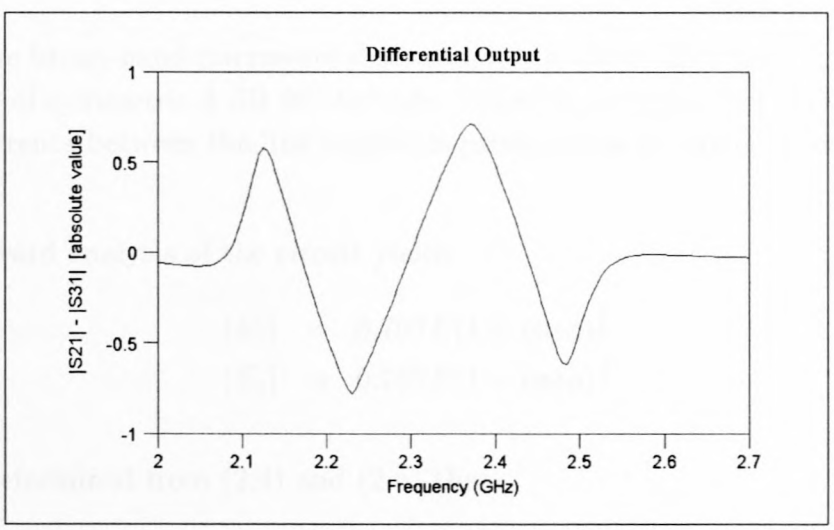

(b) Differential output.

Figure 2.9: Analysis of the Phase Discriminator.

2.3 Hybrids used with phase delay lines (the *Mohr Discriminator*)

A technique which was proposed by R.J. Mohr in 1963 [27], is very easy to design and simple to understand. There were many papers which described different approaches to designing this type of discriminator [28]–[33]. Developments of this technique, which was named the Mohr Discriminator, will be discussed in great detail in Chapter 3.

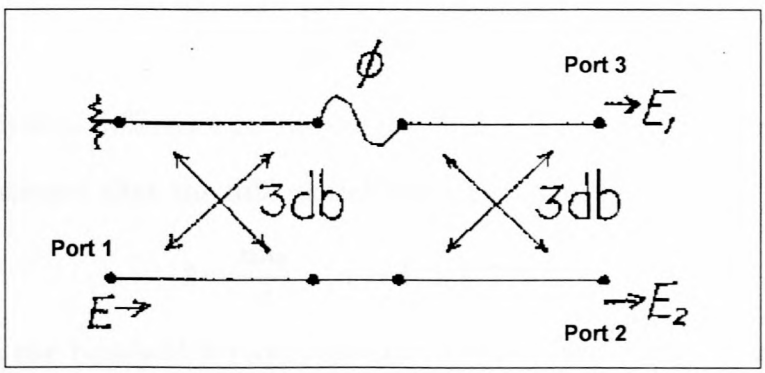

Figure 2.10: Schematic of Mohr's discriminator. [27]

2.3.1 Article discussions

(From [27]:)
A sketch of the broad-band microwave discriminator is shown in Figure 2.10. The device utilizes a pair of symmetric 3 dB 90° hybrids, joined by unequal lengths of transmission line. The difference between the line lengths is presented as a frequency dependent phase difference ϕ.

A straightforward analysis of the circuit yields

$$|E_1| = 0.707E(1 + cos\phi)^{\frac{1}{2}} \tag{2.4}$$

$$|E_2| = 0.707E(1 - cos\phi)^{\frac{1}{2}}. \tag{2.5}$$

It is readily determined from (2.4) and (2.5) that

$$|E_1|^2 + |E_2|^2 = |E|^2 \tag{2.6}$$

and that the device is then 100% efficient.

The ratio of output powers (at ports 2 and 3) is

$$\frac{P_2}{P_3} = \frac{|E_2|^2}{|E_1|^2} = \frac{\frac{1}{2}P_i[1-\cos\phi]}{\frac{1}{2}P_i[1+\cos\phi]} = \tan^2\frac{\phi}{2}. \tag{2.7}$$

Since ϕ is frequency dependent ($\phi = 2\pi(l/\lambda)$), the ratio of the output power is also frequency dependent. Equation 2.7 may be modified to

$$\frac{P_2}{P_3} = \tan^2\frac{\pi l}{\lambda} \tag{2.8}$$

where l is the physical difference in line length, and λ is the wavelength in the line.

In [29] it is mentioned that the differential line length can be set to

$$l = \frac{n\lambda_0}{4} \quad (n = 1, 3, 5, 7, 9, ...) \tag{2.9}$$

in accordance to the bandwidth requirements. λ_0 corresponds to the wavelength in the propagation medium at the center frequency f_0. Equation 2.8 may be rewritten and normalized as follows

$$\frac{P_2}{P_3} = \tan^2\frac{n\pi}{4}\frac{f}{f_0}. \tag{2.10}$$

A plot of Equation 2.10 is shown in Figure 2.11 for different values of n. From the figure it is clear that arbitrarily wide or narrow percentage bandwidths may be achieved by suitable choice of the line length difference. It is further clear that an increase in the value of n produce an increase in sensitivity for an equivalent bandwidth.

The discriminator described is highly efficient and capable of operation over bandwidths limited only by the hybrid.

(From [28]:)
It is necessary that the phase shift between the hybrid's two output ports be 90° over the band of interest (for this reason symmetric-line directional couplers were used in this article). For slight asymmetry in the coupled lines, the phase shift between the two components is different from 90° by a small amount θ which is a function of frequency. In such a case the aforementioned power relationship (Equation 2.7) gets modified to

$$\frac{P_2}{P_3} = \tan^2\left(\frac{\phi}{2} + \theta\right) \tag{2.11}$$

assuming of course that the same amount of asymmetry exists in both the 3 dB hybrids used in the discriminator.

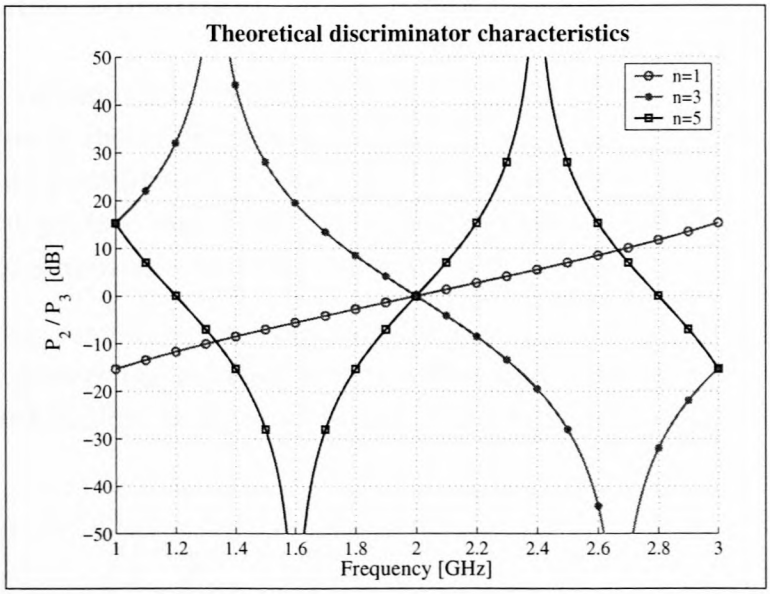

Figure 2.11: Theoretical discriminator characteristics (Eqaution 2.10 with $f_0 = 2$ GHz).

In [32] the outputs to the discriminator circuit (ports 2 and 3 of Figure 2.10), are detected by two detectors and summed in a differential amplifier. They also propose the use of a limiter to precede the RF input to the discriminator. An analysis revealed the most sensitive components of the discriminator. The major factors affecting the linearity are given in the following decreasing order of importance:

1. The detectors must be exceptionally well matched. Any residual reflections of the two detectors should track with frequency and be constant over the operating RF power range.

2. The two quadrature hybrids must have high isolation; in particular the isolation of the input hybrid is most critical for linearity. However, the linearity is relatively insensitive to coupling imbalances.

3. The internal termination must be well matched.

4. The connecting line lengths between the components should be kept as short as possible.

5. Linearity can be improved by isolation of the components through the use of pads (at the expense of decreased frequency sensitivity).

An analysis in [30] revealed that the detectors should be operated in the linear region.

2.3.2 Practical working

The phase of the transmission coefficients for the two connecting transmission lines have different slopes due to their difference in length. This difference then produce a frequency dependent in- and out-of-phase addition (constructive and destructive interference) of the signals arriving at ports 2 and 3. By increasing the value of n, the difference in phase increases, and the amplitudes vary more over frequency.

Though the theory suggest a tan^2 function for the relation of the output powers, the difference in the powers (as is taken with a differential detector circuit) actually has a cos-like triangular function, as shown in Figure 2.12 for different values of n. This function is given by

$$\begin{aligned} V_{out} &= |S_{21}| - |S_{31}| = |E_2| - |E_1| \\ &= \sqrt{\frac{1}{2}E\left(1 - cos\left(\frac{n\pi f}{2f_0}\right)\right)} - \sqrt{\frac{1}{2}E\left(1 + cos\left(\frac{n\pi f}{2f_0}\right)\right)} \end{aligned} \tag{2.12}$$

Practically Equation 2.12 has a bandwidth limitation caused by the hybrid. It will further have attenuating constants due to losses in the hybrids, transmission lines and detector circuitry. The hybrids will further not have an exact 90° phase shift between the two output ports. This deviation may cause a frequency dependent term as in Equation 2.11.

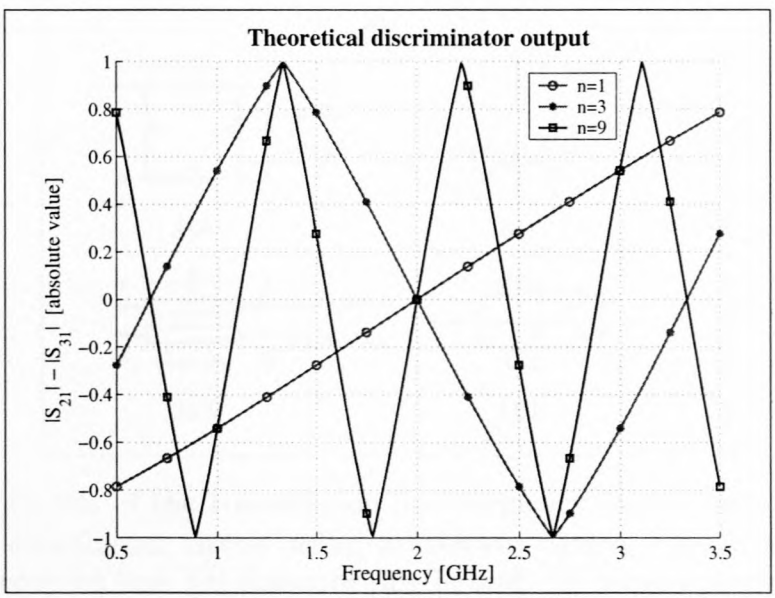

Figure 2.12: Theoretical discriminator output (V_{out} from Equation 2.12).

Design examples:
This discriminator formed the focus of the second goal of this research project. The developments at both S- and X-band, are discussed in detail in Chapter 3.

2.4 Transmission line discriminators which uses stubs

Several techniques with medium bandwidths are proposed in [34], and use a frequency splitting device together with an open and shorted stub. Bandwidths of 5% to 20% are obtained in the article, and are repeated here in design examples.

2.4.1 Article discussion (from [34])

The proposed discriminator circuits consist of a microwave device N_C and stub circuit N_L as shown in Figure 2.13 (a). For the device N_C, which serves as a power dividing as well as impedance matching section, a branch-line hybrid, a $\lambda/4$ parallel coupled line, a rat-race hybrid or a binary power divider can be used.

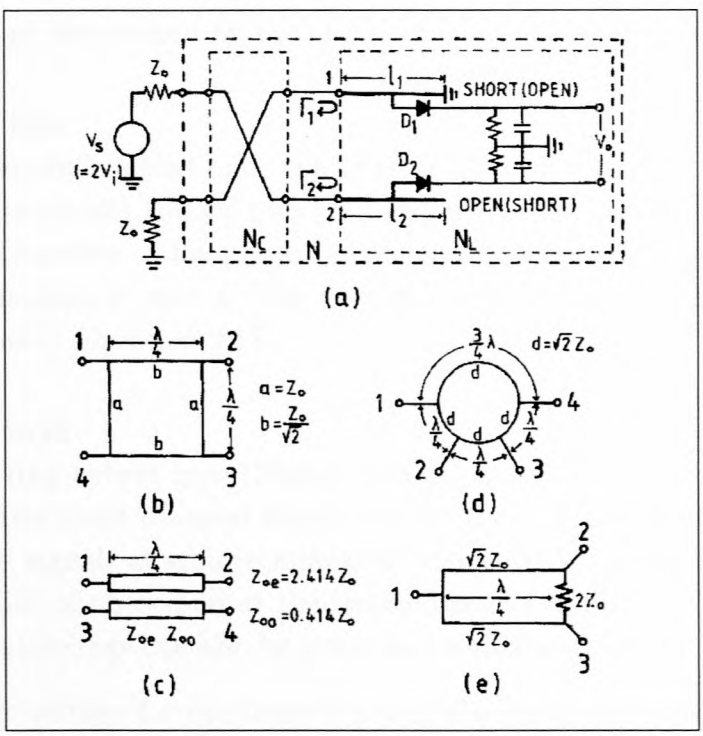

Figure 2.13: Schematic of the transmission line frequency discriminator and microwave devices. (a) Discriminator circuit using microwave device. (b) Branch-line hybrid. (c) $\lambda/4$ parallel coupled line. (d) Rat-race ring hybrid. (e) Binary power divider. [34]

Branch-line hybrid

In the 3 dB branch-line hybrid coupler type (Figure 2.13 (a) and (b)), the incident power through port 1 is coupled in equal measure to ports 2 and 3 with a 90° phase shift between ports 1 and 2, and a 180° phase shift between ports 1 and 3. If the reflection coefficients

at ports 2 and 3 (Γ_1 and Γ_2 in Figure 2.13 (a)) are chosen to be equal, the reflected signals, respectively, split into two waves that arrive at port 1 with 180° out of phase and at port 4 in phase with one another. Therefore, this circuit is matched at the driven port 1 when ports 2 and 3 are terminated with arbitrary equivalent impedances and port 4 with matched termination.

The input impedances of a shorted stub and that of an open stub are equal when the difference of the stub lengths is $\lambda/4$. The long stub is connected at port 2 so that the phase shift between port 1 and each detecting position is equal at the designed frequency. The detecting positions are located $\lambda/8$ from the stub terminations.

With an incident voltage of V_i at port 1, and incident voltages upon the stubs at ports 2 and 3 of S_{21} and S_{31} respectively, the output voltage V_o of the discriminator, can be expressed as follows:

$$V_o = 4n\left(|S_{21}|^2 \sin^2\theta - |S_{31}|^2 \cos^2\theta\right) \tag{2.13}$$

where n is a constant determined by the characteristics of the diode circuits. $\theta = \frac{\pi f}{4f_0}$.

Parallel coupled line

In the 3 dB $\lambda/4$ parallel coupled line type (Figure 2.13 (a) and (c)), the incident power through port 1 splits equally toward ports 2 and 3 with a 90° phase relationship between these two ports. Therefore, a long stub is connected at port 3, a short stub at port 2 and matched termination at port 4. The discriminator output voltage can be given as a similar expression as in Equation 2.13.

Rat-race ring hybrid

The 3 dB rat-race ring hybrid type (Figure 2.13 (a) and (d)) is a 0-180° phase response device. Therefore two stubs of equal length can be used. If the incident power is fed at port 2, the reflected signals at stub terminations connected at ports 1 and 3 arrive at the input port 2 180° out of phase and at the isolated port 4 in phase with each other. The discriminator output voltage can also be given as a similar expression as in Equation 2.13.

The relative output voltage for the three types of discriminators described previously is shown in Figure 2.14. Referring to this figure, discriminators with a bandwidth of about 5% can be achieved with these circuits. The input impedances can be well matched over the frequency bandwidth.

Binary power divider

In the binary power divider type (Figure 2.13 (a) and (e)), the fourth port (which is externally terminated with Z_0) does not exist. The divider has the advantage of excellent output port amplitude balance and in phase power division. Therefore two stubs of equal

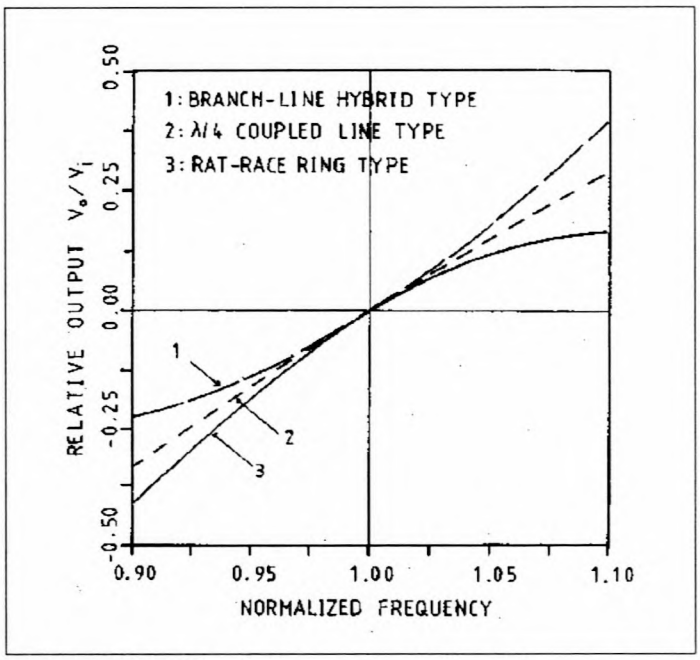

Figure 2.14: Relative output voltages for the three types of discriminators. [34]

length can be used.

When driven at port 1, the incident power splits equally between ports 2 and 3, and no power is dissipated in the internal termination $2Z_0$. On the other hand, the reflected signals at the stub terminations are dissipated in the internal termination and interfere destructively at the input port 1. The incident signals upon the two output ports 2 and 3 are equal ($S_{21} = S_{31}$). The output voltage of this discriminator can be expressed as follows:

$$V_o = 4n|S_{21}|^2 \left(\sin^2\theta - \cos^2\theta\right). \tag{2.14}$$

The relative output voltage for the binary power divider type discriminator is shown in Figure 2.15. The linearity is acceptable over approximately 20% bandwidth. In that frequency range, the input impedance can also be well matched.

A similar looking discriminator was also used in [6]. Their MIC transmission line design is linear from 2500 to 2700 MHz. The frequency selective elements are formed by two 70 Ω transmission lines $13/8\lambda$ long, one open-circuited, the other short-circuited. Harmonics generated by the detector diodes are absorbed by properly placed dissipative elements in the transmission lines.

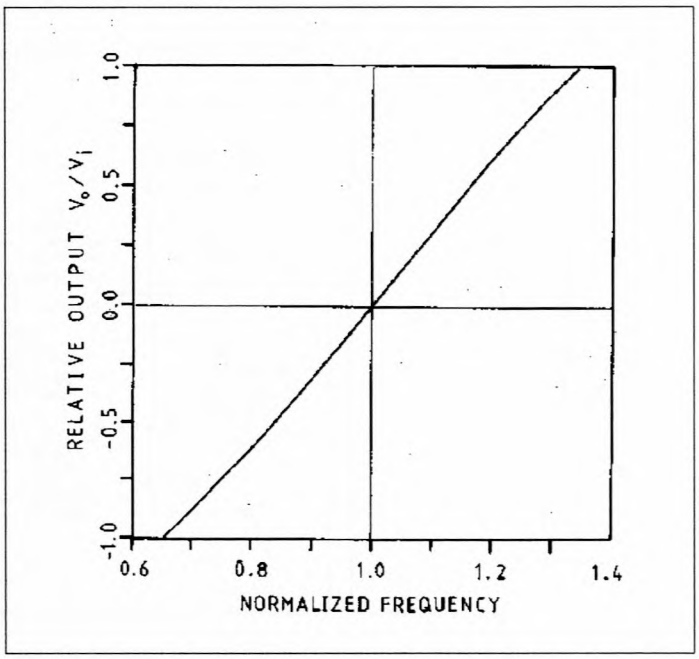

Figure 2.15: Relative output voltage for binary power divider type discriminator. [34]

2.4.2 Design examples

Designs were done for the four types of discriminators. The circuits which were used for the analysis in Microwave Office [61], is shown in Figure 2.16. The center frequency is given by $f = 2.5$ GHz. The configurations in which the circuits are described in the article, did not have satisfactory responses, and had to be modified slightly.

The transmission lines with electrical lengths *ea* and *eb* (TL7 and TL8 respectively in all the circuits), are there for matching purposes. For both the branch-line hybrid type and parallel coupled line type, a difference of 90° is needed. 0° and 90° is used for *ea* and *eb* respectively in the branch-line hybrid type, and 90° and 0° in the coupled line type. The rat-race ring hybrid type and binary power divider type both need equal lengths, which can be set to multiples of 90°, depending on the matching and linearity which is needed. It was set to 90° and 0° in the rat-race and divider types respectively.

The length of the stubs could be set to an electrical length of

$$es = eo = \pi \frac{2n+1}{4} \qquad n = 0, 1, 2, \ldots \tag{2.15}$$

(given in [35]). The values for *eo* and *es* (the electrical lengths of the open and shorted stubs – TL5 and TL6), were set to 45° and 225°, and the analysis of both cases are shown in Figure 2.17. The impedance OutZ0 is set to 70.71 Ω so that the stub/port-split is matched to the rest of the circuit.

These discriminators do not have a remarkable linearity or sensitivity, and can only be used over a small portion of their S-curve.

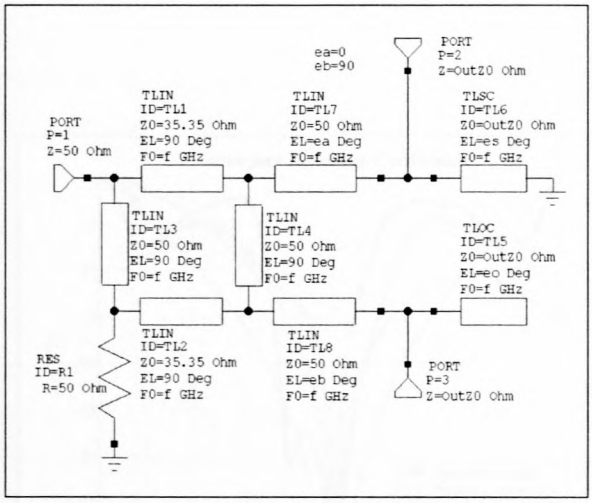

(a) Branch-line hybrid type.

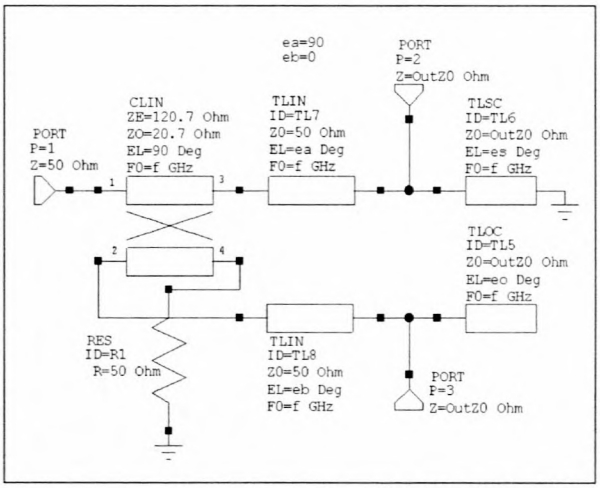

(b) $\lambda/4$ parallel coupled line type.

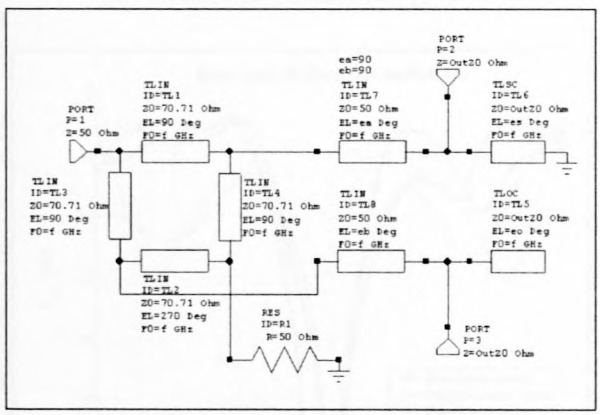

(c) Rat-race ring hybrid type.

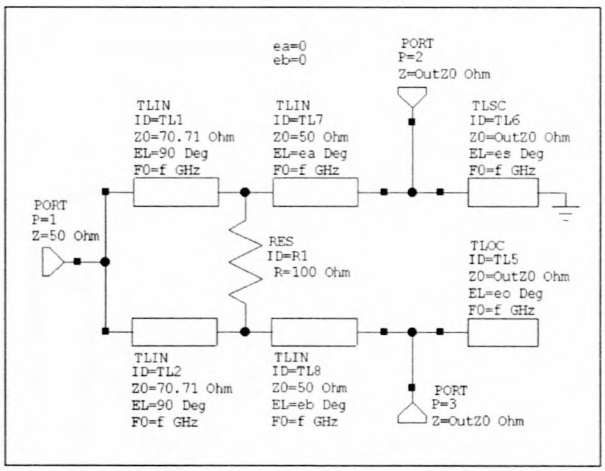

(d) Binary power divider type.

Figure 2.16: Circuits used in the analysis of the stub-type transmission line frequency discriminators.

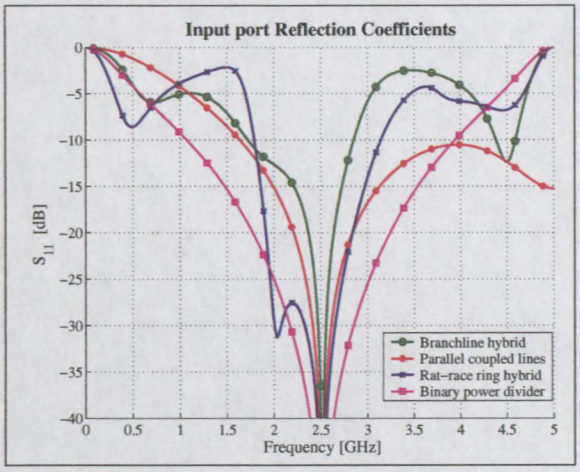

(a) Reflection coefficients ($\theta = 45°$).

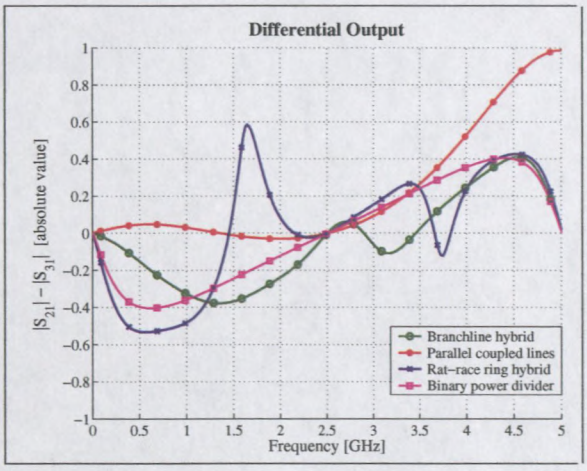

(b) Differential output ($\theta = 45°$).

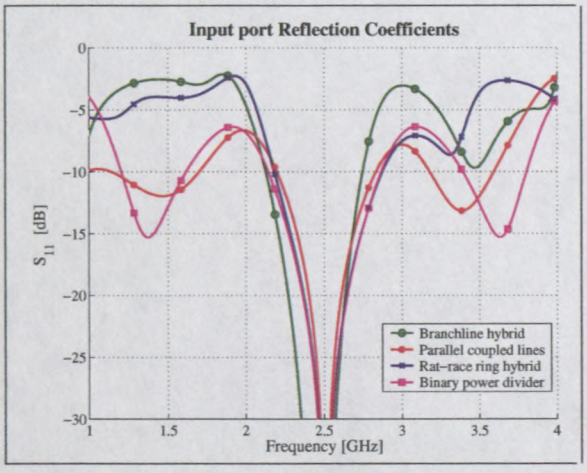

(c) Reflection coefficients ($\theta = 225°$).

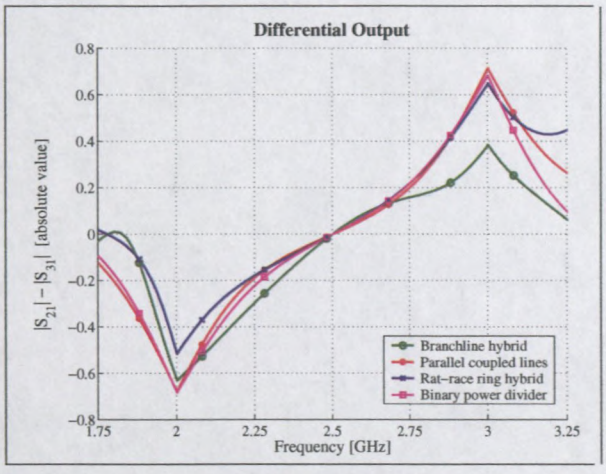

(d) Differential output ($\theta = 225°$).

Figure 2.17: Analysis of the stub-type transmission line discriminators.

2.5 Super wide-band technique (bridge type)

Work done by C.W. Lee, *et. al.* [35][36][34], fills a gap between lower frequency discrete discriminators, and the usual higher frequency discriminators. Both proposed bridge type discriminators have a very broad bandwidth, and practical results are shown at center frequencies of 85 MHz and 3.2 GHz with a 40% and 50% linear deviation.

2.5.1 Article discussions

(From [35] and [36]:)
This FM line discriminator is analyzed from the viewpoint of the impedance of a short-circuited and an open-circuited transmission line which varies with the frequency deviation of the impressed FM signal. The bridge type configuration of transmission lines and pure resistors is shown in Figure 2.18.

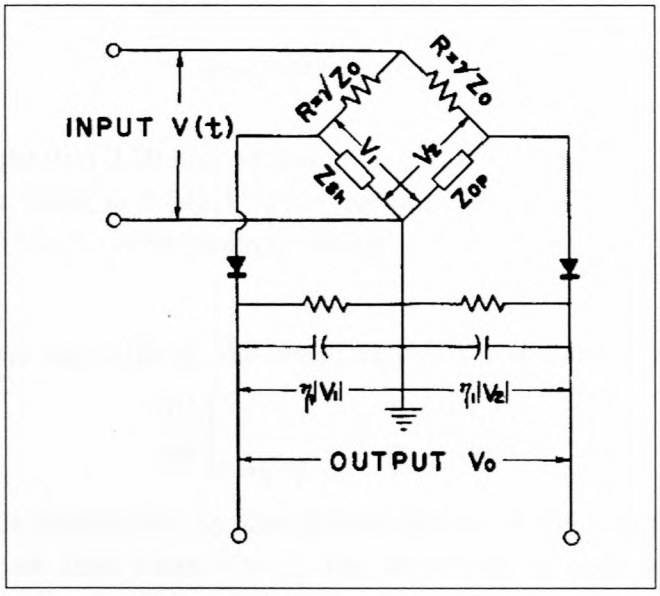

Figure 2.18: Circuit diagram of bridge type transmission line discriminator. [36]

If the loss of the transmission line is negligible, the input impedances of the short-circuited and the open-circuited transmission lines can be given by

$$Z_{sh} = jZ_0 \tan\theta \tag{2.16}$$

$$Z_{op} = -jZ_0 \cot\theta \tag{2.17}$$

$$\text{where} \quad \theta = 2\pi\frac{l}{\lambda}. \tag{2.18}$$

Referring to Figure 2.18, using Equations 2.16 and 2.17, if V_1 and V_2 are applied to linear detectors and the input FM signal has a constant amplitude from the limiter, the output voltage V_0 of the discriminator can be expressed as

$$\begin{aligned} V_0 &= \eta_1 \left(|V_1| - |V_2| \right) \\ &= \eta_1 V \left(\frac{1}{\sqrt{1 + \gamma^2 \cot^2 \theta}} - \frac{1}{\sqrt{1 + \gamma^2 \tan^2 \theta}} \right) \end{aligned} \tag{2.19}$$

where

η_1 is a constant determined by the characteristics of the diode,
V is the amplitude of the input signal, and
$\gamma = R/Z_0$ is the coupling resistor constant.

Inspecting Equation 2.19, it is seen that when $\theta = \pi \left(\frac{2n+1}{4} \right)$, where $n = 0, 1, 2, \ldots$, the output voltage is zero. The operating point should be chosen there, which corresponds to a line length of $l = \lambda_0 \left(\frac{2n+1}{8} \right)$, where λ_0 is the wavelength of the carrier frequency. The sensitivity at the operating point is given by

$$\left. \frac{\partial V_0}{\partial \theta} \right|_{\theta = \pi \left(\frac{2n+1}{4} \right)} = \frac{4\gamma^2 \eta_1 V}{(1 + \gamma^2)^{\frac{3}{2}}}. \tag{2.20}$$

By differentiating Equation 2.20 and setting $\gamma = \sqrt{2}$, it can be shown that the sensitivity is maximum and its value is $1.54\eta_1 V$ volts/radian. On the other hand, when $\gamma = 1$, the sensitivity is $1.414\eta_1 V$ volts/radian, which is only 8.18% less than the maximum sensitivity.

If square-law detectors are utilized, the sensitivity of the discriminator is

$$\left. \frac{\partial V_0}{\partial \theta} \right|_{\theta = \pi \left(\frac{2n+1}{4} \right)} = \frac{8\gamma^2 \eta_2 V^2}{(1 + \gamma^2)^2} \tag{2.21}$$

where η_2 is a constant determined by the characteristics of the diode. The differentiation of Equation 2.21 shows that when $\gamma = 1$, the sensitivity is maximum and the value is $2\eta_2 V$ volts/radian.

It is further shown in [36] that when $\gamma = 1$, the input impedance changes only to the characteristic impedance of the transmission line Z_0 and becomes independent of frequency. Judging by these results, it is desirable to set the coupling resistor constant γ at unity. The output voltage can then be written as

$$V_0 = \eta_1 V \left(|\sin \theta| - |\cos \theta| \right). \tag{2.22}$$

Through a lengthy Fourier analysis and Bessel function expansion, it is shown that even when the frequency deviation of the input signal is 100%, the harmonic distortion is only

2.67% for linear detectors. For square-law detectors, the harmonic distortion is 12.17% for 100% frequency deviation of the input signal, and 2.67% for 50% frequency deviation. $n = 0$ was used in all the calculations.

Experiments were performed to verify the analytical results obtained. The total length of the transmission line is 35.6 cm and the corresponding theoretical center frequency is 102.74 MHz. However, because of the unsymmetrical characteristics of crystal diodes, etc., the center frequency moves down to 85.5 MHz. The characteristic curve of the discriminator, when the input signal is 100 mV, is shown in Figure 2.19, which shows that the curve is linear for a frequency deviation of 40% from the center frequency. The measured input impedance is within ±14% of the ideal 50 Ω and the phase angle is less than 5°.

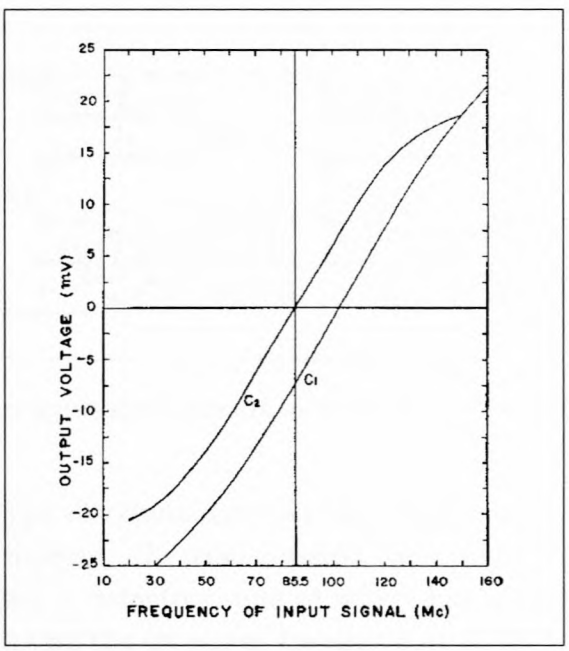

Figure 2.19: C_1 represents the curve drawn according to Equation 2.22 and C_2 shows the measured characteristic curve of the bridge type discriminator when the input signal is 100 mV. [36]

(From [34]:)
The bridge circuit can also be realized using microstrip lines and slotlines as shown in Figure 2.20. In the experimental discriminator designed at 3.2 GHz as shown in Figure 2.21, matched detectors are used in place of the coupling resistors and detecting circuits. The measured output voltage from 2.4 GHz to 4.0 GHz is shown in the article, and is linear over the given band. For an input power of -10 dBm, the discriminator has a sensitivity of ~37.5 mV/GHz. The 50% bandwidth operation confirmed by the experiment is in good agreement with the theory.

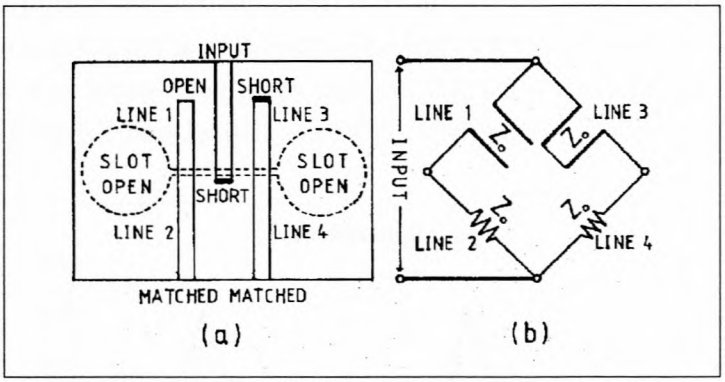

Figure 2.20: (a) Layout configuration for the bridge circuit (b) Equivalent circuit diagram of bridge-type transmission line discriminator. [34]

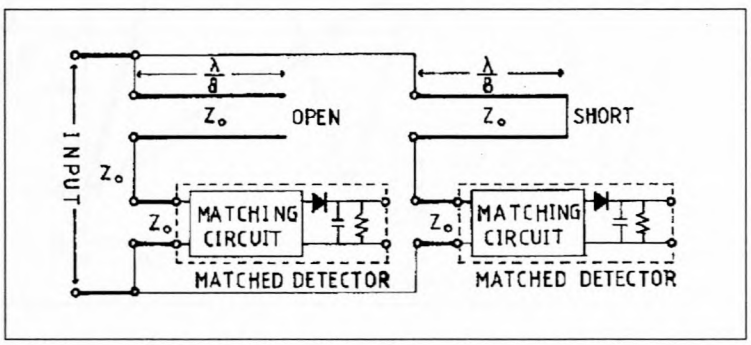

Figure 2.21: An equivalent circuit of a bridge type discriminator. [34]

The wide-band bridge type discriminator was also implemented in a satellite television receiver system [37]. However, the transmission lines were replaced by their lumped element equivalent circuits – inductors, one of which has a variable capacitor in series. The capacitor was used to set the crossover frequency at 80 MHz (the IF of this system). A linear response ($\sim$ 1% deviation from linearity) was achieved with this approach over the band from 60 to 100 MHz.

2.5.2 Design example

The circuit of Figure 2.18 was analyzed in Microwave Office [61] without the detecting circuitry. The output port impedance (which would be the input impedance of the detectors) was set to 100 Ω for improved input port matching and differential output linearity. The lumped resistors was set to 50 Ω ($\gamma = 1$), and the lengths of the transmission lines was set to 45° and 225° ($n = 0$ and $n = 2$ respectively).

The results are compared to the theoretical output given by Equation 2.22, with $\eta_1 = 0.4$, in Figure 2.22. The input port is well matched, and both configurations have an S_{11} better than -16.9 dB over the whole frequency range. This discriminator is not very efficient, but can have a very broad bandwidth, has a good linearity and sufficient sensitivity.

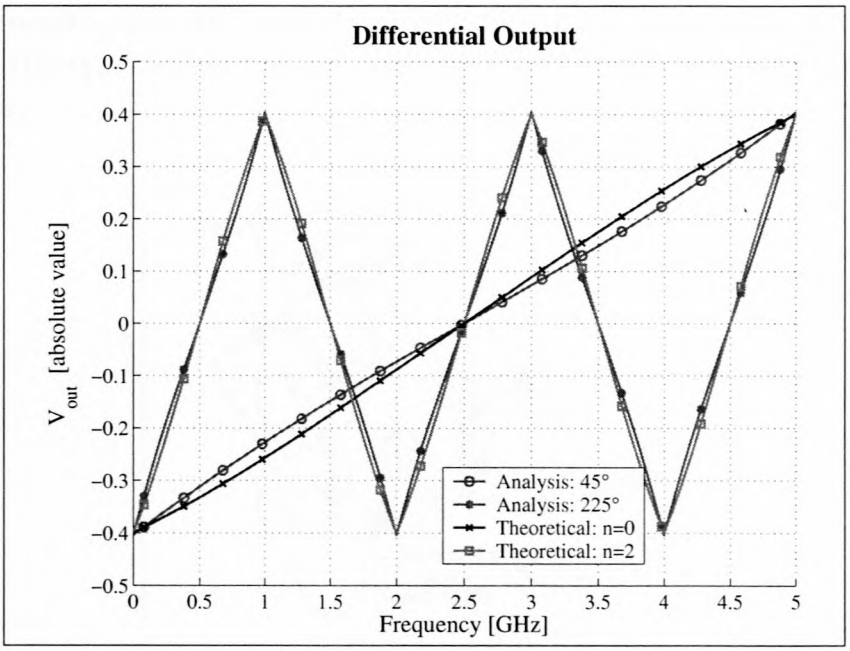

Figure 2.22: Practical and theoretical analysis of the bridge type transmission line discriminator.

Remark: The techniques to follow were not analyzed, and will only consist of article discussions.

2.6 Techniques using circulators

2.6.1 A delay line type

A delay line type discriminator which uses circulators to achieve its splitting and combining of signals, was proposed in 1968 [38]. Due to modeling problems, this technique was not analyzed. The article itself has a good example which will be included in this discussion.

(From [38]:)
The discriminator is of the delay line type. It uses ferrite circulators and intentionally introduced variable mismatches to permit simple compensation for delay line loss and easy adjustment to the desired input carrier frequency. For the article's intended application, it is necessary to have the capability of tuning the device to any one of many carrier frequencies extending over the band from 5925 to 6425 MHz. The discriminator must have high sensitivity, excellent linearity (for frequency deviations up to ±5 MHz), and a low group delay.

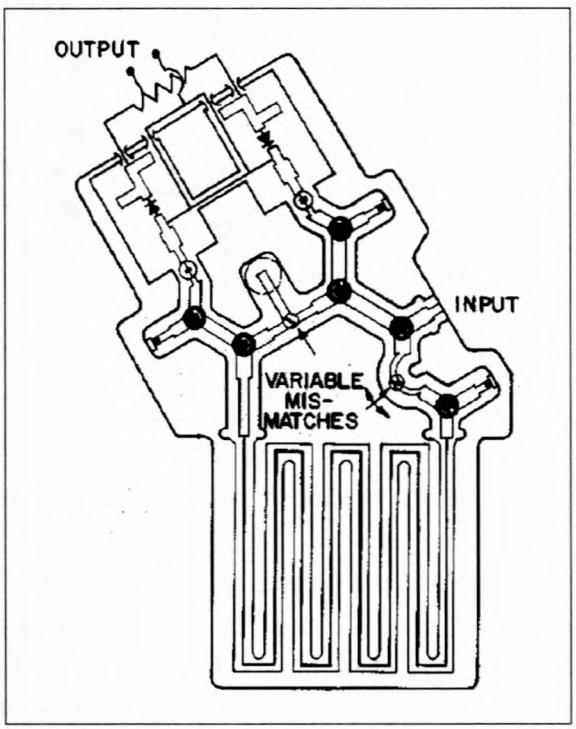

Figure 2.23: Circuit layout for the circulator/delay line type discriminator. [38]

A layout of the discriminator is shown in Figure 2.23. The stripline circuitry in the discriminator is of two types. In the vicinity of the circulators and detectors, thin film technology is used on a thin ceramic substrate suspended between two ground plates. A cross section of the circulator is shown in the article. The delay line is in fully loaded stripline (normal stripline). The dielectric used is alumina and the centre conductor is also defined by thin film techniques.

The power splitting and combining network and the delay line are shown in Figure 2.24. The FM input signal is coupled through a circulator to the line on which the variable depth, variable position mismatch is located. Adjustment of the magnitude of this first mismatch controls the amount of signal transmitted through it and the amount reflected. Adjustment of its position controls the phase between the signals. The signal reflected

from this mismatch is coupled through several circulators to the second mismatch, which is set to 3 dB. Half of the non-delayed signal is thus sent to each detector. The signal transmitted through the first mismatch and the delay line, reaches each detector similarly. For the highest sensitivity the delayed and non-delayed signal levels should be equal. Since the delay line has some loss, this condition is achieved by making the transmitted signal at the first mismatch larger than the reflected signal.

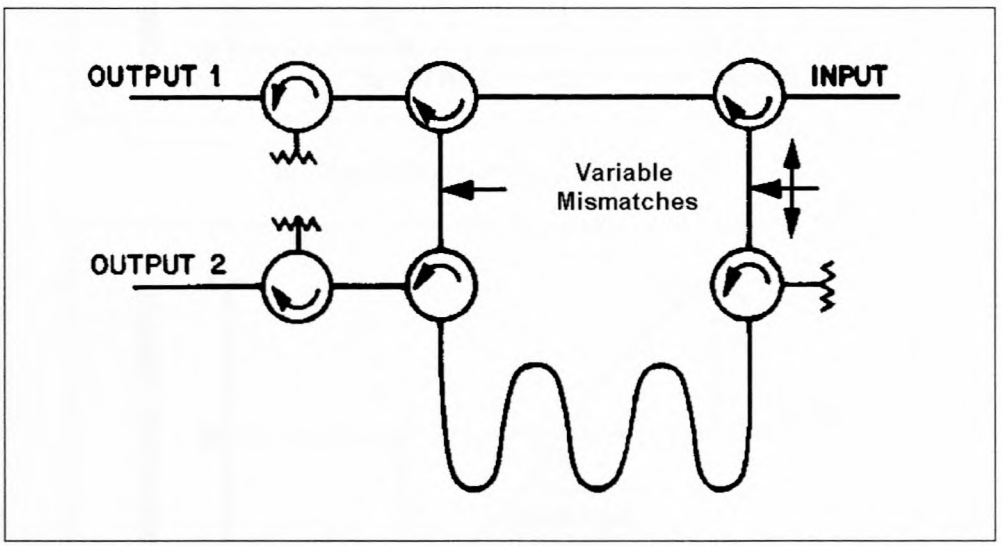

Figure 2.24: Simplified diagram for the circulator/delay line type discriminator. [38]

In order for the circuit to function, it is necessary for the signals reflected and transmitted at the second mismatch to be 90° out of phase. For a lossless mismatch, this condition is automatically satisfied. The delayed and non-delayed signals reaching each detector add on a vector basis to produce the amplitude response shown in Figure 2.25 (a). The detector currents, made opposite in sign by opposite polarization of the diodes, combine to produce the discriminator function shown in Figure 2.25 (b).

The meandering delay line has a delay of 8 ns. A larger value would provide greater sensitivity but would not permit meeting the linearity requirements. In addition it would mean increased group delay for the complete discriminator. The delay line is a 50 Ω line in a channel fully loaded with dielectric. The full loading is used to decrease the velocity of propagation, and therefore minimize the physical length. The line is approximately 30 inches long and has a loss of about 3 dB. A computer analysis has shown that a return loss for the complete delay line of better than 35 dB across the 500 MHz band, can be achieved when it is terminated in a 50 Ω load. This high return loss is necessary since multiple reflections of the delay line adding in phase would significantly degrade the linearity of the discriminator.

The two detectors shown in Figure 2.23 are identical except for the opposite polarity

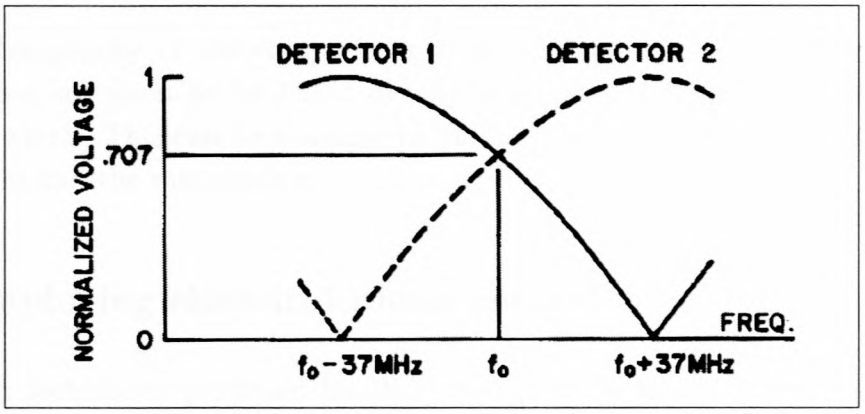

(a) Normalized detector input voltage.

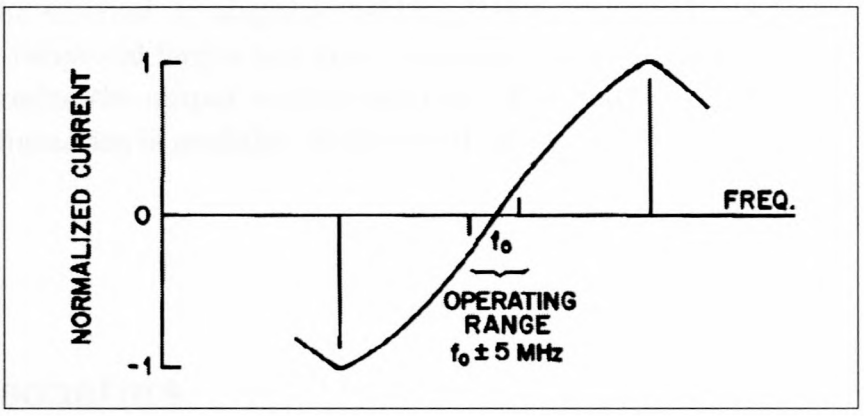

(b) Normalized current of combined detectors.

Figure 2.25: Normalized analysis of the circulator/delay line type discriminator as a function of instantaneous frequency. [38]

of the diodes. The detectors are floating at a relatively high DC potential. Blocking capacitors are used to isolate the detectors from the remainder of the stripline structure. Filters provide the necessary RF short circuits behind the diodes and prevent leakage on the baseband outputs.

Models of the discriminator have been built and tested. The discriminator is operated with an input power of +13 dBm and the diode detectors operate in the linear region. The output current from each diode, at the carrier frequency, is 6 mA. The sensitivity is approximately 0.25 mA/MHz of frequency deviation, when operating into a low impedance filter. Non-linearity of less than 1% has been achieved over the required frequency deviation.

Discussion:
Due to the complexity of the components, a design example was not attempted. This technique does not seem to be linear over a large part of its S-curve, and has a very narrow bandwidth. This can be a simple technique, if a method is available of employing the circulators and the mismatches.

2.6.2 Employing electrical phase control

One of many techniques proposed by W.Y. Seo [39], employs the method of electrical phase control to adjust the phase difference very accurately. Two circulators are used to precisely adjust the phase difference to $\pi/2$ between two transmission channels by controlling the external dc magnetic field applied to the circulator. The circulator is a stripline non-reciprocal ferrite wye type. Faraday's rotation angle in ferrite is given and used to determine the output voltage function. The math involved is complicated, and very little information is available on this method.

2.7 Resonators

2.7.1 Modal excitation

The first of two resonator-discriminator techniques discussed here use either a microstrip resonator [7] or a dielectric resonator (DR) [8] to excite two orthogonal modes at two frequencies f_1 and f_2.

2.7.1.1 Microstrip resonator

A 5.2 GHz microstrip Gunn oscillator has been frequency stabilized by means of a discriminator and feedback loop [7]. The thin-film discriminator is shown in Figure 2.26 (a). It consist of a double-mode microstrip resonator with a pair of detector diodes. The resonator has the geometrical shape of a rectangle with truncated corners. The RF input signal excites two orthogonal resonances, as shown in Figure 2.26 (b), which are determined by the electrical dimensions of the rectangular resonator. The transmitted signal is detected by a reversed diode pair giving the output signal shown in Figure 2.26 (c). Frequency tuning of the discriminator is achieved by either adjusting the resonator lengths or by dielectrically loading the resonator along the resonance axes.

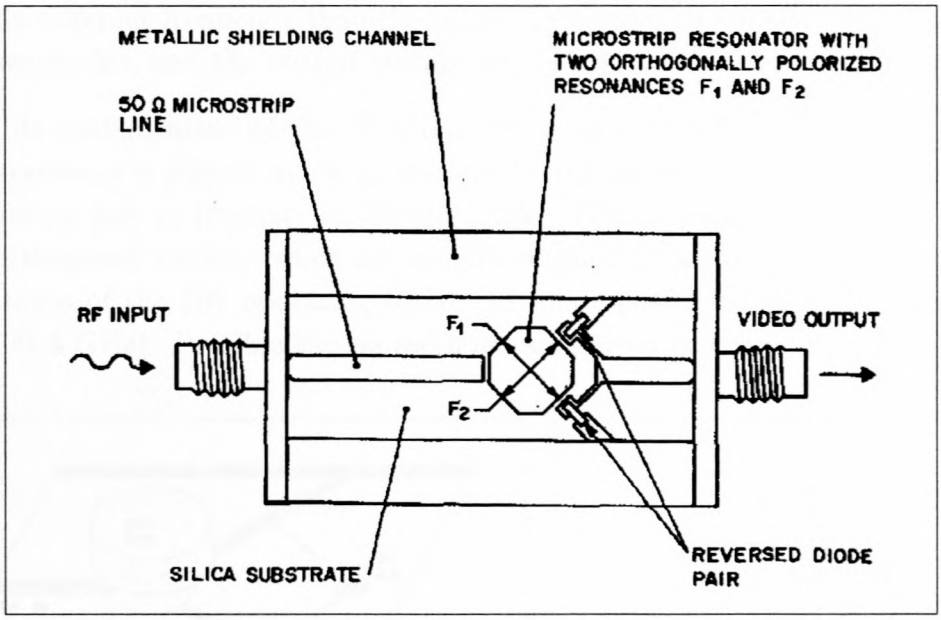

(a) Circuit configuration showing how each diode is capacitively coupled to one of the two orthogonal modes of the microstrip resonator.

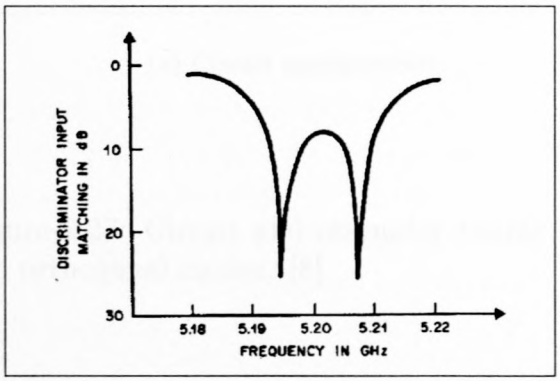

(b) Return loss of the input signal.

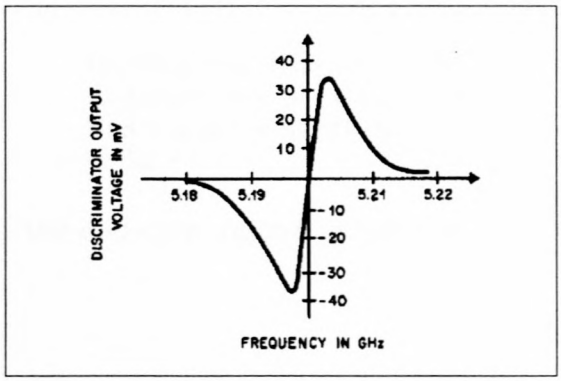

(c) Detected output signal.

Figure 2.26: Circuit and measurements of the microstrip-resonator discriminator with two orthogonal modes. [7]

2.7.1.2 Dielectric resonator

A dual mode dielectric resonator frequency discriminator [8] offers a much higher Q and stability than the previous circuit. Similar to a waveguide cavity configuration, two orthogonal modes are excited in a cylindrical or square DR. One of the modes is tuned to a slightly different frequency than the other. Two opposite polarity diodes are coupled to these two modes, and the output voltage combines into a discriminator curve.

One possible configuration of the discriminator is shown in Figure 2.27 (a). A high Q dielectric resonator is placed on low loss support (to maximize the Q factor) and is excited by a microstrip line to resonate in HE11δ mode. This particular mode can be resolved into two orthogonal modes, which are weakly coupled to a reversed diode pair. One of the advantages of the DR operating in HE11δ mode is the flexibility and tuning range (500 MHz @ 4 GHz). Possible tuning methods are shown in Figure 2.27 (b).

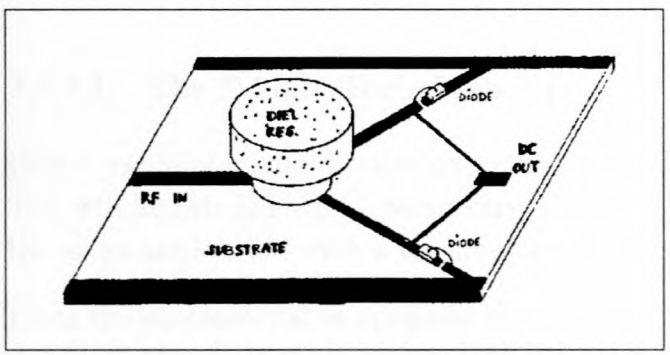

(a) Circuit configuration.

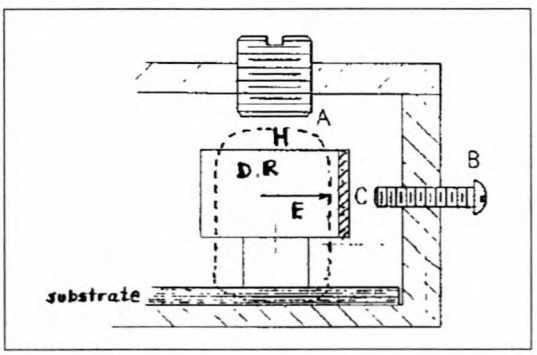

(b) Frequency tuning of the HE11δ mode. A: Large screw perturbing magnetic field. B: Screw perturbing electric field. C: Notch or flat.

Figure 2.27: Circuit and resonator tuning of the dielectric resonator discriminator with two orthogonal modes. [8]

2.7.2 The Pound discriminator

Possibly the first microwave discriminator to be published, was proposed by R.V. Pound in 1946 [9][10]. It uses a resonant cavity and two magic tees as discriminator to stabilize a microwave oscillator. It was improved by J.R. Ashley *et al.* by separating the waveguide channels [17]. A more modern approach to this design was implemented on microstrip and uses a dielectric resonator as 'cavity' [11].

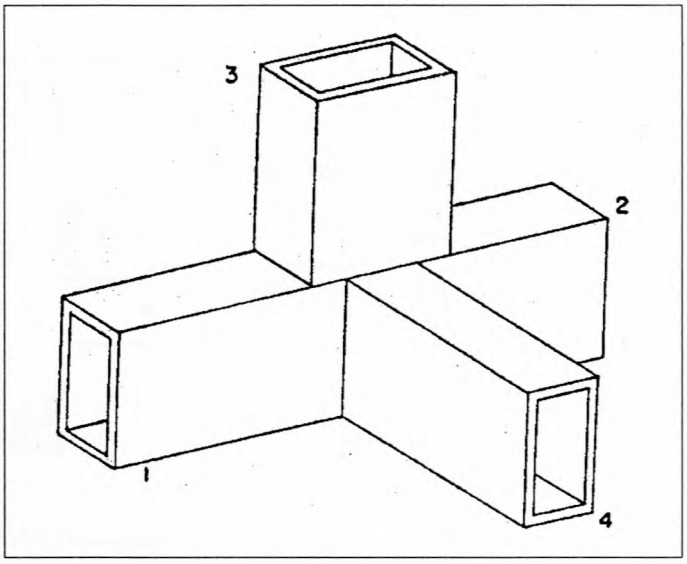

Figure 2.28: Schematic of waveguide 'Magic Tee'. [9]

2.7.2.1 The 'Magic Tee' (from [9])

Before explaining the discriminator, the special microwave circuit known as the 'Magic Tee' will be introduced. A perspective sketch of this device is given in Figure 2.28, where the arms are labeled with a terminology which will be used in this section.

From the symmetry it is apparent that a wave sent into arm 3 excites arms 1 and 2 with waves of identical phase and amplitude at points equidistant from the center plane of the junction. A wave sent into arm 4, conversely, excites 1 and 2 with waves of equal amplitude and opposite phase at symmetrical planes. Because of this 'even' and 'odd' symmetry associated with arms 3 and 4, respectively, there is no direct excitation of arm 3 by a wave in arm 4 or *vice versa*. It can be shown by a simple argument based on the reversibility of waves that a wave into arm 1 will directly excite only 3 and 4 and not 2. The device is thus the equivalent of a 4 terminal-pair 'hybrid coil' with identical characteristic admittances at all 4 terminals. A set of transformation equations are described in the article. A more thorough description of this device is given in [40]. A modal analysis was also done in [41].

2.7.2.2 Pound's circuit [9]

A symbolic diagram of one form of this discriminator is shown in Figure 2.29 (a). The numbers on the arms of the two magic tee circuits correspond to those of Figure 2.28. An explanation of this circuit is given as follows: At frequencies far from resonance the waves reflected from the cavity on arm 2 and the short circuit on arm 1 of the upper tee are $\pi/2$ radians out of phase as they reconverge so that equal components of even and

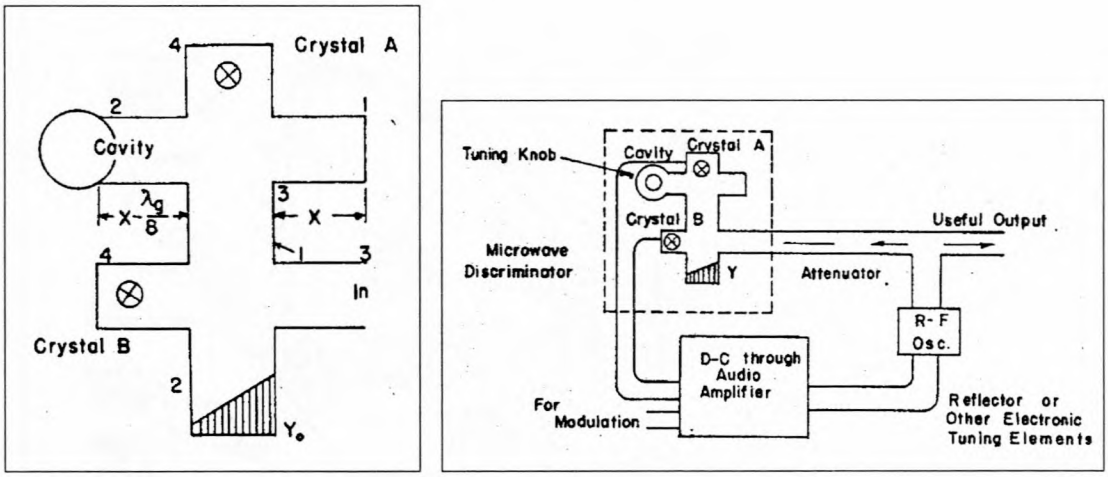

(a) Magic Tee discriminator. (b) The stabilization circuit.

Figure 2.29: The Magic Tee Pound discriminator stabilization circuit. [9]

odd symmetry exist. Thus, waves of equal amplitude travel out arms 3 and 4. A matched crystal on arm 4 detects this wave whereas one-half the power sent out arm 3 is detected by a matched crystal on arm 4 of the lower tee. The complete function of the lower tee is to pick up the reflected wave without direct coupling to the input wave.

At resonance, the cavity reflection coefficient is also real so that again the waves out arms 3 and 4 are equal and crystal B detects half the power of crystal A. Just either side of resonance the reflection coefficient of the cavity has an imaginary component so that on one side the power at crystal A is increased and at B decreased, and on the other that at crystal B is increased and at A is decreased.

If the power into crystal A is reduced by 3 dB, or if the output voltage is reduced to be equal to that of crystal B when the cavity is detuned, a symmetrical discriminator curve is obtained by taking the difference between the output voltages of the two crystals. This discriminator was developed for stabilizing oscillators in systems such as that shown in Figure 2.29 (b).

2.7.2.3 Improvements by Ashley [17]

A schematic of the improved discriminator is shown in Figure 2.30. This discriminator differs from Pound's circuit by separating the waveguide channels for the signal reflected from the cavity resonator and the reference signal for the phase detector. Notice further that the discriminator cavity resonator receives its signal from a three-port circulator rather than a magic tee or 3 dB hybrid. This provides a total of 6 dB threshold improvement.

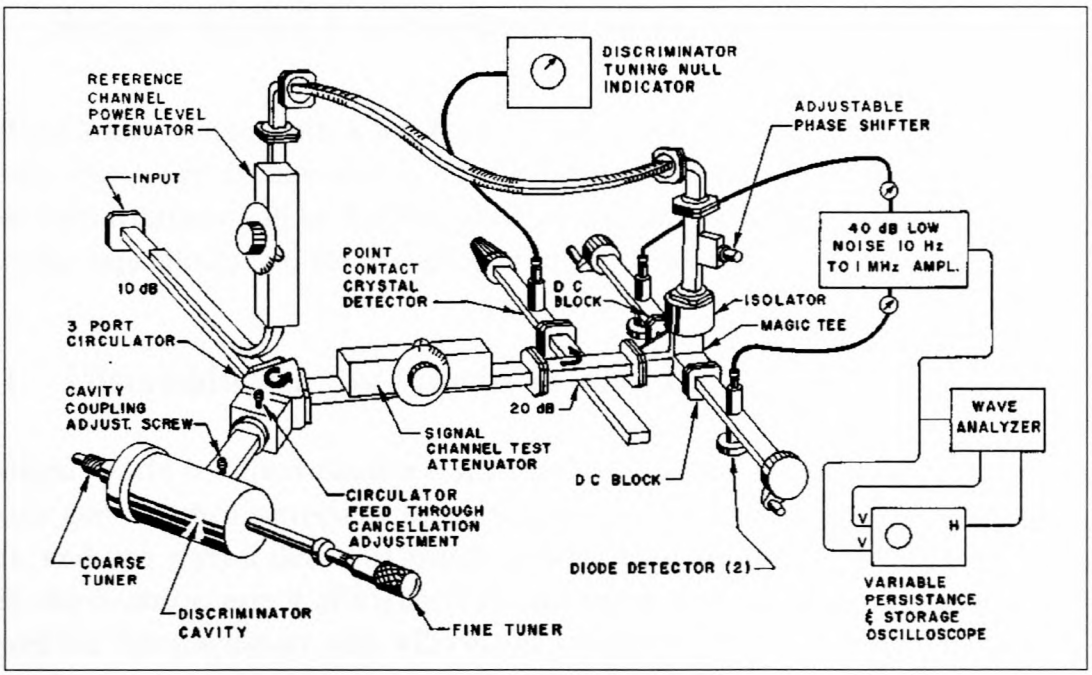

Figure 2.30: The Pound-Ashley discriminator. [17]

2.7.2.4 Microstrip Pound discriminator

An article describing dielectric resonators as microstrip circuit elements [11], applied their techniques to illustrate the use of such a resonator in a practical Pound discriminator circuit. The microstrip Pound discriminator is shown in Figure 2.31, where ring hybrids are used as the splitting device, and the dielectric resonator acts as the reference cavity. It was designed at 6.25 GHz. The sensitivity of the results are 30 mV/MHz for a $Q_0 \approx 415$ resonator, and 400 mV/MHz for a resonator with $Q_0 \approx 5400$.

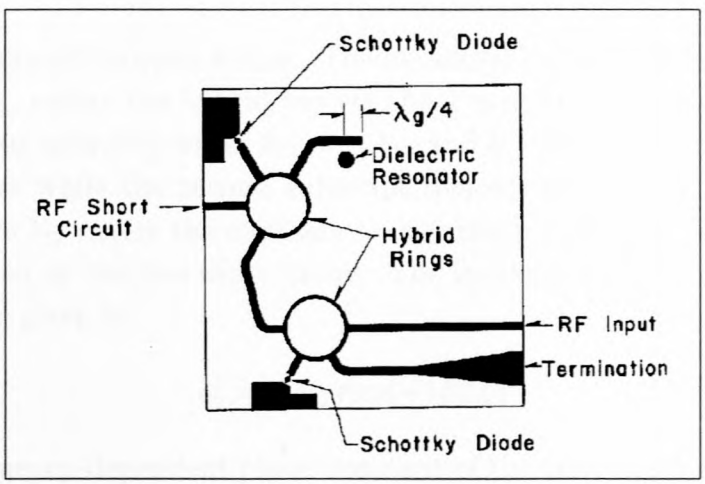

Figure 2.31: Microstrip Pound discriminator circuit. [11]

2.8 Single hybrid techniques with a Magic Tee

A method which employ only a single magic tee, a transmission line [42] and a circulator [43], were developed extensively by T.P. Chattopadhyay and B.N. Biswas [44]–[49]. Only the two initial circuits will be discussed here, since the developments only included further measuring capabilities and the inclusion of injection locking.

2.8.1 Discriminator by Nigrin *et al.* [42]

The single hybrid tee discriminator is schematically shown in Figure 2.32. It consist of an ordinary non-matched waveguide tee, a transmission line terminated by a movable short circuit, and two crystal detectors which match terminate the E and H arms of the tee. **Note:** the E-arm is arm 4 of Figure 2.28 and the H-arm is arm 3. These numbers have swapped for this discussion, and will change totally in the following discussion.

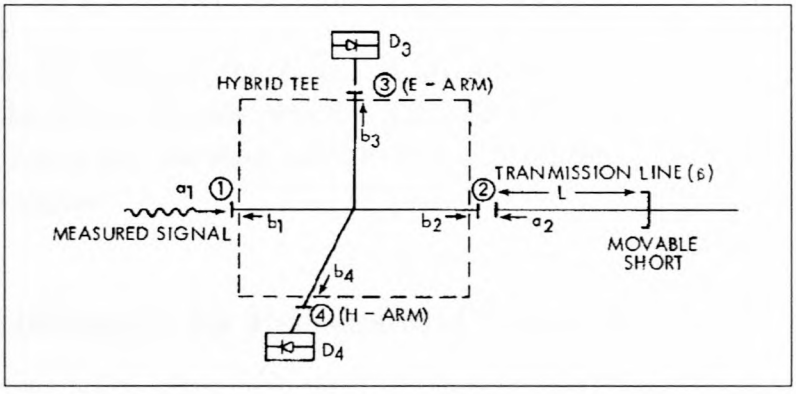

Figure 2.32: Single hybrid tee frequency discriminator. [42]

The principal of operation is quite simple. The measured signal represented by an incident normalized wave a_1, enters the hybrid tee via the 1 arm and is split into the H, E and 2 arms giving rise to emerging waves b_{13}, b_{14}, b_{12} and b_{11} (the first subscript denotes the number of the wave while the second subscript denotes the arm from which the wave emerges). The wave b_{12} enters the auxiliary transmission line and travels the distance L before being reflected by the line short circuit. The incident wave returning to the hybrid tee via the 2 arm is given by

$$a_2' = -b_{12} \exp(-j\beta 2L) \tag{2.23}$$

where β is the frequency-dependent phase constant of the transmission line. The a_2' wave undergoes similar splitting as the wave a_1 and gives rise to waves b_{23}, b_{24}, b_{21} and b_{22}. Since the phase difference of the waves b_{13} and b_{23} as well as b_{14} and b_{24} depends on

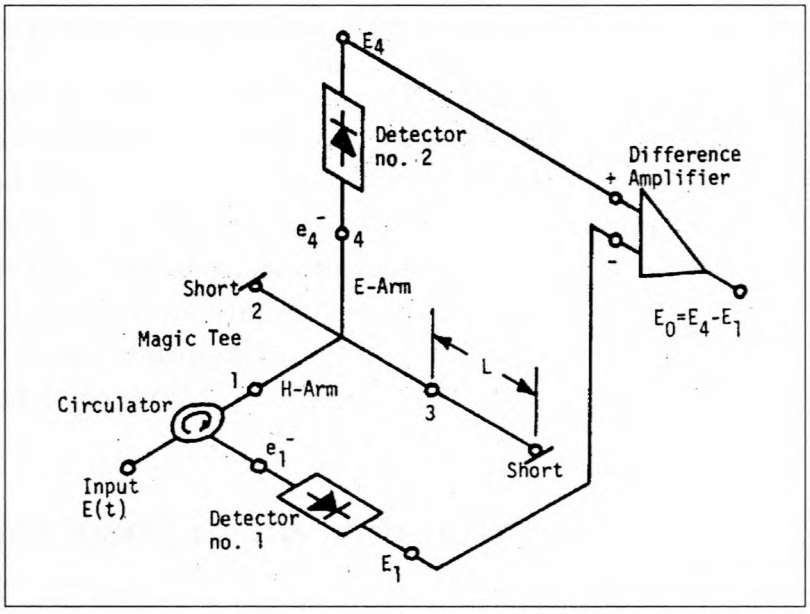

Figure 2.33: The microwave discriminator. [43]

the factor $(\beta 2L)$, the waves in the E and H arms interfere. The envelope of the signals emerging from the E and H arms, which is also affected by additional reflections between the input of the 2 arm and the short circuit, thus depends on the amplitude and frequency of the measured signal.

2.8.2 Discriminator by Peebles and Green [43]

A similar microwave discriminator was designed for operation at 35 GHz with a 400 MHz bandwidth [43]. In the simplest construction the device requires one magic tee, one circulator, two line-matched detectors, a length of line, and two shorts. The configuration of these components are shown in Figure 2.33.

An input signal is directed by the circulator to port 1 (H-arm) of the magic tee. It is split to cause ideally equal-amplitude, equal-phase waves to emerge from ports 2 and 3 (colinear arms). No output occurs at port 4 (E-arm) due to the input. The waves emerging from ports 2 and 3 are reflected by conductive short circuits as shown. The short on port 2 is at the magic tee while that at port 3 is at the end of a line of physical length L.

The waves reflected from the short circuits reenter the magic tee with that at port 3 phase delayed relative to that at port 2. The wave incident on port 2 is split into two equal-amplitude, equal-phase signals that emerge from ports 1 and 4 (no output occurs at port 3). The wave incident at port 3 is also split to cause equal amplitude waves to emerge from ports 1 and 4 (no output at port 2), however, the wave emerging from port

4 is the negative of that emerging from port 1.

Two waves emerge at ports 1 and 4, which have the same amplitude but differ in phase according to the behaviour of the magic tee and the line length L. Thus there will be constructive and destructive interference of the two waves at each port as a function of the frequency of the input signal because the phase delay of the line length L is frequency dependent. The circulator separates the incident and emergent waves at port 1 so that diode detectors (assumed to be impedance-matched to the lines) produce voltages E_1 and E_4 proportional to the magnitudes (for linear detectors) of the composite waves emerging from ports 1 and 4 respectively.

2.9 Mixers used in discriminators

The discriminator developed by J.R. Ashley *et al.* for FM noise measurements [17] (see Section 2.7.2.3) was again improved by omitting the resonator cavity [18]. There were comments in [50] whether this discriminator is a delay-line discriminator or a transmission line resonator-discriminator. The problem arose when the signal recirculating between the slide screw tuner and the short was neglected in their discussion [51].

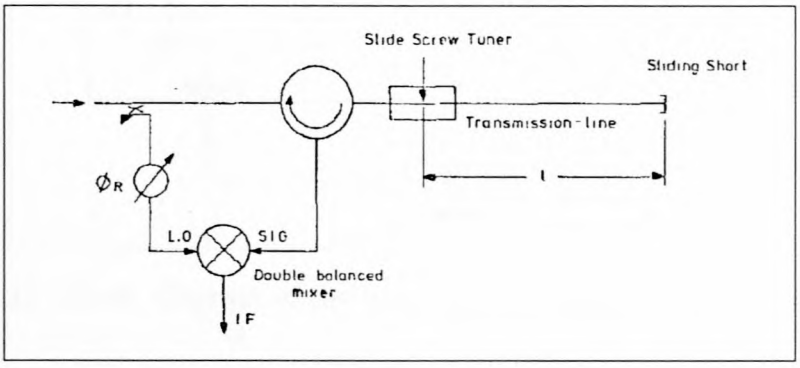

Figure 2.34: Transmission line resonator-discriminator. [50]

The simplified circuit shown in Figure 2.34 is a transmission line resonator-discriminator. When the slide screw tuner is removed or substituted by an attenuator [19], it is called a delay line discriminator. Instead of phase interference, these discriminators mix the two signals (the reference signal at LO and the tuned frequency signal from the circulator at SIG).

These circuits operate fairly similar. An analysis of both circuits are done in both [19] and [50]. An analysis was also done in [20] with a magic tee and two shorted lines. Various lower frequency (from HF) discriminators were also proposed which use hybrids and two shorted transmission lines instead of the circulator and the single line [18][51].

2.10 The divider/delay line type

There are several ways in which dividers and delay lines are configured to form discriminators. Most of these techniques are developed for implementation in instantaneous frequency-measuring receivers (IFR), and use multiple discriminators to increase the resolution of their measurement.

A single chip MMIC discriminator covers the frequency range from 2 to 4 GHz [52]. It consist of five identical discriminators connected with different delay lines. A block diagram of the monolithically realized frequency discriminator is shown in Figure 2.35. It consist of three Wilkinson dividers, a two-stage amplifier and two balanced mixers. The dividers are realized with lumped elements, since distributed structures will be too large for realization on GaAs in this frequency range – a two-stage tandem structure was used for better performance.

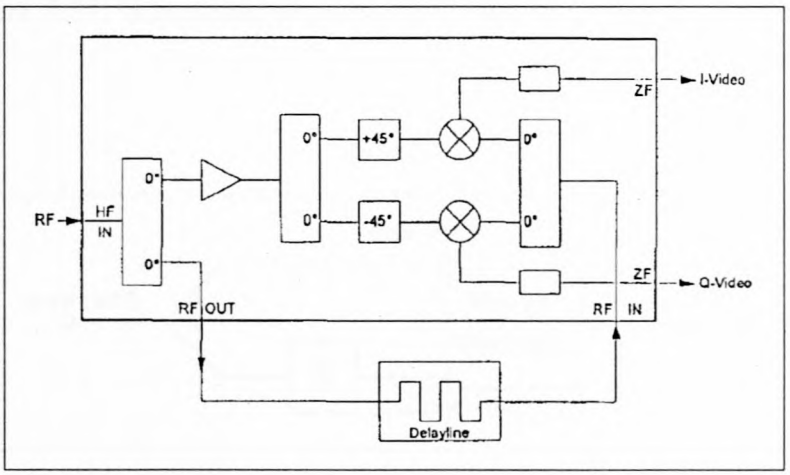

Figure 2.35: Block diagram of the monolithic frequency discriminator. [52]

Another discriminator has two dividers, a delay line and three hybrids [24]. A schematic of this circuit is shown in Figure 2.36. It is implemented in a system which uses two discriminators with 45° and 90° delay lines respectively. It is also realized in an MMIC, and is used as a channel detector which operate from 2 to 6 GHz with 250 MHz resolution.

A coplanar waveguide unit [25] has eight discriminators with different delay line lengths from two different splitting structures to increase its resolution. It is capable of measuring from 6 to 18 GHz with 12 bits resolution. A single discriminator and the topology of its phase bridge, is shown in Figure 2.37.

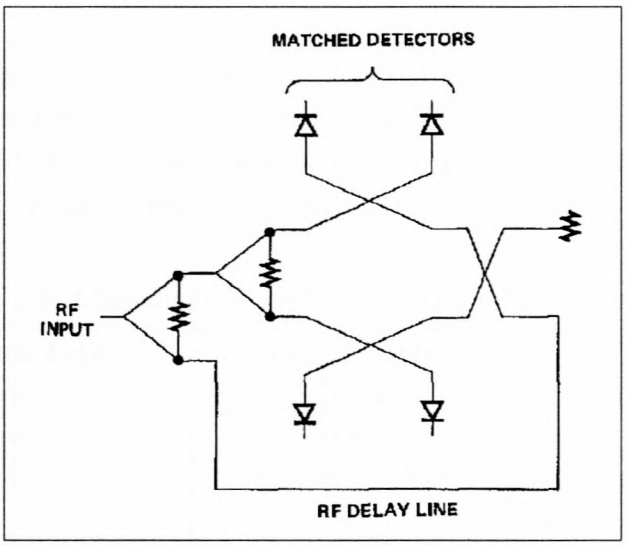

Figure 2.36: Schematic of a divider/delay line discriminator. [24]

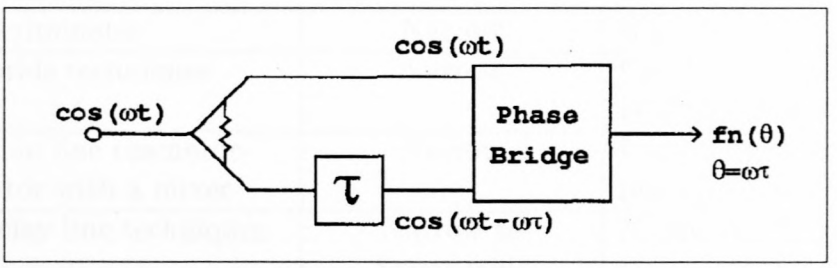

(a) Delay line discriminator.

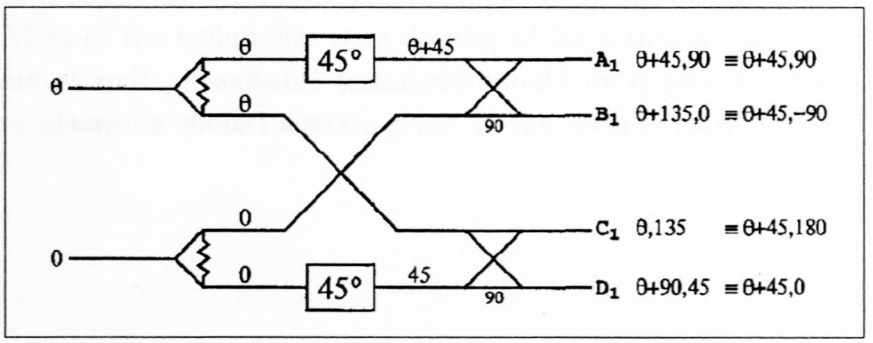

(b) Phase bridge topology.

Figure 2.37: Simple delay line discriminator. [25]

2.11 Comparison and Conclusion

The techniques discussed in this chapter are listed in Table 2.1. The bandwidth are roughly classified as follows: narrow is less than 5%, medium is between 5 and 20%, wide is between 20 and 40%, and super wide means it has greater than 40% bandwidth. General comments on either its performance or other characteristics are also given.

Table 2.1: Classification of the discriminator techniques.

Discriminator type	**Bandwidth**	**Comments**
Slope discriminator	Narrow	Not highly linear
Phase discriminator	Narrow	Possible multiple bands
Mohr discriminator	Medium to Wide	Easy to design Can be made highly linear
Stub-type discriminators	Narrow to Medium	Not highly linear Not very efficient
Super wide-band (bridge-type)	Super wide	Enormous bandwidth
Delay line type with circulators	Narrow	Structural complexities
Modal resonators	Narrow	High Q
Pound discriminator	Narrow	High Q
Single hybrids techniques	Narrow	Can be implemented at mm-waves
Transmission line resonator- discriminator with a mixer	Narrow	Used for FM noise measurements
Divider/delay line techniques	Narrow to Super wide	MMIC implementation Easily cascaded

There do exist many techniques of implementing a frequency discriminator at microwave frequencies. Most of the techniques were developed for a specific application, but can be used for others as well. A suitable technique should be chosen to fit the given specifications, where attention should also be given to the level of complexity which will suite your budget.

Chapter 3

The Mohr Discriminator

The discriminator proposed by R.J. Mohr [27] is suitable for medium to wide bandwidths. The theory and practical working of this technique are discussed in Section 2.3.

In this chapter a brief overview of previous implementations of the Mohr technique will be given. The hybrids which are used in the discriminator, form an integral part of its design. Their development will receive some attention. Discriminators were developed at both S- and X-band for an application in the direct demodulation of wide-band FM signals. A detailed discussion on the design and development of these discriminators will include some good measurements.

3.1 Previous implementations

Three articles described different techniques for implementing the hybrids used in the Mohr discriminator: using coupled lines [28]; waveguides with a magic tee as hybrid [29]; a hybrid/wiggly coupler with improved linearity [32]. An interesting application in a DCPSK detector/AFC discriminator [31] will also be discussed.

3.1.1 Coupled line hybrids [28]

Each 3 db hybrid consist of three sections, with broadside coupling for the central section (k=0.83) and coplanar coupling for the outer sections (k=0.15). Three sections were used in preference to a single section to reduce the coupling variation over an octave frequency band.

The construction of this implementation is shown in Figure 3.1. The striplines are printed on individual boards which are placed facing each other. At the broadside coupled sections, the lines are separated by thin teflon strips (S1 and S2). The line denoted l is $3\lambda/4$ longer.

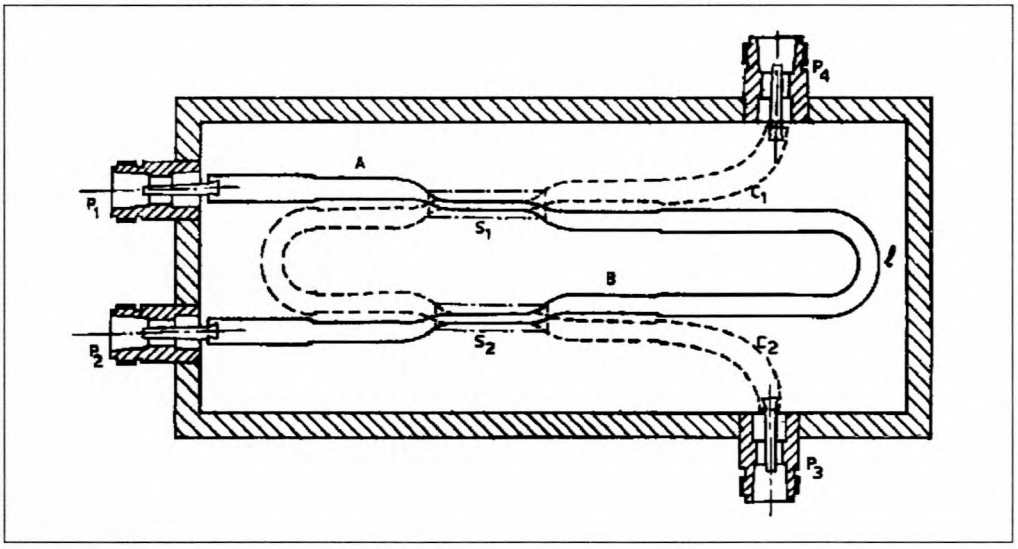

Figure 3.1: Schematic layout of the discriminator (dotted stripline printed on separate board). [28]

3.1.2 Waveguide using Magic Tees [29]

Two magic tees are used as the hybrids, and an additional line length are obtained by using waveguide flange spacers. Flanges of varying length (thickness) could be conveniently used to vary the mid-frequency of the required bandwidth. A schematic layout for this implementation (for $l = 3\lambda_{g0}/4$) is shown in Figure 3.2. The H-arm of the lower magic tee forms the input, and the E- and H-arms of the upper tee form the two outputs. For the case of $l = 9\lambda_{g0}/4$ the input arm was taken as one of the two side arms of the magic tee. With this configuration a VSWR of better than 1.1 was obtained; however, the geometry becomes quite complicated and it requires a larger number of components. Matching of the input arm is achieved by using susceptance screws.

3.1.3 Hybrid/Wiggly coupler [32]

The design consist of a gain equalizer, two quadrature hybrids, a delay line section and two detectors. The quadrature hybrids have a 2.8 dB midband coupling and consist of two cascaded 8.08 dB wiggly couplers (described in [55]). The couplers have approximately 25 dB isolation and a VSWR less than 1.2 over the band from 7 to 11 GHz.

The detectors are the most complex elements. Their design provide a flat response, low VSWR and a controlled impedance for the higher harmonics generated in the detector diodes. The harmonics are reactively terminated by the matching networks, which are

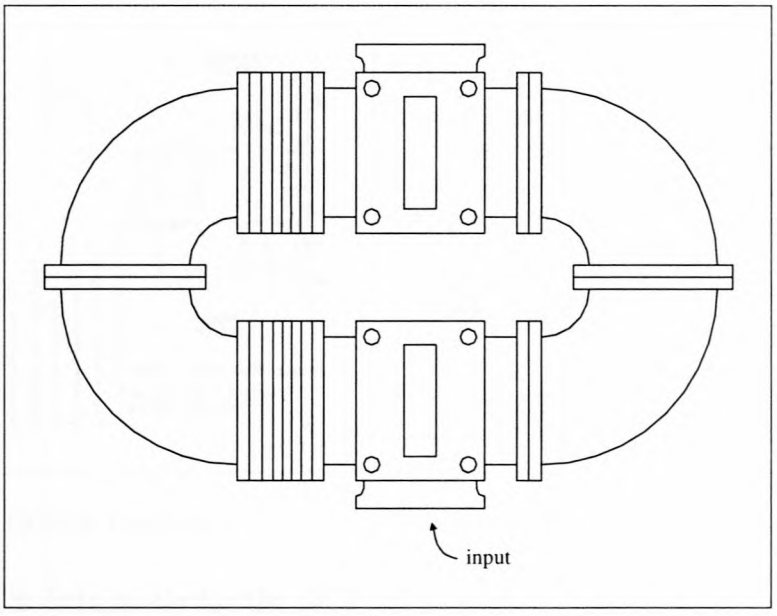

Figure 3.2: Layout of the waveguide implementation for the Mohr discriminator.

designed as low-pass filters – the stop-band requirements are eased by the use of an anti-parallel diode pair. The total system provide a linearity better than ±0.85%.

3.1.4 An L-band DCPSK detector/AFC discriminator [31]

An interesting application in a differentially coherent phase-shift keying (DCPSK) detector slash automatic frequency control (AFC) discriminator is given in [31]. The circuit operates at the 1.404 GHz IF of a millimeter-wave system, and have a baud rate of 280.8 Megabits/s.

The DCPSK detector is similar to the Mohr discriminator, but has an even function (with $l = 5\lambda$). It is used to delay half of the signal in the delay line, and compare the present signal's phase with the previous bit. The schematic of this part of the circuit is shown in Figure 3.3 (a).

The AFC discriminator was accomplished by 'tapping' the delay line at a point corresponding to 5/4 wavelengths with two 4.8 dB couplers as shown in Figure 3.3 (b). Recombining these 'tapped' signals in a 3 dB coupler provides the discriminator characteristic required. The voltage unbalance between points A and B is differentially amplified and used as the AFC error signal.

The five directional couplers in the circuit are four-line interdigitated quarter wavelength couplers with wire crossovers (described in [56]).

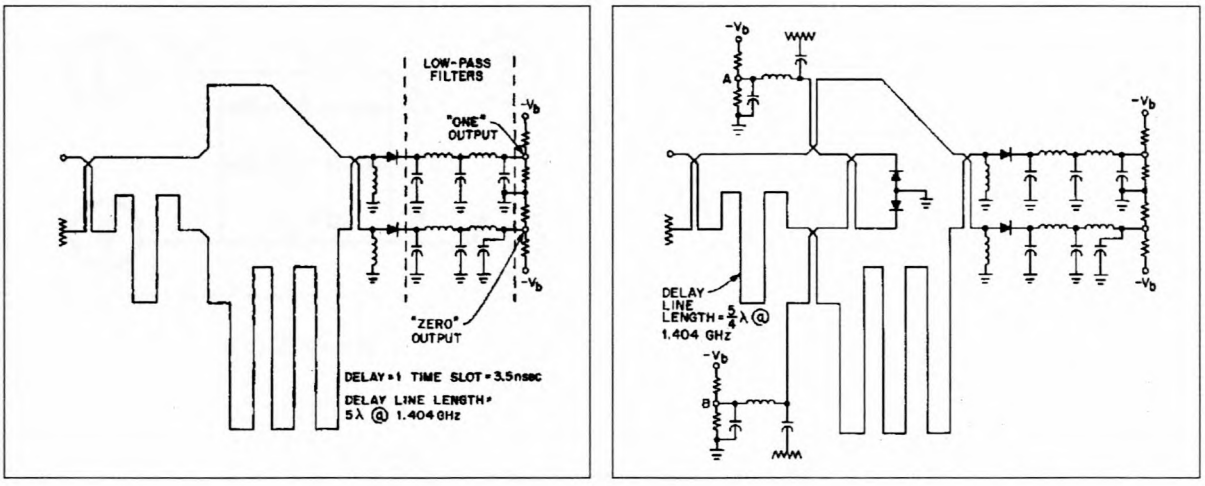

(a) DCPSK Detector (b) DCPSK Detector/AFC Discriminator

Figure 3.3: Schematic for the DCPSK Detector/AFC Discriminator. [31]

3.2 Hybrid considerations

As seen in the previous section, many different techniques are used to implement the hybrids used in the discriminator. They mostly use coupled lines and variations thereof in their hybrids. It was decided to experiment with the implementation of the branchline hybrid coupler. It offers the advantage of combining co-directional coupling characteristics with structural simplicity, thus avoiding narrow line gaps, the need for bond-wires or other complexities, as is necessary for the previously mentioned couplers.

3.2.1 Branchline hybrid

The working and basic expansion of the branchline hybrid is analyzed in [57]. A schematic of the two-arm and three-arm branchline hybrids are shown in Figure 3.4. The two-arm hybrid has normalized admittances of $a = 1$ and $b = \sqrt{2}$ for a 3 dB directional coupler (impedances of $Z_a = 50\,\Omega$ and $Z_b = 35.35\,\Omega$ in a $50\,\Omega$ system).

For improved bandwidth more cross arms can be added to the hybrid of Figure 3.4 (b) (ideal values for up to 6 arms are tabulated in the article). A broader band three-arm hybrid is shown in Figure 3.4 (c). For a 3 dB coupler the normalized admittances are $a = \sqrt{2} - 1$ and $b = c = \sqrt{2}$ (impedances of $Z_a = 120.7\,\Omega$ and $Z_b = Z_c = 35.35\,\Omega$ in a $50\,\Omega$ system).

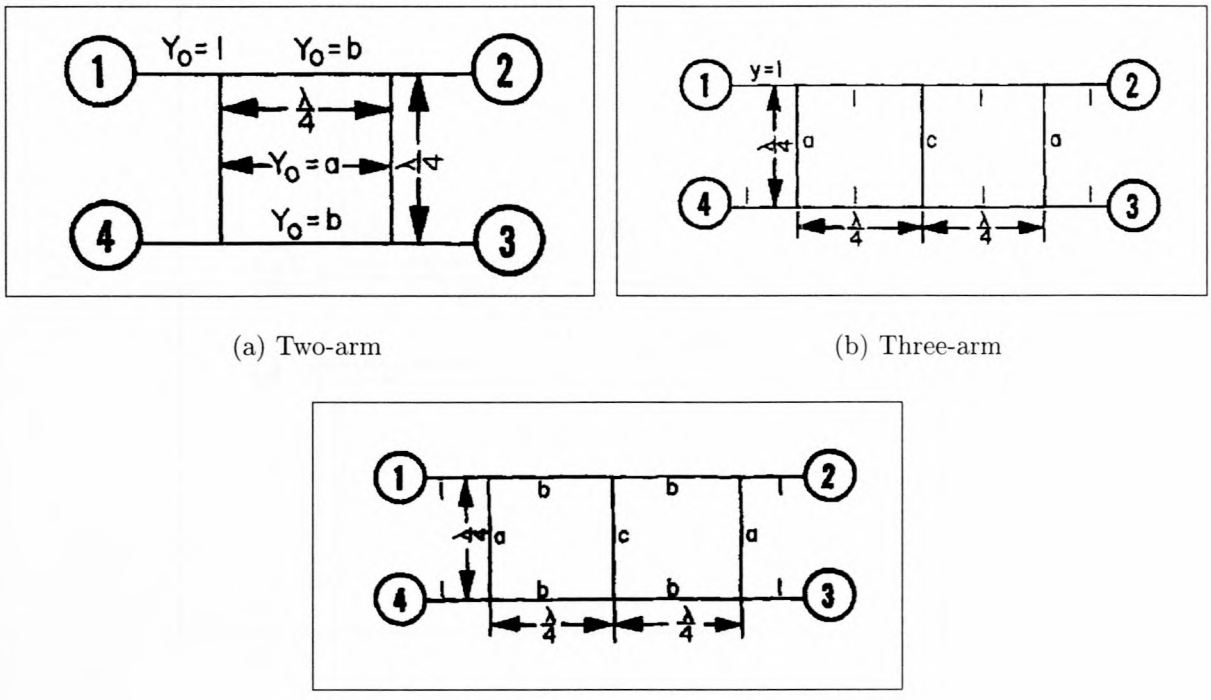

(a) Two-arm

(b) Three-arm

(c) Broader band three-arm

Figure 3.4: Schematics of branchline hybrids with two and three cross arms. [57]

3.2.2 Improved branchline hybrid

Two disadvantages exist for the above mentioned (normal) branchline hybrids: they have

- inconvenient line impedances and
- narrow operating bandwidths.

Branchline couplers with improved design flexibility and a broader bandwidth are described in [58]. Two of their techniques were used in later designs, and are shown in Figure 3.5.

Both extend the two-arm hybrid with two half-wavelength transmission lines. In the first design one of the lines are added as an open-circuited stub at the hybrid's ports. The characteristic impedances for this circuit are $Z_1 = 39.5\,\Omega$, $Z_2 = 55.9\,\Omega$, $Z_3 = 92.7\,\Omega$ and $Z_4 = 67\,\Omega$. The two lines are connected in series for the second design. The characteristic impedances for the second circuit are $Z_1 = 38.62\,\Omega$, $Z_2 = 54.57\,\Omega$, $Z_3 = 85.5\,\Omega$ and $Z_4 = 34.43\,\Omega$.

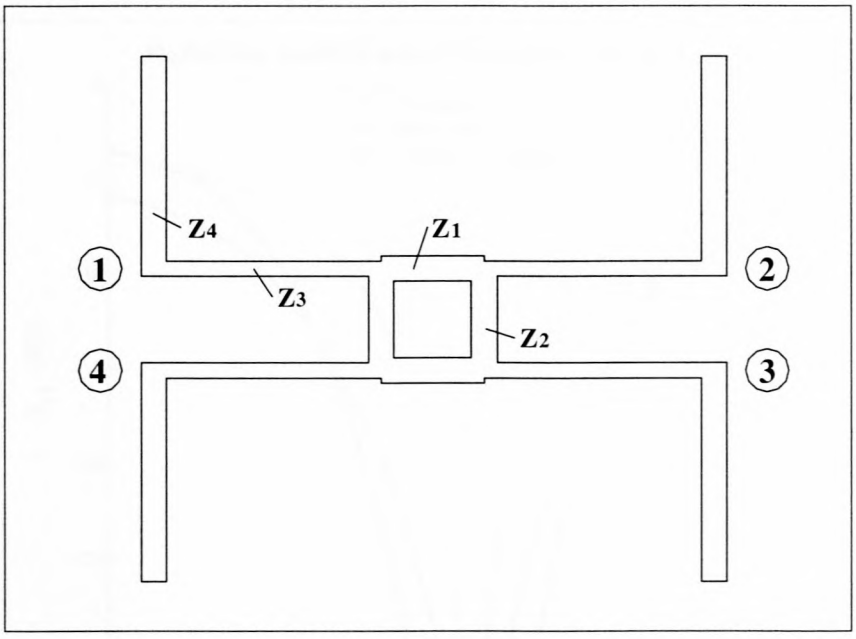

(a)

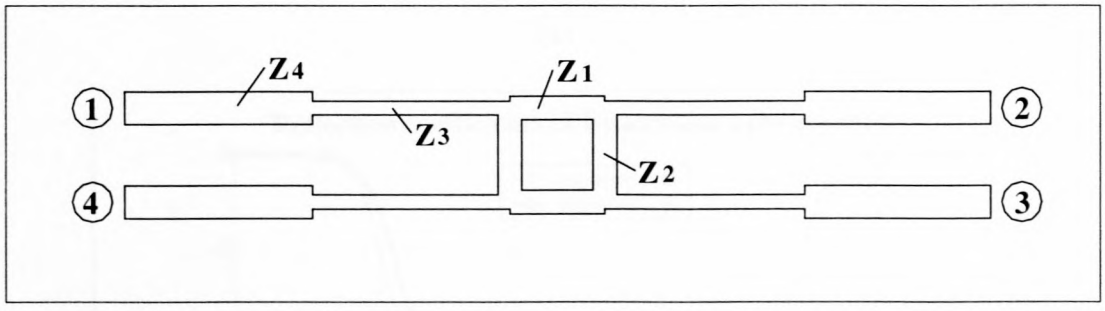

(b)

Figure 3.5: Layout of two improved branchline hybrid couplers.

3.2.3 Analysis

An analysis of the five hybrids given above are shown in Figures 3.6 to 3.8 [1]. It is clear from the graphs that the improved hybrids have a broader bandwidth with a good reflection coefficient and isolation of the ports. The transmission coefficients (co-directional coupling) have an exceptional improvement. It has an almost even power split and good phase difference over the whole band for which it is matched.

The improved hybrids have the further advantage that it has design flexibility – i.e. it can be optimized. More manageable line impedances was achieved with the optimization of

[1] These simulations was done with ideal transmission lines, at a center frequency of 2 GHz.

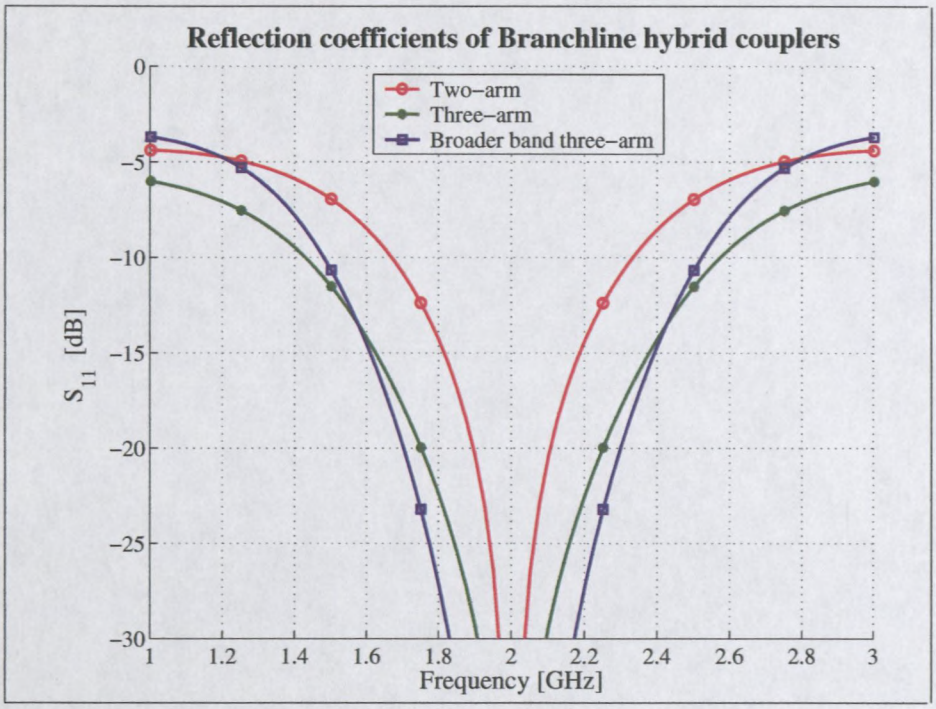

(a)

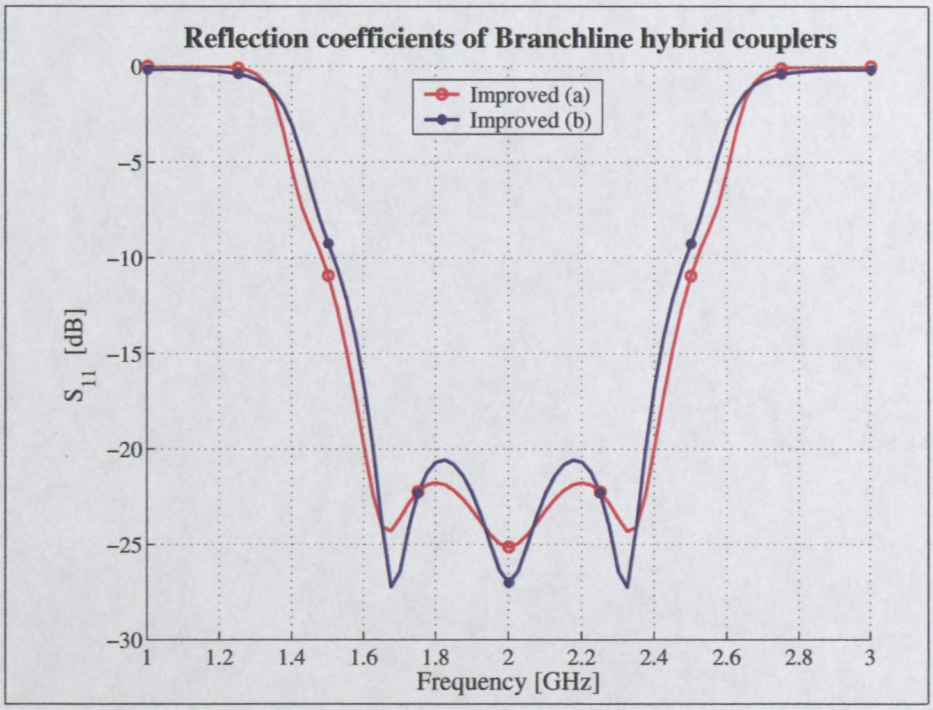

(b)

Figure 3.6: The reflection coefficients of the five types of branchline hybrid couplers.

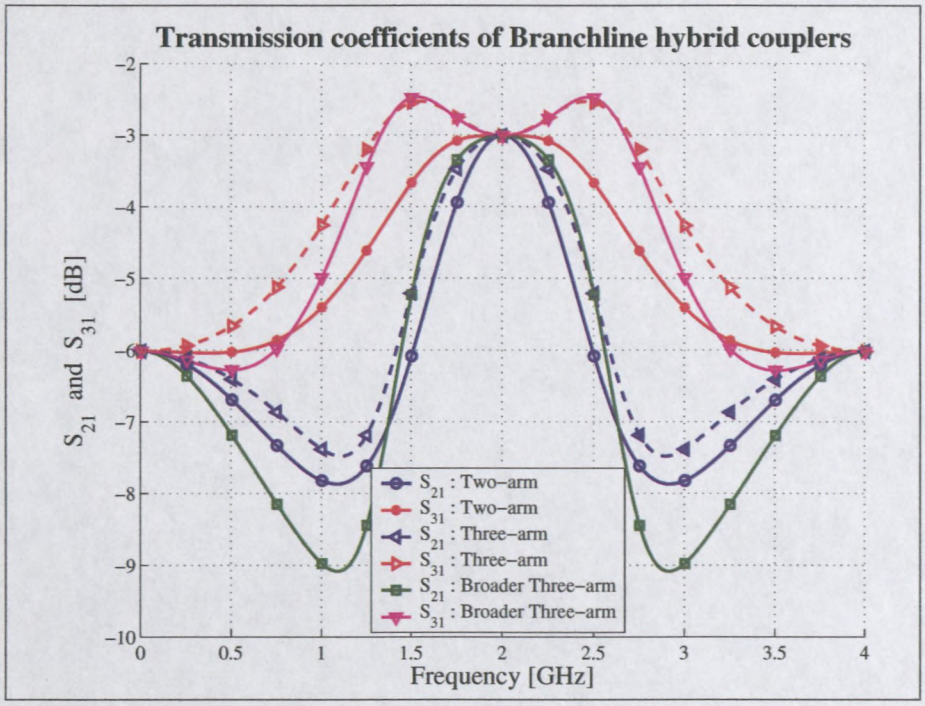

(a)

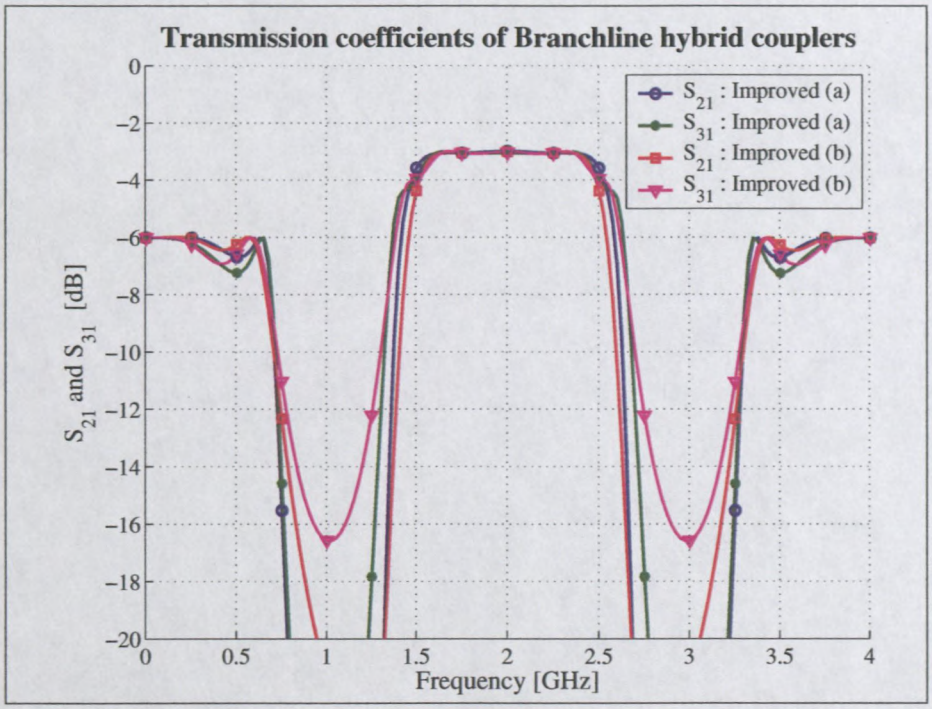

(b)

Figure 3.7: The transmission coefficients of the five types of branchline hybrid couplers.

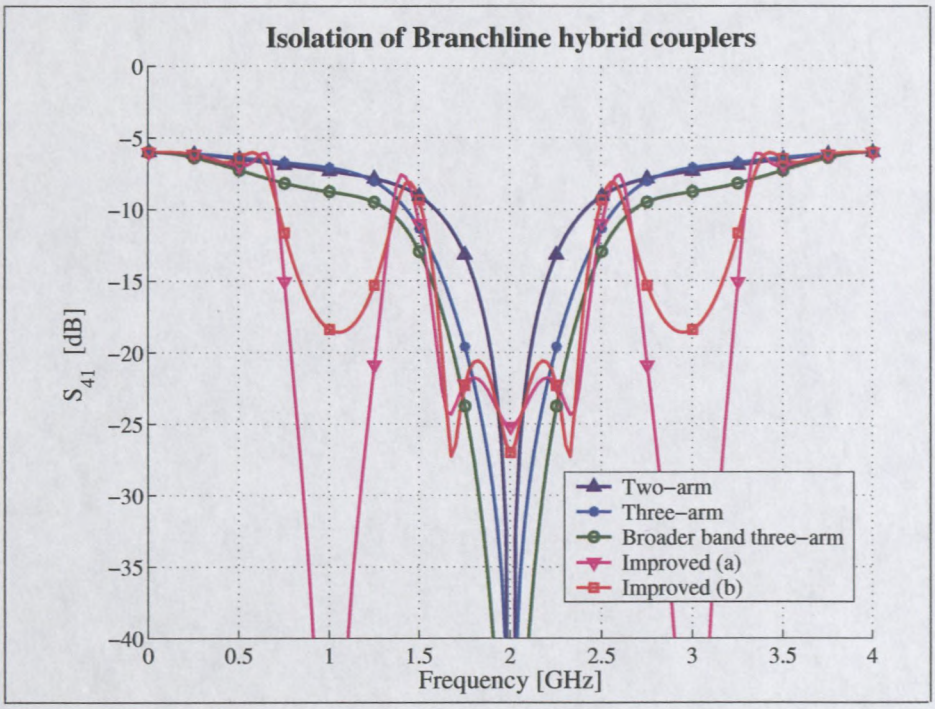

(a)

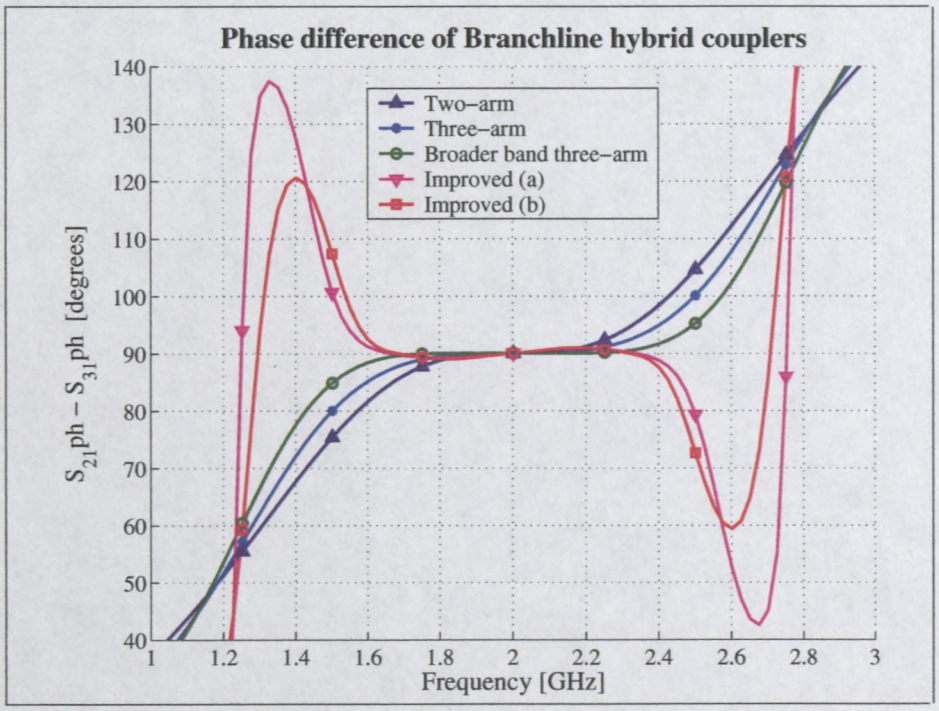

(b)

Figure 3.8: The isolation and co-directional phase difference of the five types of branchline hybrid couplers.

the discriminator systems. These improvements resulted in an unequal power split, but had a broader bandwidth with a 90° phase difference. These results are shown with the development of the discriminators (Sections 3.4 and 3.5 – Figures 3.18 (a) and 3.19).

3.2.4 Comments

Through experimentation it was found that the following hybrid properties are needed for improved operation of the Mohr discriminator:

1. A good 90° phase split.
2. Not necessarily an equal 3 dB power split. For a high linearity of the complete S-curve, it is preferable though that the split is as equal as possible. (This will be explained in Section 3.5.4.)
3. Well matched ports.
4. A good isolation between the output ports are usually a result of the other properties.

3.3 S-band Mohr discriminator

3.3.1 Developments

The development process was started with a simple example, consisting of two two-arm branchline hybrid couplers, and two transmission lines named A and B. The length of path A was chosen as $\lambda_0/4$ ($EA = 90°$), and path B had an extra $n\lambda_0/4, \quad n = 1, 3, 5, \ldots$ ($EB = 90° + n90°$). Tests were done in Libra [63] to investigate the discriminator.

The circuit was then analyzed on a microstrip substrate. Different substrates was investigated for more manageable line widths. T-junctions and bends was added for the realization of the circuit.

3.3.1.1 Right-angle Bend in Microstrip

An optimally compensated (chamfered) bend was used for the analysis. The relative compensation, in percent, is defined in Hoffmann [59] (with reference to Figure 3.9 (a)) as

$$S^* = 100\frac{s}{d} = \left(1 - \frac{b}{w\sqrt{2}}\right). \tag{3.1}$$

Optimal compensation for any $w/h \geq 0.25$, $1 \leq \epsilon_r \leq 25$ and $f \cdot h < 10\text{GHz} \cdot \text{mm}$ is empirically described by

$$S^*_{\text{opt}} = 52 + 65 \exp\left(-1.35\frac{w}{h}\right). \tag{3.2}$$

The model used in Libra, is the MBEND3 – *Optimum 90-Degree Bend in Microstrip*, as shown in Figure 3.9 (b). The value of L is calculated as follows:

$$\frac{L}{W} = \sqrt{2}\left[1.04 + 1.3 \exp\left(-1.35\frac{W}{H}\right)\right] \tag{3.3}$$

where W (the line width) is part of the bend's definition and
H (the substrate height) is part of the substrate's definition.

With the use of the geometry and Equation 3.1, it can be shown that the chamfering given by Equations 3.2 and 3.3 are equal.

The equivalent length of the bend ($2\Delta l$) can be determined from

$$\frac{2\Delta l}{h} = 0.5\left(\frac{w}{h}\right)^{1.08} - \left(\frac{0.45}{\sqrt{\epsilon_r}}\right) - 0.12. \tag{3.4}$$

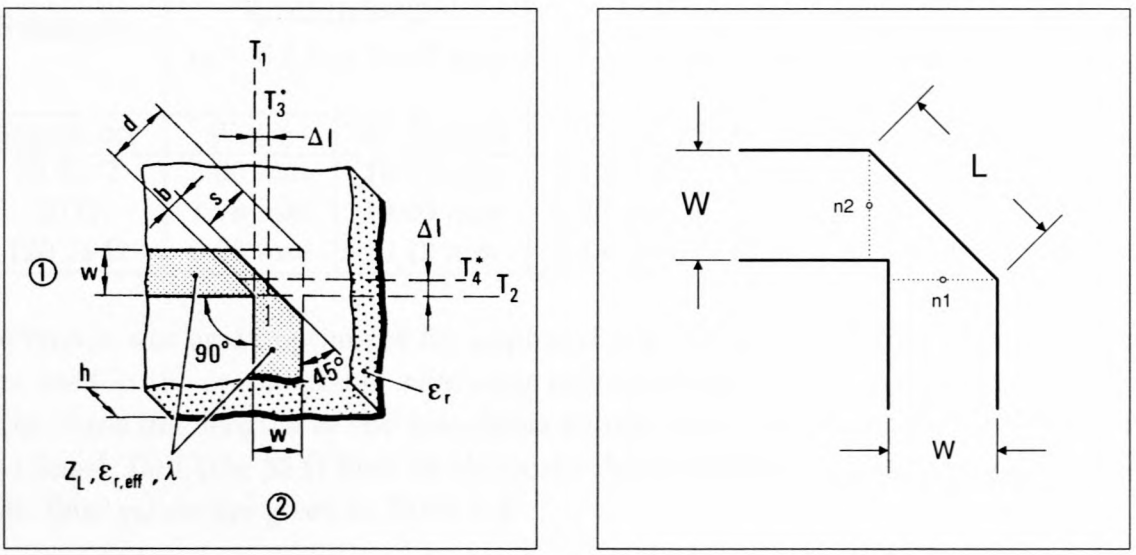

(a) Chamfered bend in microstrip. [59]

(b) Model used in Libra.

Figure 3.9: 90 degree bend in microstrip: (a) Definitions for theoretical analysis (b) Definition for model used in Libra.

3.3.1.2 Broader band hybrid

For improved bandwidth, the broader band three-arm branchline hybrid was employed (see Section 3.2.1). A design was done in microstrip on a GML1000 substrate with height

$h = 0.762\ mm$ and dielectric constant $\epsilon_r = 3.2$. The path difference was chosen with $n = 5$ ($EA = 6 \times EB$). The lengths of the lines in the hybrids and that of paths A and B, were optimized for maximum bandwidth of the discriminator. The circuit file is given in Appendix A.1 in conjunction with the final design. The parameters and simulation results are compared with the final design in Tables 3.1 and 3.2, and Figures 3.11 and 3.12.

3.3.2 Final design

To further simplify the construction[2], the discriminator was redesigned for a stripline substrate with dielectric constant $\epsilon_r = 3.05$ and earth plane spacing $b = 3.048\ mm$. The line impedances and widths are listed in Table 3.1 (for both microstrip and stripline designs). The circuit file with both the microstrip and stripline circuits, is given in Appendix A.1.

Table 3.1: Line dimensions for the S-band Mohr discriminator design.

Substrate:	**Microstrip** GML1000 030 $\epsilon_r = 3.2$ $h = 0.762\ mm$		**Stripline** GML1000 060 $\epsilon_r = 3.05$ $h = 1.524\ mm$ $b = 3.048\ mm$		
Impedance	Width	90° Length	Width	90° Length	Rounded Width
35.35 Ω	3.00 mm	18.70 mm	3.19 mm	17.51 mm	3.20 mm
50 Ω	1.79 mm	19.09 mm	1.86 mm	17.51 mm	1.85 mm
120.71 Ω	0.25 mm	20.12 mm	0.18 mm	17.51 mm	0.30 $mm \rightarrow 106\ \Omega$

The circuit was again optimized for improved matching and isolation. The only parameters used in the optimization, were some element lengths in the paths A and B, as well as the three line lengths in the branchline hybrid: L9M (the two 120 Ω and the middle 35 Ω lines), L9V (the 35 Ω lines on the port-side) and L9B (the 35 Ω lines on the inside). Their final values are given in Table 3.2.

Libra only have limited models for stripline elements, and only have an unchamfered bend (with a changeable angle) in stripline. A theoretical model for a bend in stripline was not found in the available sources. The equivalent length of the bend in stripline was then gauged according to the bend's properties in a microstrip substrate with half the height. A similar bend to the one used in the previous microstrip design was used here, and

[2]The construction of a box for the microstrip structure is more complex than cutting two metal plates and putting screws through them. Putting a microstrip structure in a box will further cause electromagnetic coupling with it, which will change the characteristics of the structure.

Table 3.2: Optimized line lengths for the S-band Mohr discriminator.

Element	Microstrip Length	Stripline Length
Path A		
LA (sides)	6.20 *mm*	6.00 *mm*
LM (mid)	6.50 *mm*	5.50 *mm*
Path B		
LBA	5.90 *mm*	5.05 *mm*
LBB	18.95 *mm*	17.85 *mm*
LBC	6.00 *mm*	5.00 *mm*
LBD	48.60 *mm*	45.50 *mm*
Hybrids		
L9M (mid)	18.15 *mm*	18.30 *mm*
L9V (port side)	19.50 *mm*	17.20 *mm*
L9B (inside)	19.85 *mm*	16.95 *mm*

an equivalent length of 0.98 *mm* was determined from Equation 3.4. A normal stripline line-element with a length of 1 *mm* was used to model the bend.

The layout for this circuit was done in AutoCad. The dimensions of the lines were rounded to the nearest 0.05 *mm* for reduced tolerance. The layout for the stripline circuit is shown in Figure 3.10. The simulations of both microstrip and stripline circuits are shown in Figures 3.11 and 3.12. The measurements will be shown in Section 3.3.4.

3.3.3 Improved analysis

With the acquisition of Microwave Office 2000 [61], the circuit could be analyzed with more accuracy[3]. Our stripline bend was not an available stripline element, and had to be analyzed with the built-in electromagnetic (EM) simulator (EMSight – uses a full-wave, three-dimensional solution based on the spectral-domain method of moments).

The model for stripline T-junctions assumes that W1 is equal to W2 (the widths of the two opposite facing ports). If this assumption is not true, then the model assumes W1 = W2 = (W1 × W2)/2. It is further recommended that $0.2 \leq \frac{\sqrt{Z_1 Z_2}}{Z_3} \leq 2$ for proper working of the model. The outer junctions (on the port-side) has a value of 0.35, but those on the inside have a value of 2.2. The inner T-junctions were then also substituted with EM-structures.

[3]This analysis was done after construction of the device.

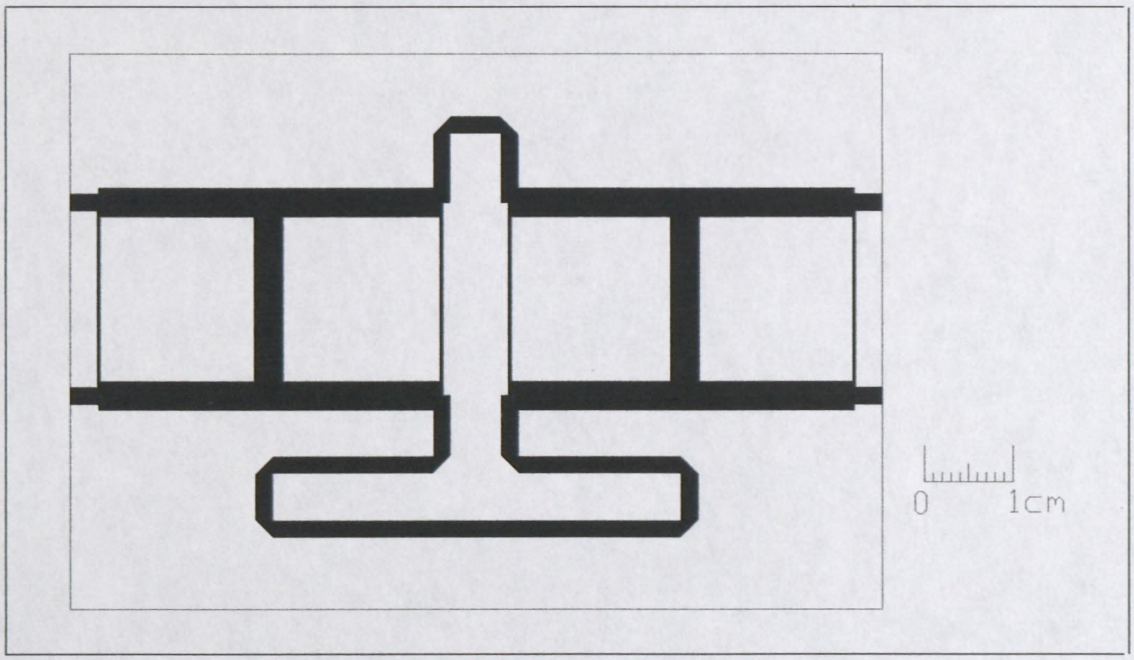

Figure 3.10: Layout of the stripline S-band Mohr Discriminator.

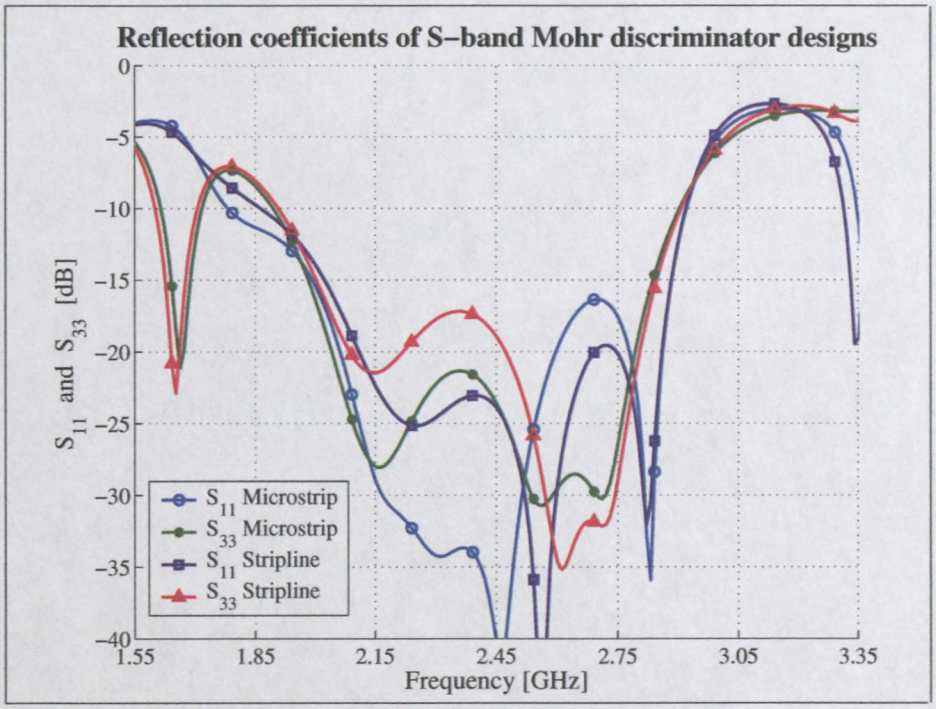

Figure 3.11: Reflection coefficients for the microstrip and stripline S-band Mohr Discriminator designs.

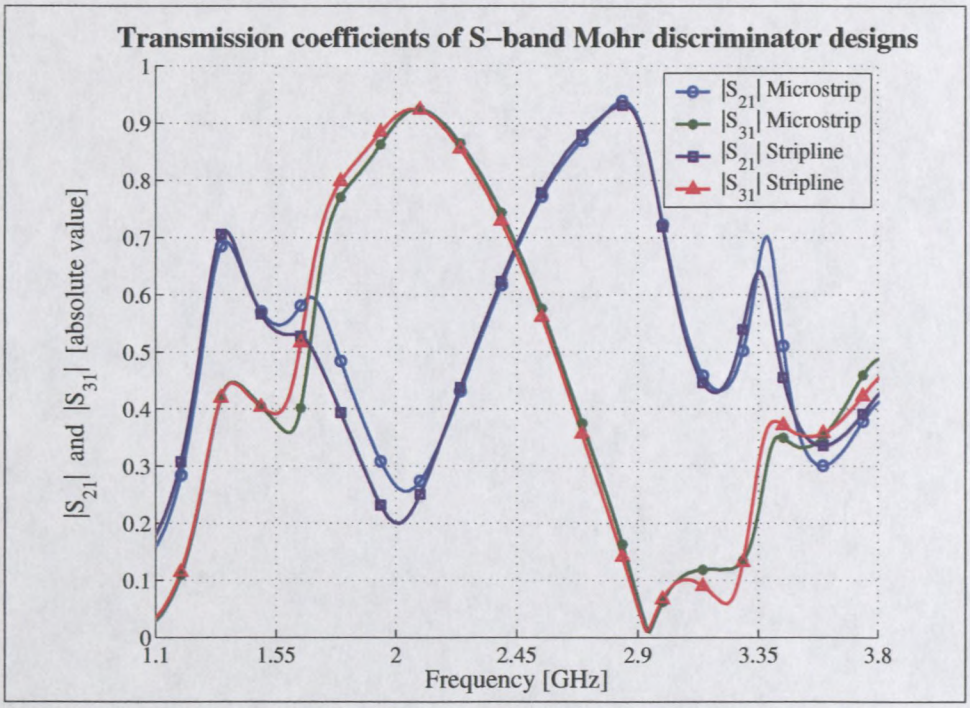

(a) Transmission Coefficients

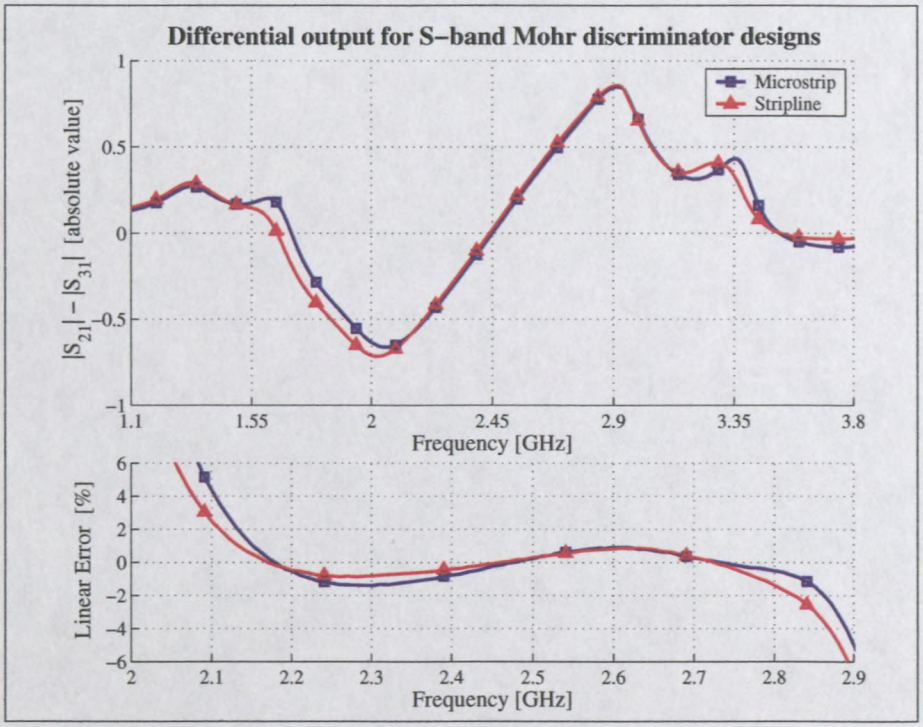

(b) Differential Output

Figure 3.12: Simulation of microstrip and stripline S-band Mohr Discriminator designs.

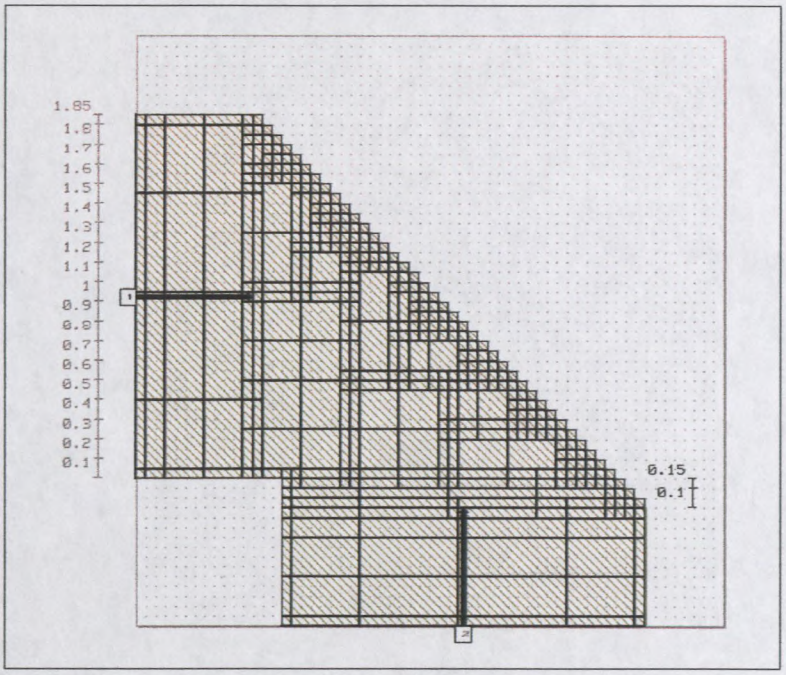

(a) Meshing of SBEND4

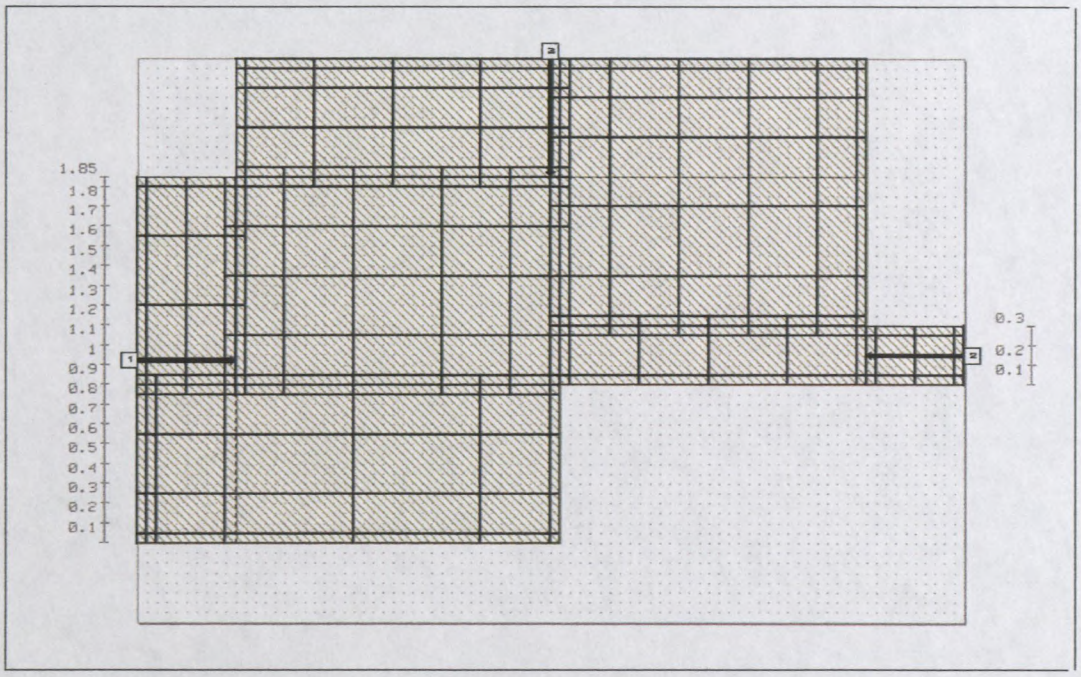

(b) Meshing of STEE4

Figure 3.13: The EM-structures for the bend and inner T-junction used for simulation in Microwave Office.

Both EM-structures are shown in Figure 3.13, where a normal meshing were used for both structures. The solutions are deembedded up to the edge of the 'structure under test' (the bend or the T-junction), as indicated by the arrows.

3.3.4 Measurement

The ports were numbered as in Figure 2.10, with ports 1 and 2 on the shorter transmission line's side. The total four-port device was measured with a Network Analyzer by consecutive full two-port measurements, with the other two ports terminated. The measurements for the different measured entities looked fairly similar. A photograph of the discriminator is shown in Figure C.2.

The improved analysis proved to be a more accurate match to the measured data. The initial Libra design, the improved Microwave Office analysis and the measured data are compared in Figures 3.14 and 3.15. The differential output between ports 2 and 3, and the linearized error thereof, are shown in Figure 3.16. The linear fit shown in Figure 3.16 (a) are of the measured data, and has its cross-over at 2.418 GHz. The linear error functions of Figure 3.16 (b), are from individual linear fits done between 2.1 GHz and 2.8 GHz (28.5% bandwidth). Both simulated sets of data are within $\pm$ 1% linear over most of the band. The measured data are within $\pm$ 1.5% linear. This discriminator was also tested with detectors, and the measurements will be shown in Section 4.5.1.

3.4 X-band Mohr discriminator

3.4.1 Development and Design

To reduce the differences in line dimensions, the improved branchline hybrids were employed (see Section 3.2.2 from page 52). Two discriminators were designed with transmission line differences of $n = 5$ and $n = 9$, and a center frequency of 10.5 GHz. They were named XMohr1 and XMohr2, and use the hybrids from Figure 3.5 (a) and a modified version from Figure 3.5 (b) respectively. A third design was done with the second hybrid (in stripline), and will be discussed as a design example in Section 3.5.

The realization of the discriminators were done on a microstrip substrate with dielectric constant $\epsilon_r = 2.3$ and thickness $h = 0.508\,mm$. The layout for these discriminators are shown in Figure 3.17. The simulations were done in Microwave Office, and are shown in Figure 3.18. Both differential outputs are highly linear over the 1 GHz bandwidth from 10 to 11 GHz. They were optimized to be linear over a 2 GHz band, but the edges never

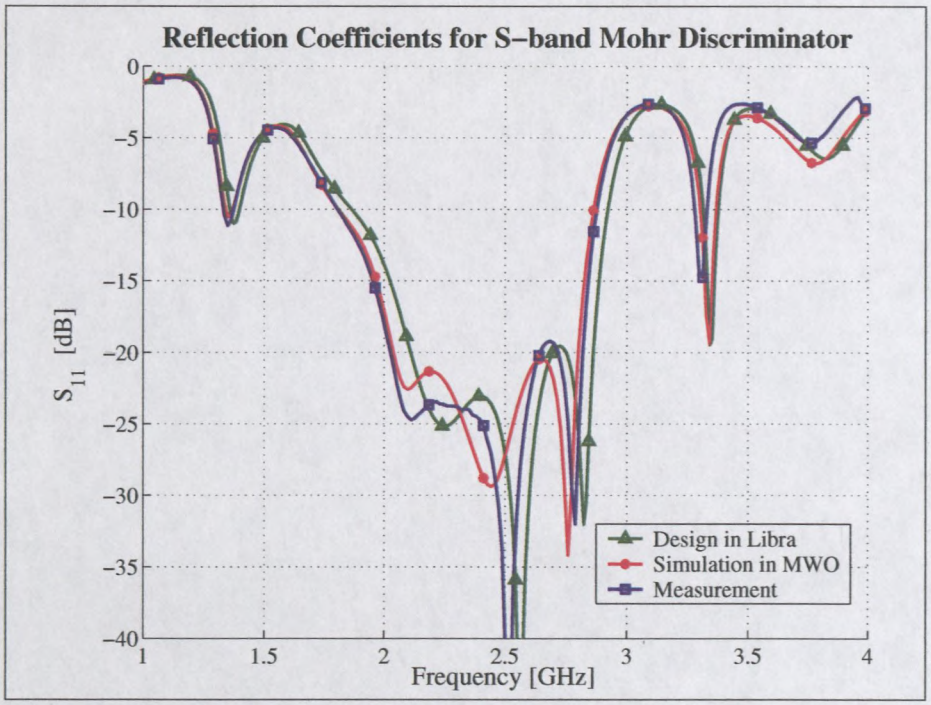

(a) Reflection Coefficients: S_{11} ($\sim S_{22}$)

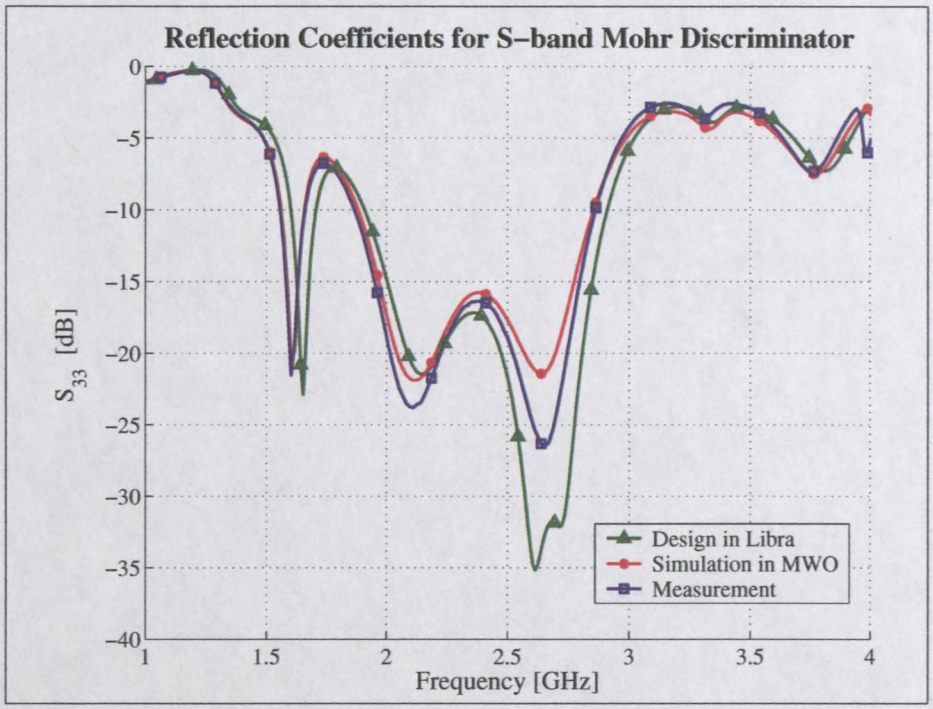

(b) Reflection Coefficients: S_{33} ($\sim S_{44}$)

Figure 3.14: Comparison of simulations and measurements for the S-band Mohr Discriminator. (Reflection Coefficients)

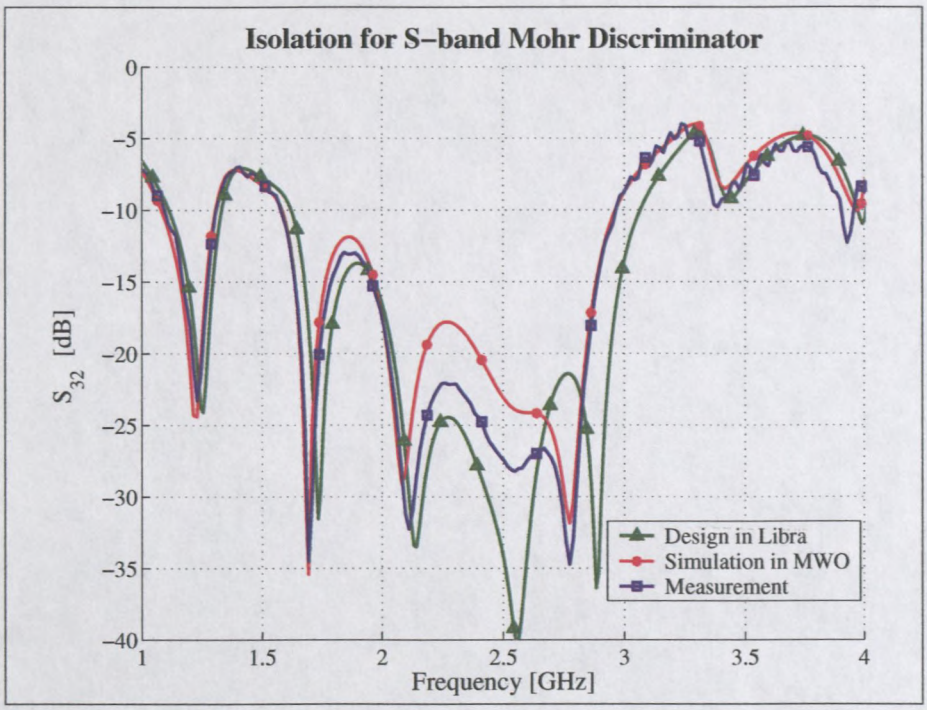

(a) Isolation: S_{32} ($\sim S_{41}$)

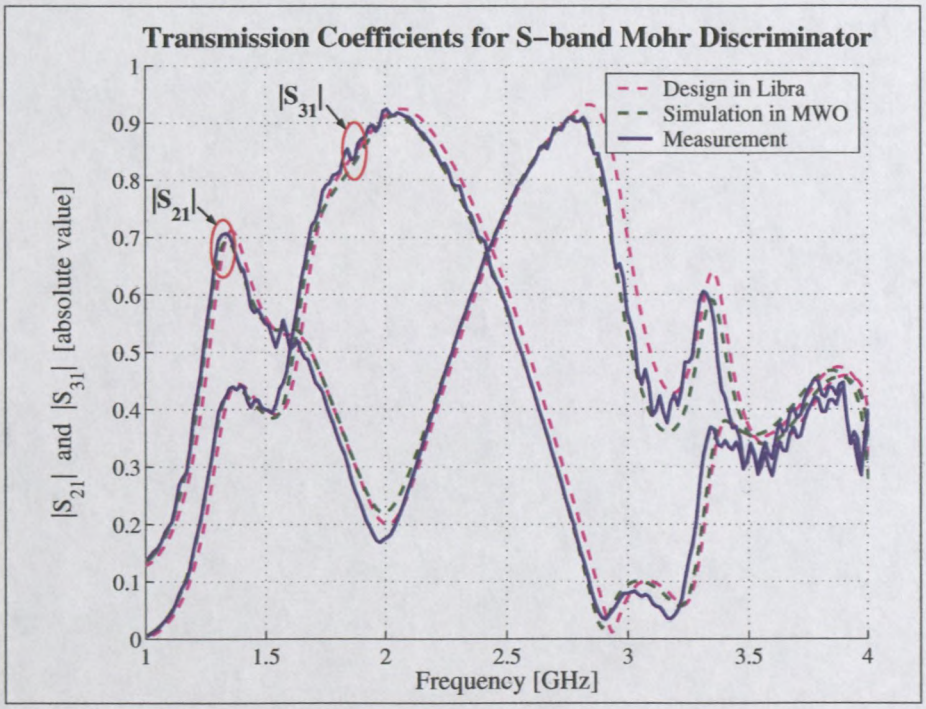

(b) Transmission Coefficients: S_{21} and S_{31}

Figure 3.15: Comparison of simulations and measurements for the S-band Mohr Discriminator. (Isolation and Transmission Coefficients)

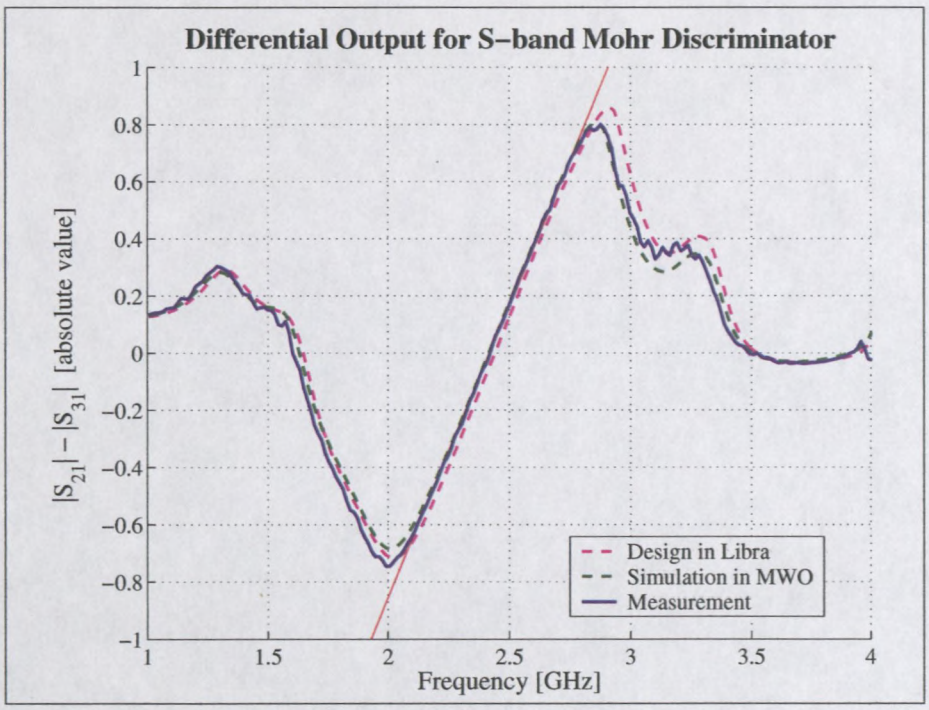

(a) Differential Output: $|S_{21}| - |S_{31}|$

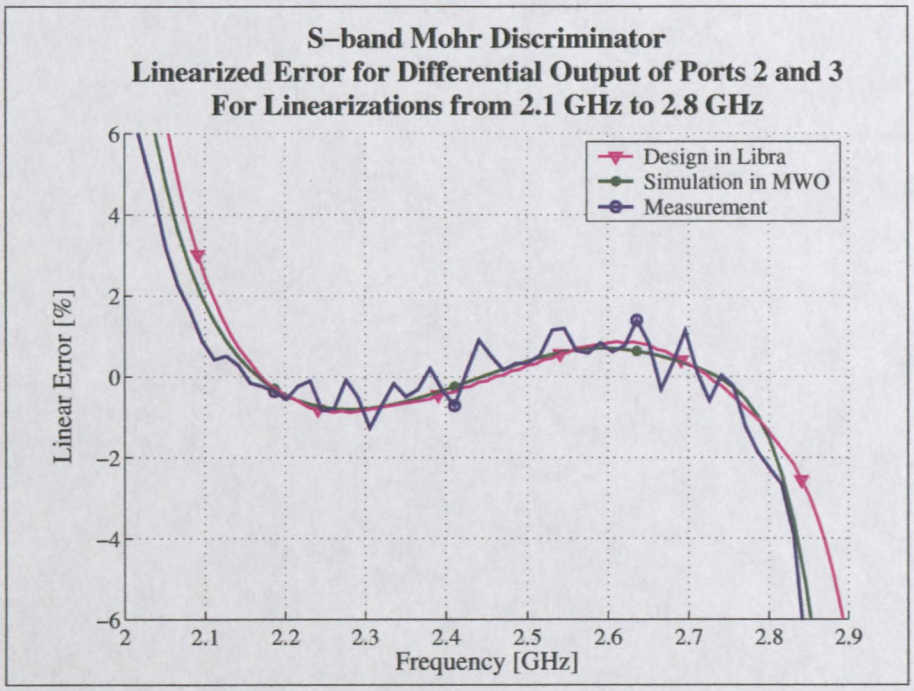

(b) Linearized Error for Differential Output

Figure 3.16: Comparison of simulations and measurements for the S-band Mohr Discriminator. (Differential Output)

seemed to curve back. The hybrids also seem to influence the transfer functions, since their bandwidth are just not wide enough for full operation.

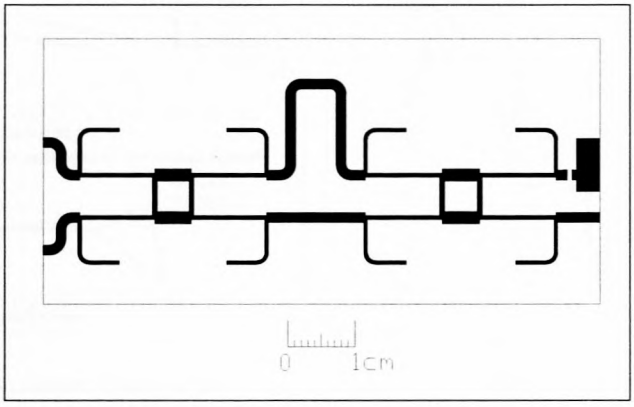

(a) XMohr1

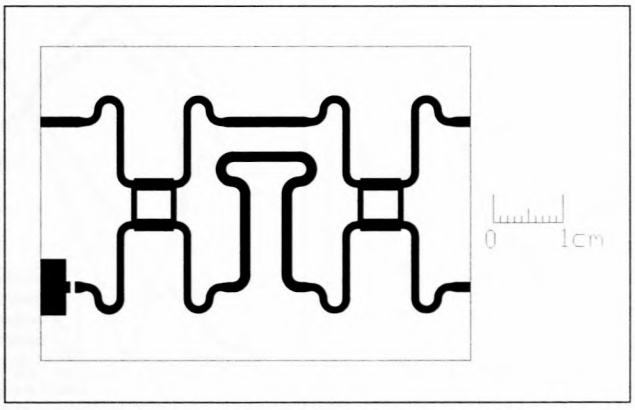

(b) XMohr2

Figure 3.17: Layout for two X-band Mohr Discriminators.

3.4.2 Comments on the measurements

The measurements were not nearly as expected, and are shown in Appendix B.2. With a slight imagination, the transmission coefficients look almost like the designed responses, but have much higher losses, and a seemingly rippled response. This is most probably due to the ports not being well matched, as concluded from the measured reflection coefficients. The isolation is not that bad.

An improvement of these devices were not attempted, neither were second iterations. The third X-band discriminator yielded more promising results, as will be seen in the following section.

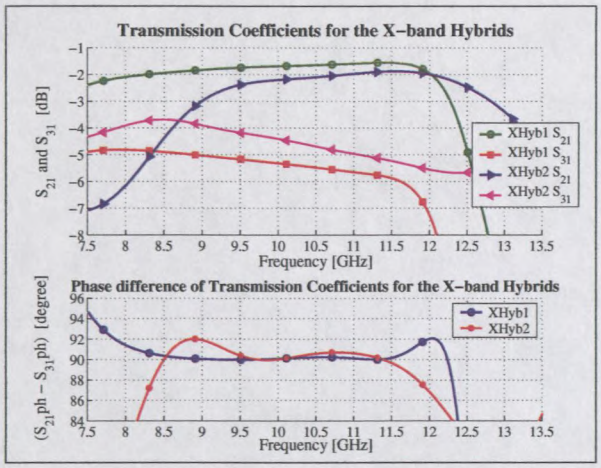

(a) Hybrid Transmission Coefficients

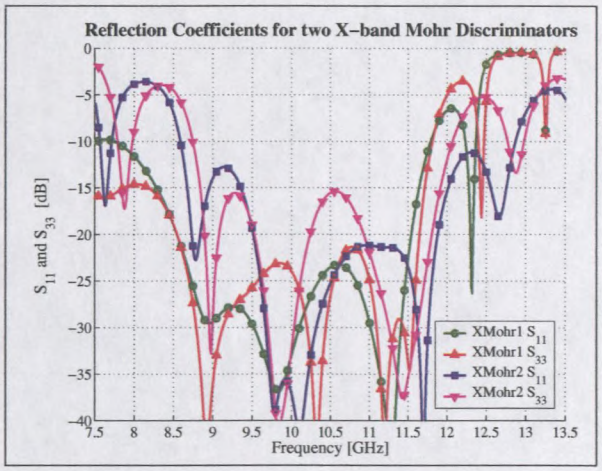

(b) Reflection Coefficients

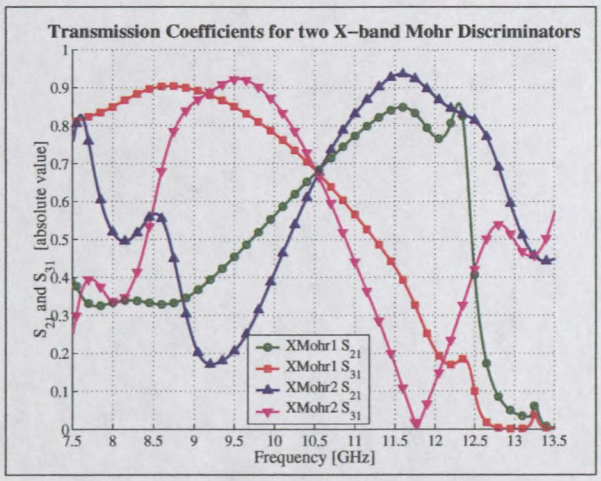

(c) Transmission Coefficients

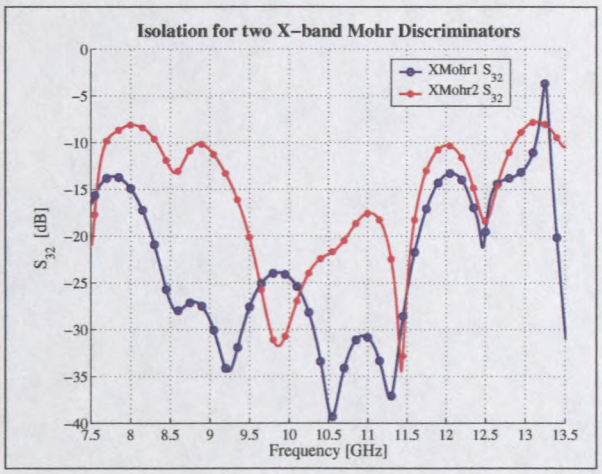

(d) Isolation

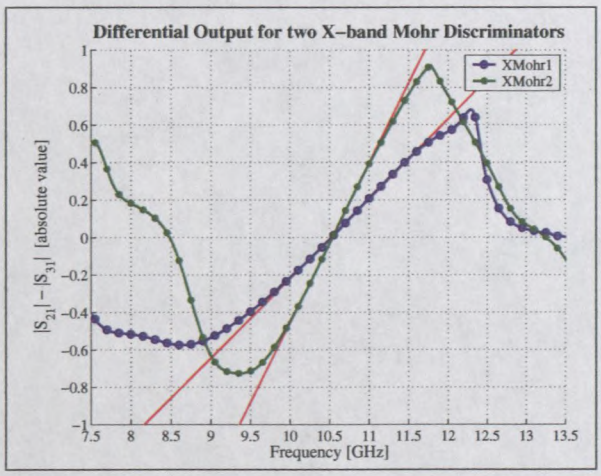

(e) Differential Output

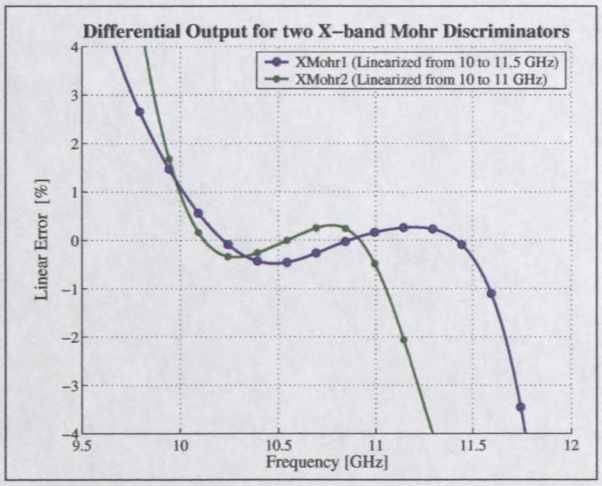

(f) Linear Error

Figure 3.18: Analysis of two X-band Mohr Discriminators.

3.5 An X-band design example

As a design example, an X-band Mohr discriminator will be discussed in detail. The process will kick off by setting the goals to the design. An ideal transmission line circuit and its stripline equivalent will be designed. It will then be meandered to make it more practical. With all imperfect models substituted with EM-structures, the circuit will be optimized to improve all aspects of its performance. The final circuit was built, and its measured data will be compared to the analysis, with comments on its performance.

3.5.1 Design Goal

A highly linear discriminator with a center frequency at 10.5 GHz and a 1 GHz bandwidth is required (9.5% bandwidth). The sensitivity should be good, and the device must be well matched in a 50 Ω system.

Realization:
The second improved branchline hybrid design (see Figure 3.5 (b)) will be used for this implementation. The length of path A is set to 180° and with $n = 11$ for a good sensitivity, the length of path B is 1170°. The line difference was increased to ensure that the S-curve fall within the bandwidth of the hybrid, and so reduce the effects the hybrid's imperfections have on the discriminator's performance.

3.5.2 Ideal Transmission Lines converted to Stripline

The line impedances for the second improved branchline hybrid is tabulated in Table 3.3. This ideal transmission line circuit has exceptional performance and will be compared to the stripline conversion and final design later in this chapter.

The choice of the stripline substrate proved to be a lengthy process. The initial substrate was not in stock. A second design was on a substrate with $\epsilon_r = 3.2$ and $b = 1.016\,mm$. It was later found that the 50 Ω line was much thinner than the normal stripline SMA connector's launch pad. To simplify the construction, it was decided to rather redesign it for the thicker GML1000 substrate with $\epsilon_r = 3.05$ and $b = 3.048\,mm$ (has a $\tan\delta = 0.004$ at 10 GHz). The process was completed up to the layout for all the realizations – only the last design will be shown here.

The line dimensions given in Table 3.3, were calculated with Microwave Office's TXLine. The lengths of L1 and L2 had to be adjusted to compensate for the parts swallowed by the T-junctions (for which an EM-structure was used similar to that of Figure 3.13 (b)).

Table 3.3: Line dimensions for the X-band Mohr discriminator design (no optimization).

Element	**Transmission line**		**Stripline**	
	Impedance	Length	Width	Length
Z1	38.62 Ω	90°	2.84 *mm*	2.49 *mm*
Z2	54.57 Ω	90°	1.61 *mm*	3.91 *mm*
Z3	85.5 Ω	180°	0.59 *mm*	8.16 *mm*
Z4	34.43 Ω	180°	3.35 *mm*	8.16 *mm*
	50 Ω	(90°)	1.88 *mm*	(4.08 *mm*)

The transmission coefficients for the stripline hybrid is compared to the ideal transmission line circuit in Figure 3.19 – the analysis of the final design's hybrid is also shown, and will be discussed in due coarse. The uneven power split for the two paths through the hybrid, is due to the change in the lengths of the mid-sections (Z1 and Z2).

3.5.3 Meandering and optimization

The ports of the hybrid will be too close to manufacture if the lines of sections Z3 and Z4 were left straight. Furthermore, the line difference of paths A and B necessitate a meandering of path B. There are many ways in which this meandering can be accomplished, as can be seen in the other implementations shown here: Figures 3.10 and 3.17 (a) and (b).

For this design, section Z3 is meandered with two 90° curves, and path B uses eight 90° curves. The curves are defined by the radius of the center-line and the width of the line. A curve has a more accurate model than a bend, and is easier to work with. The configurations of these meanders and the names given to each line-section, are shown in Figure 3.20. To make the optimization process simpler, the length of path A (la) is also contained in path B. All the lines are further spaced and constrained in such a way that there will be the least amount of coupling (if any) between close-proximity lines.

Full-wave step junctions are used for the steps in line-width between Z3 and Z4, as well as Z4 and the 50 Ω lines. The lines in the branch-part (Z1 and Z2) were modeled with coupled line sections to ensure that any coupling between these lines were not ignored. Before construction of the final circuit, the complete ring-structure were analyzed with EMSight. This analysis is shown in Figure B.1.

As explained in Section 3.3.3, the stripline T-junction model assumes the average width for the facing lines. The T-junctions were therefore rather analyzed with EM structures to improve the accuracy of the simulations. An EM structure is rigid and can not be changed during optimization. Therefore it had to be changed after each convergence to

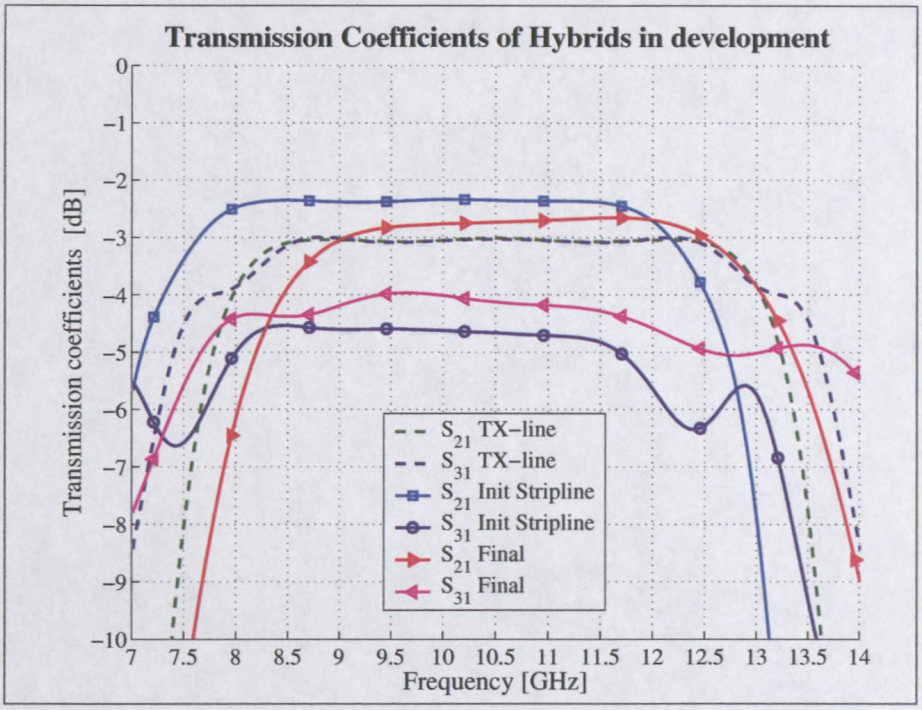

(a) Transmission Coefficients

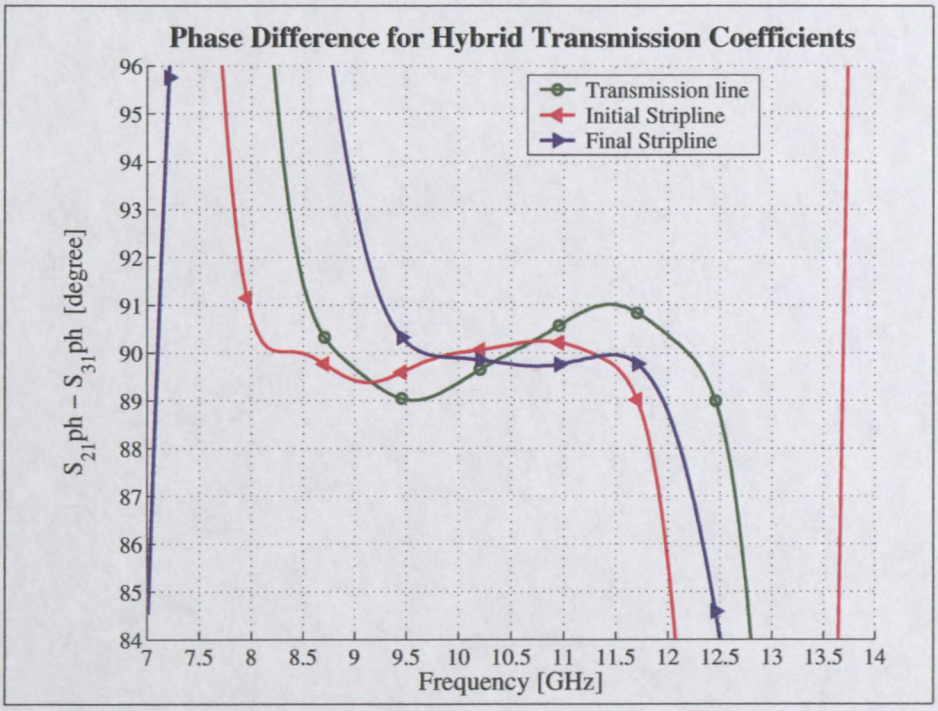

(b) Phase difference of Transmission Coefficients

Figure 3.19: Analysis of the hybrids used during the development of the stripline X-band Mohr Discriminator.

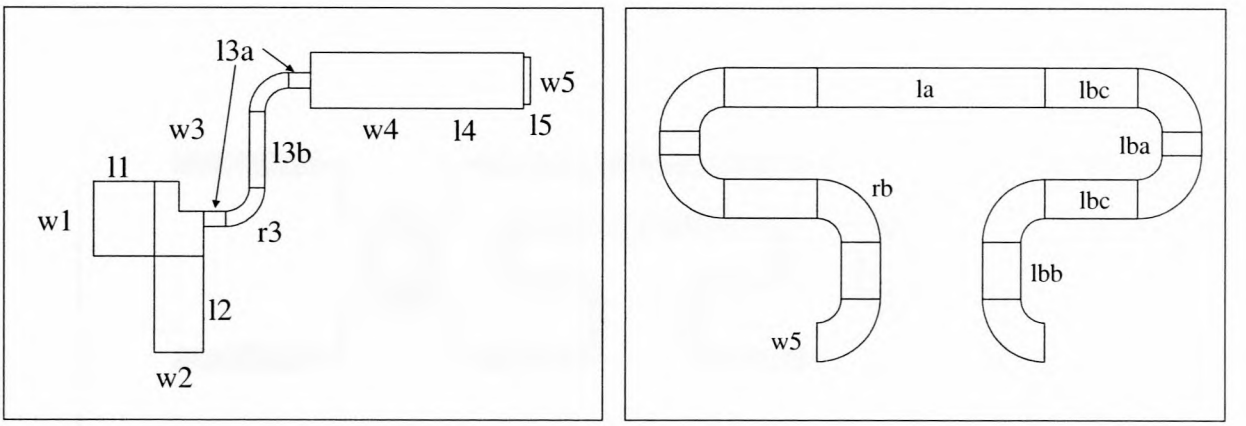

(a) Quarter of the Hybrid (b) Path B of the discriminator

Figure 3.20: Construction and Meandering of the lines in the X-band Mohr Discriminator.

Table 3.4: Optimized Line dimensions for the X-band Mohr discriminator.

Line Widths		**Hybrid Lengths**		**Paths A and B**	
Section	Width	Section	Length	Section	Length
w1	2.62 *mm*	l1	2.11 *mm*	la	11.0 *mm*
w2	1.72 *mm*	l2	3.38 *mm*	lba	1.0 *mm*
w3	0.54 *mm*	l3a	0.76 *mm*	lbb	2.4 *mm*
		l3b	2.66 *mm*	lbc	3.93 *mm*
		r3	1.095 *mm*	rb	1.85 *mm*
w4	1.96 *mm*	l4	7.5 *mm*	**Port Extensions**	
w5	1.66 *mm*	l5	0.25 *mm*	lp	4.0 *mm*

decrease the errors in the simulation.

The circuit was optimized with the following goals: an $S_{11} < -20$ dB and $S_{33} < -20$ dB over the band from 9.5 GHz to 11.5 GHz; a linear goal was put to the differential output ($|S_{31}| - |S_{21}|$) between the points (-0.75, 9.7 GHz) and (0.75, 11.3 GHz). The final optimized values for the parameters of the hybrid and paths are given in Table 3.4. The port extensions are there for the connectors' launch pads.

3.5.4 Final design and Simulation

The layout of the final circuit is shown in Figure 3.21. Its analysis is compared with the ideal transmission line circuit and the initial stripline circuit in Figures 3.22 and 3.23. The practical circuits have losses, which cause the transmission coefficients to be lower

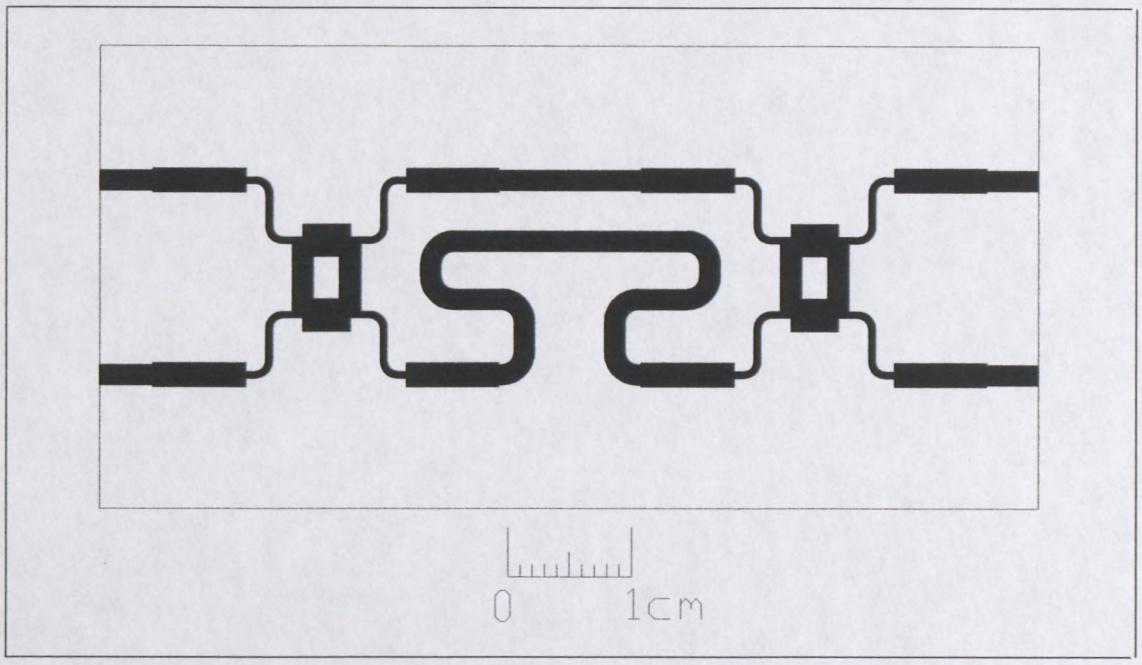

Figure 3.21: Layout of the stripline X-band Mohr Discriminator.

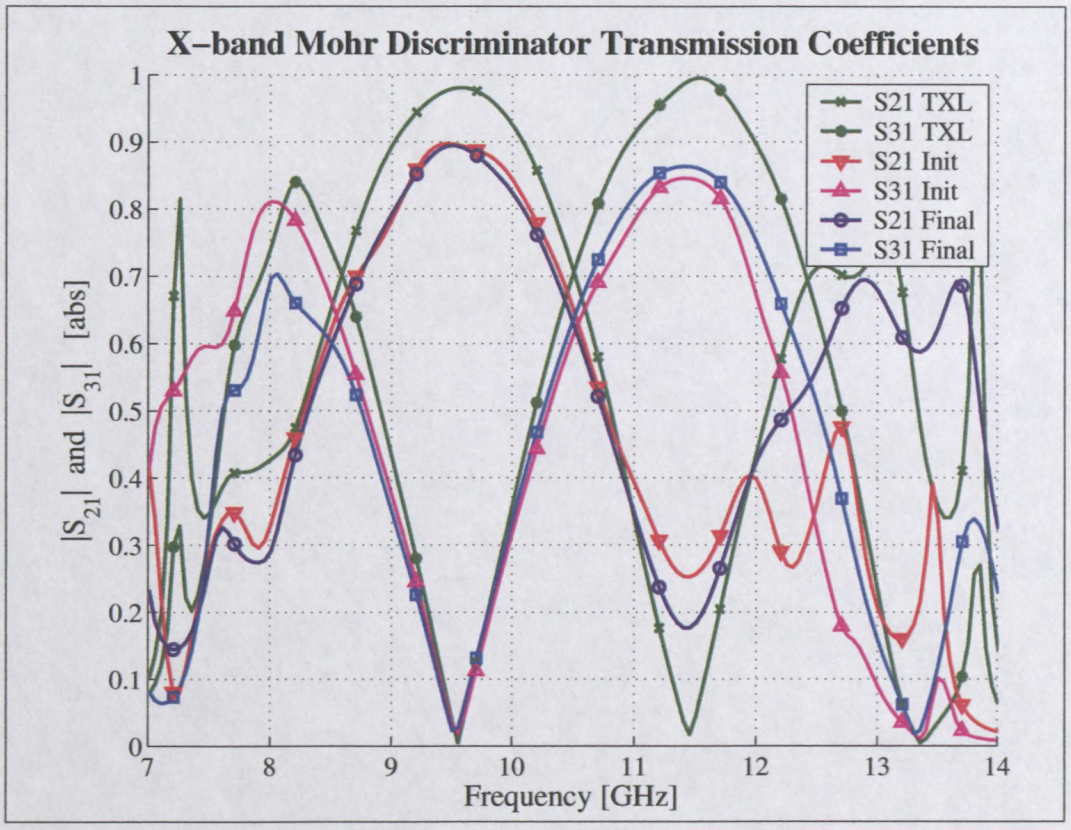

Figure 3.22: Transmission Coefficients for the Stages in the Development of the X-band Mohr Discriminator.

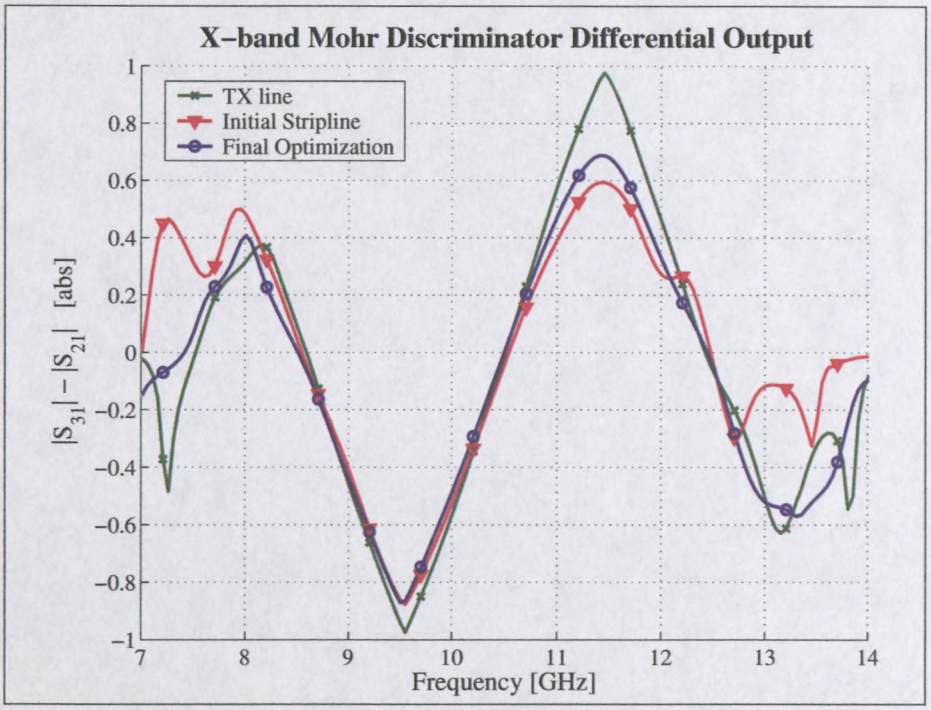

(a) Differential Outputs: $|S_{31}| - |S_{21}|$

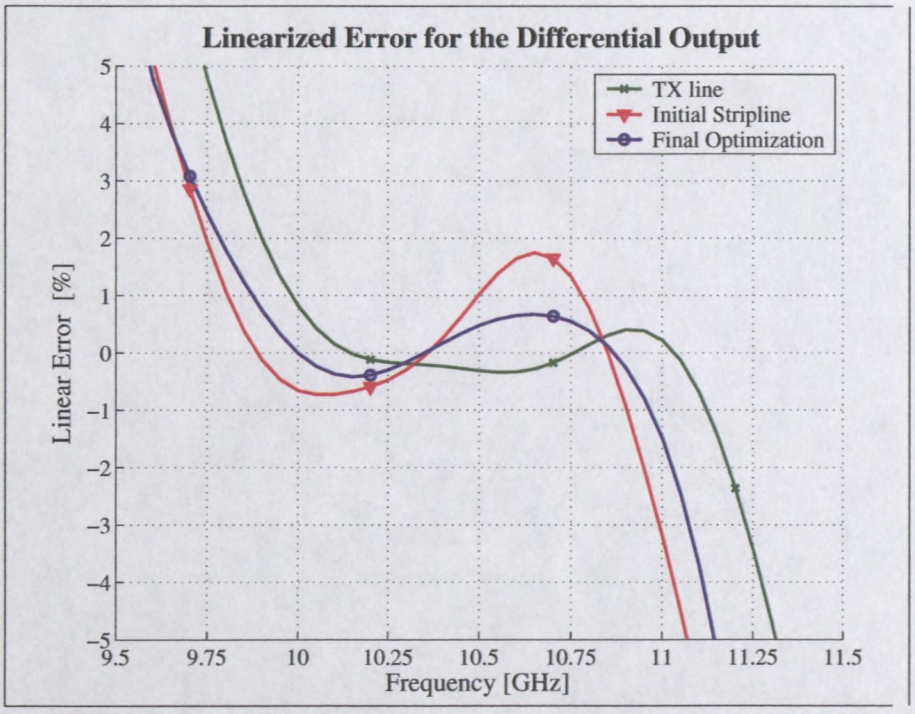

(b) Linearized Error (for linear fits from 10 to 11 GHz)

Figure 3.23: Comparison of the simulation for the Stages in the Development of the X-band Mohr Discriminator.

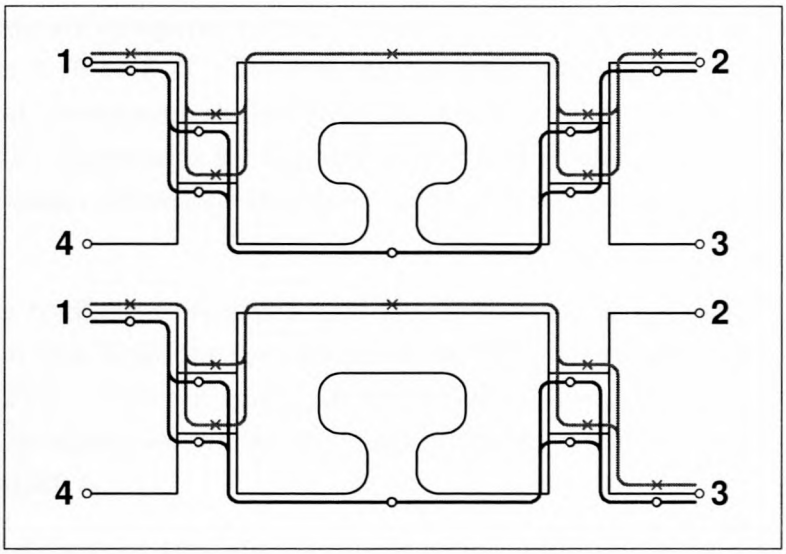

Figure 3.24: Explanation of the cause of incomplete destructive interference.

than with transmission lines, but also cause the path going straight (either S_{21} or S_{34}) to have an incomplete destructive interference.

This incomplete destructive interference is best explained through Figure 3.24. The hybrids have an unequal power split, as was seen in Figure 3.19 (a). The paths going from port 1 to port 2 (or equivalently from port 4 to 3), either have twice an S_{21} or an S_{31} of the hybrid affecting its attenuation. The two signals arriving at port 2 through these two paths, then have double the effect of this unequal split, and do not have a complete destructive interference. The paths from port 1 to port 3 (or port 4 to port 2), both have an S_{21} and S_{31} to contend with. The signals only have a small extra loss due to the longer transmission line, and have a good destructive interference.

The optimized circuit does work better, but this occurrence cause the differential output to start deviating early from the ideal transmission line case, and substantially influence the linearity. This occurred with all previous implementations of the Mohr discriminator as well, as can be seen in Figures 3.12 (a), 3.15 (b) and 3.18 (c).

3.5.5 Measurement

The circuit was built and a photograph of it can be seen in Figure C.4. The ports are defined as follows, referring to Figure 3.21: the upper left-hand port is port 1, and continuing clockwise, the ports on the right is 2 and 3, and at bottom-left is port 4. Ports 1 and 4 have female SMA connectors, while ports 2 and 3 have male SMA connectors. This was due to a shortage in female SMA connectors.

The measurements are compared to the Microwave Office simulation of the final optimized design in Figures 3.25 to 3.27. The reflection coefficients and the isolation of the ports looks good. Most resonances shifted slightly, which is an indication of some structural imperfections. The dimensions for this design were set to the nearest 1 mm, and at these high frequencies small deviations may have a large influence in the characteristics of the device.

The transmission coefficients revealed that the substrate has a slightly larger dissipation factor. The given specifications for this substrate indicates a dissipation factor of 0.004 at 10 GHz and 25°C. Through tuning in Microwave Office, it was found to be closer to 0.0065. A shift in some resonances are again noticed. These may also be a result of a frequency dependent ϵ_r.

The differential output for this discriminator have highly linear transfer functions. The measured functions do not have a maximum deviation due to higher losses. A system with port 1 as input, will not be as linear as one with port 4 as the input and port 1 terminated. The output taken as $|S_{24}| - |S_{34}|$ is well within 1% linear, except close to 11 GHz where the incomplete destructive interference cause an early deviation from linearity. Port 4 is also better matched over the 1 GHz band.

This discriminator was also tested with detectors, and the measurements will be shown in Section 4.5.2. The overall result looks very good. It shows that systems like this one can be implemented in transmission line structures at these frequencies, using low-cost substrates.

3.6 Conclusion

Previous implementations of the Mohr discriminator used complex hybrids and couplers. A simpler branchline hybrid was implemented in the S-band discriminator. The expansion of the hybrid, with its improved design flexibility and more manageable dimensions, helped to improve the linearity of the X-band discriminators. The final X-band discriminator was developed through the experience gained from previous mistakes, and was discussed as a design example. Good measurements were shown of both the S- and final X-band discriminators. They both have a good linearity and bandwidths of 28.5% and 9.5% respectively. The Mohr discriminator is a simple technique which is easy to design and develop.

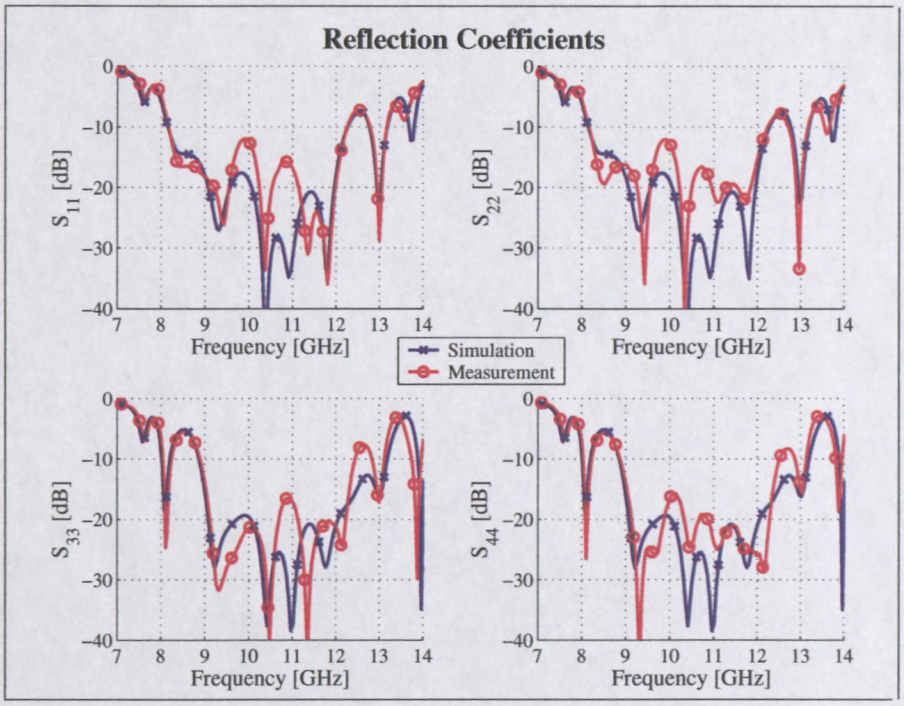

(a) Reflection Coefficients

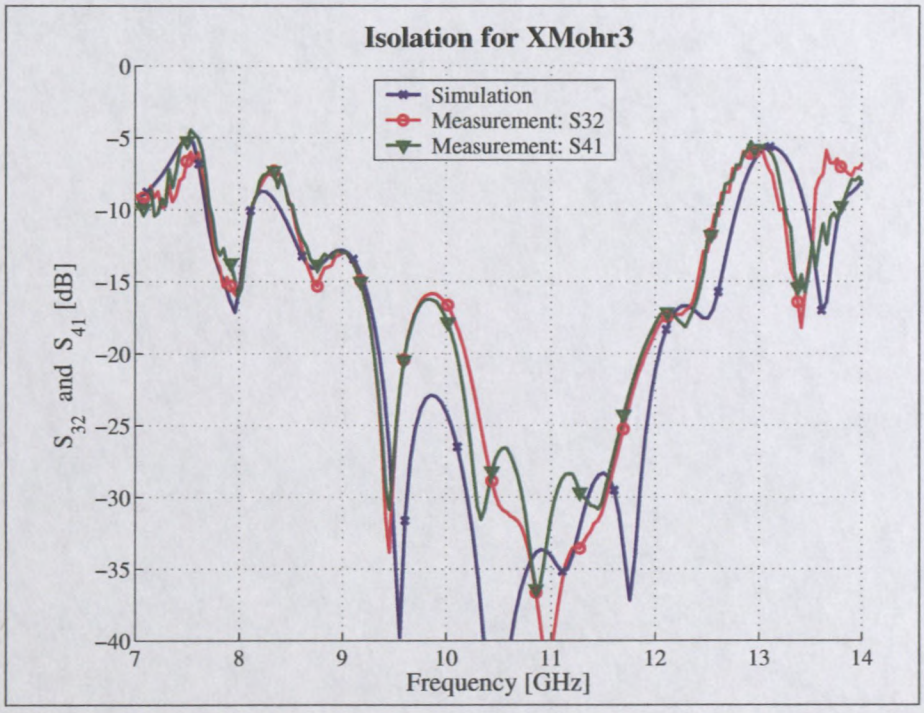

(b) Isolation

Figure 3.25: Comparison of the simulated and measured data for the X-band Mohr Discriminator.

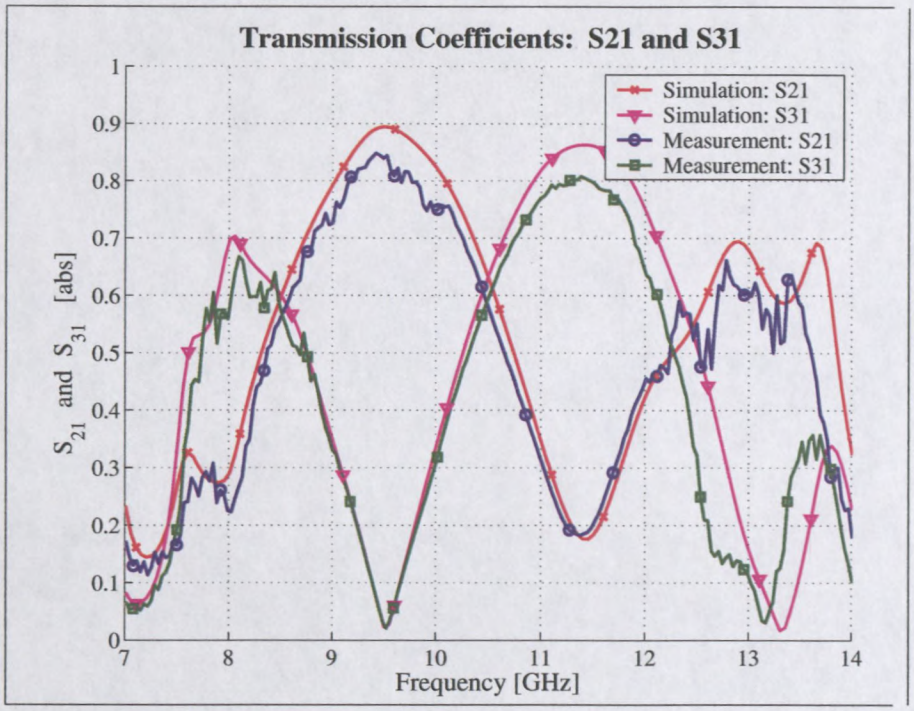

(a) Transmission Coefficients: S_{21} and S_{31}

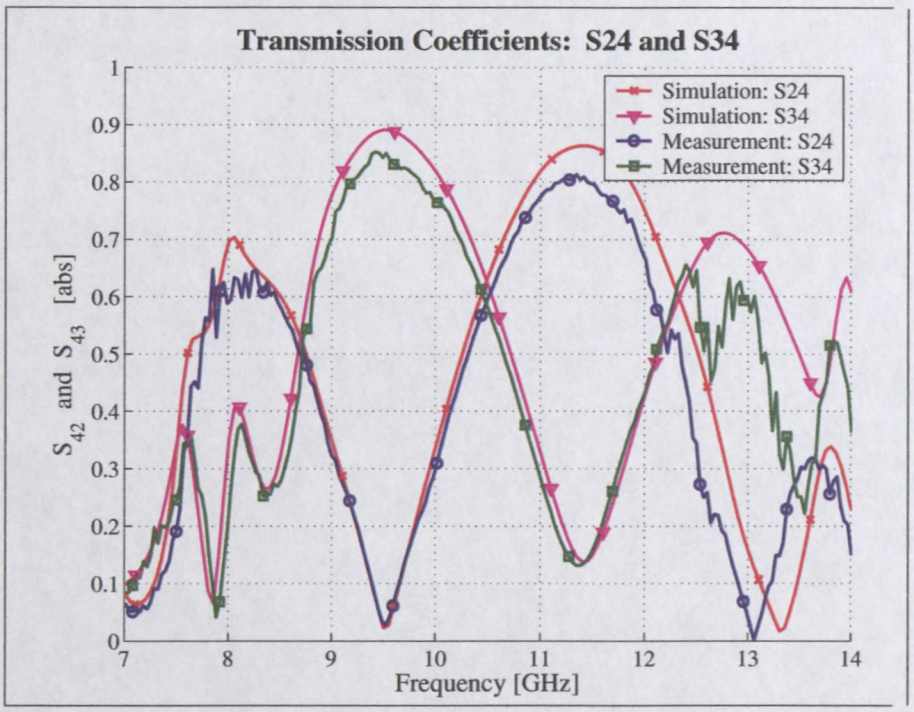

(b) Transmission Coefficients: S_{24} and S_{34}

Figure 3.26: Comparison of the simulated and measured data for the X-band Mohr Discriminator.

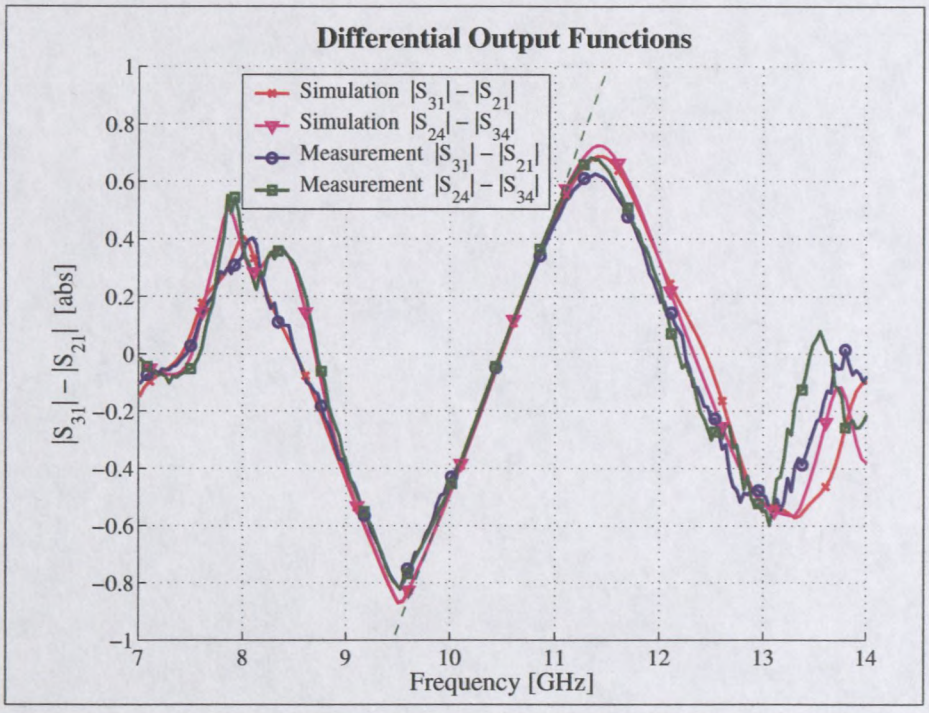

(a) Differential Outputs: $|S_{31}| - |S_{21}|$ and $|S_{24}| - |S_{34}|$

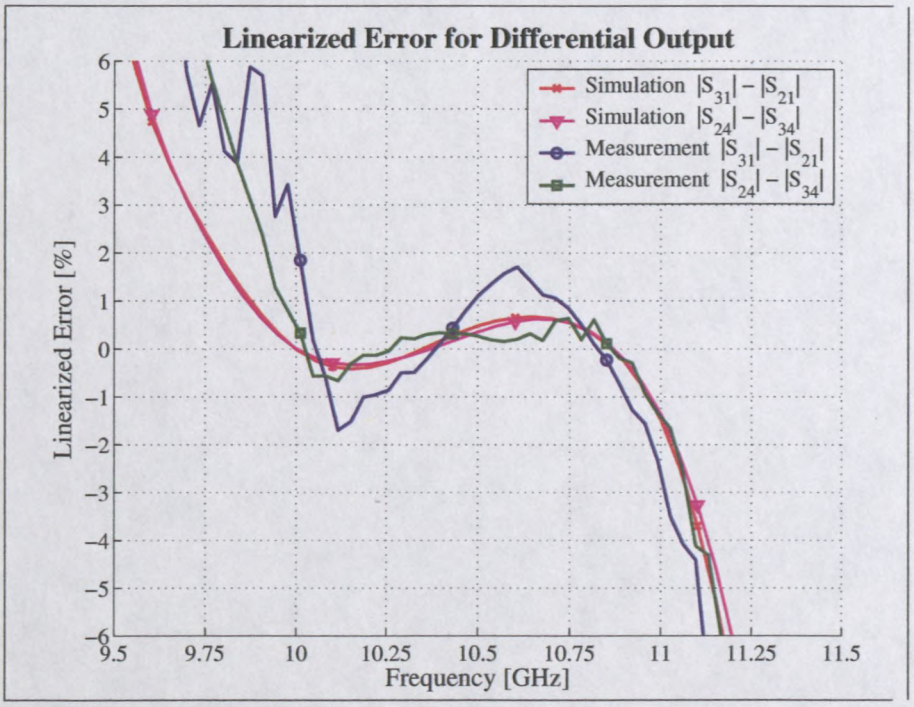

(b) Linearized Error (for linear fits from 10 to 11 GHz)

Figure 3.27: Comparison of the simulated and measured data for the X-band Mohr Discriminator.

Chapter 4

The Discriminator System

In this chapter an overview of the complete discriminator system will be given. A practical discriminator system consists of more than just the transmission line structures discussed in Chapters 2 and 3. The systems which were used to test the S-band and X-band Mohr discriminators, will be discussed as examples, and measurements thereof will be shown.

4.1 Topology

A general discriminator system consist of four parts – see the diagram of Figure 4.1. The discriminator is responsible for changing the amplitude of the signal according to the frequency thereof (it was the main topic of this document thus far). These amplitude changes must then be detected by detector diode circuits. There usually exist two outputs to the discriminator, and the difference between these detected signals are usually needed. A differential amplifier are used to calculate the differential output of the system. The fourth part of the system is a limiter or gain control circuit at the input of the discriminator.

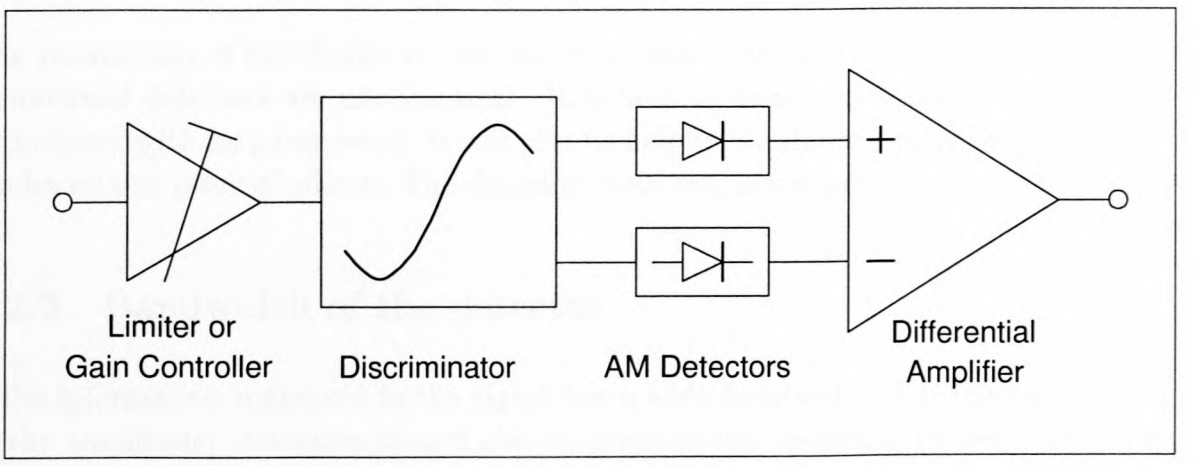

Figure 4.1: A general discriminator system.

4.2 Detectors

The amplitude variation of the RF signal caused by the discriminator, can be detected by an AM detector to retrieve the information in the signal. If the system is good enough, a direct translation is possible of the frequency of the system's input signal, to a dc-voltage value for the differential output signal.

4.2.1 Linear or Square-law

Depending on the discriminator that are used, either a linear or a square-law detector can be employed. The linear detector is a peak detector and has a linear relation between the peak values of the input RF signal and the dc-voltage at its output. A square-law detector's output reflects the power of the input signal (the magnitude squared). Some discriminators have a flattened S-curve, for which the linearity may be improved if a square-law detector is used.

4.2.2 Linearity aspect

The detectors and the discriminator should work together as a unit to provide a linear translation of the frequency to a dc-voltage. The linearity of the detector thus plays an equal role in the performance of the system.

The two detectors should have identical transfer functions (of input versus output voltage). This will provide equal detection of the output signals from the discriminator, and if the differential amplifier gives an accurate difference signal, the linearity of the system will be good.

The parameters of the diodes in the detectors vary with each piece of silicon, therefore commercial detectors are not identical. It is best to design each detector separately in accordance with its parameters. It will also be helpful if a diode pair is used with the two diodes on one piece of silicon. The detectors were not developed.

4.2.3 Bandwidth of the detector

If the information contained in the signal has a wide bandwidth (i.e. has fast deviations in the amplitude), attention should also be given to the operating (video) bandwidth of the detectors used. Since a detector consist of both a diode and a low-pass filter, it will have a certain operating bandwidth.

4.2.4 Measurements

Linear detectors were used to test with the Mohr discriminators. Two zero bias Schottky detectors from MICA Microwave, with model number ZP0208CC01, was used with the S-band system. Their frequency range is from 2 to 8 GHz. The detectors have serial numbers which end in 057 and 058, and will be named as such. Their input and output have SMA connectors.

For the X-band system, two detectors were chosen from 7. They were all measured to find the closest match of the input versus output voltage functions. These detectors are from Marconi Instruments with type number 6002/1. One had the marking 'A2' on it, and the other was named 'MP' (it still had a nice sticker). They have an N-type connector on the RF-input, and a BNC at the output.

MICA Detectors: The measurements of the input power versus the output voltage at 2.45 GHz is shown in Figure 4.2. For these measurements, the output of the detectors was connected directly to the oscilloscope, and thus has a 1 MΩ load. The input power was measured separately on the Spectrum Analyzer.

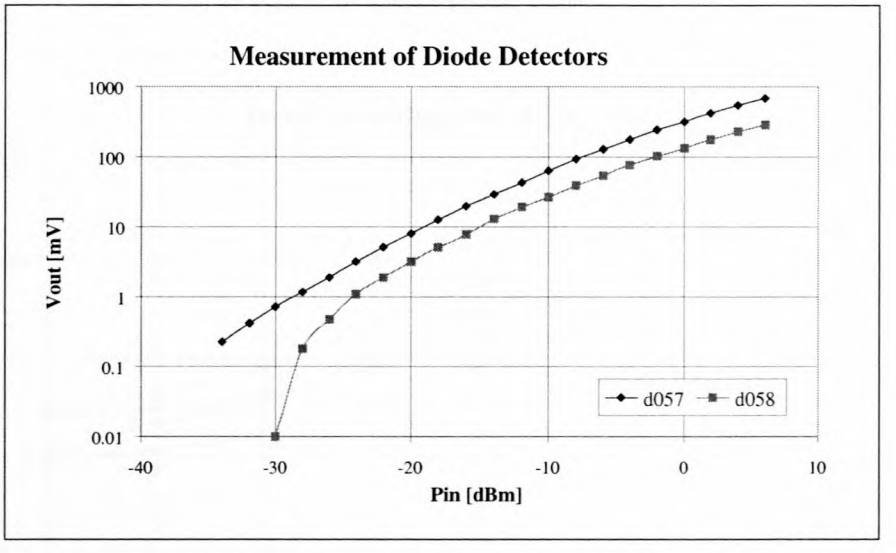

Figure 4.2: Measurements of the two MICA detectors.

The 058 detector was damaged previously, but with a 2.4 times amplification of the detector's output signal, a similar relation to the 057 detector can be achieved. A high-speed non-inverting op-amp circuit, with a voltage gain of 2, was built with a current-feedback amplifier. The circuit and the measurements thereof (for both detectors), are shown in Figure 4.3. Vdet and Vamp was measured before and after the amplifier with 10×-probes, as indicated in the diagram. The amplifier itself will form part of the discussion on the differential amplifier.

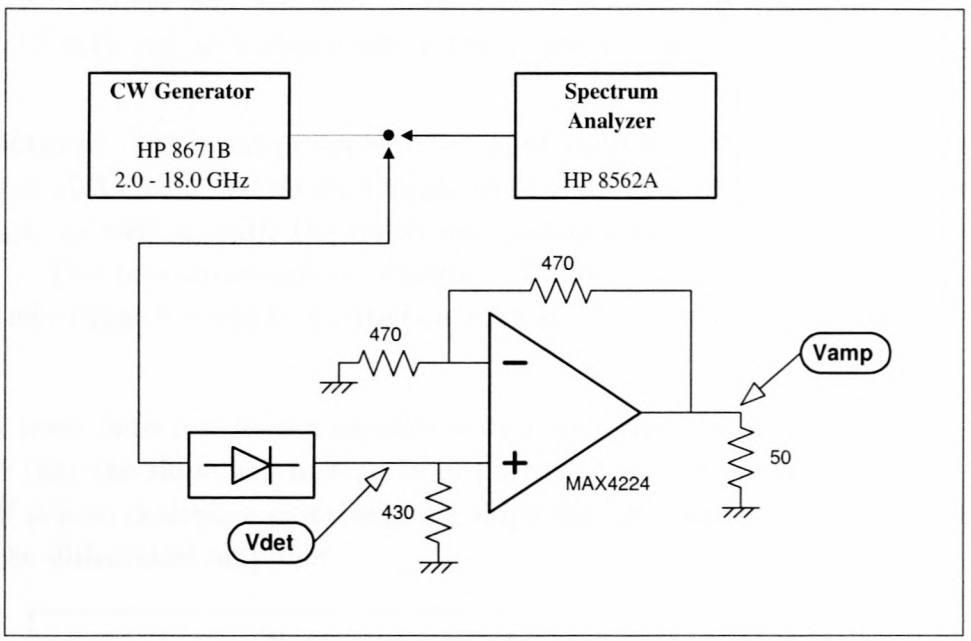

(a) The measurement diagram

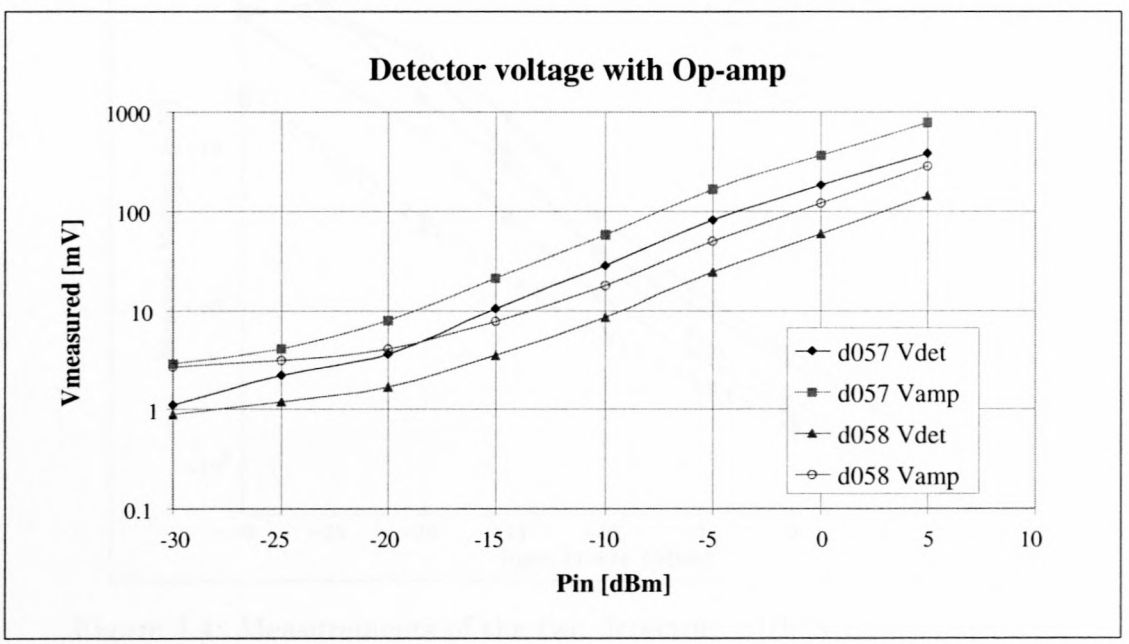

(b) Measurements

Figure 4.3: Measurements of the two detectors connected to a buffering op-amp.

These measurements are an indication of the voltages which will exist if the detectors are connected to the differential amplifier, and are almost half that of the previous set. This is due to the load the detectors now have. Notice that the amplifier has an output noise floor of ~2.7 mV, and also adds noise to the input voltage.

MI Detectors: The input power versus output voltage of the two chosen detectors were measured at 10.5 GHz. The measurements were done with the detectors connected to the oscilloscope, as well as with the buffering op-amp circuit (the same as for the MICA detectors). The measurements are shown in Figure 4.4, where those with the op-amp were shifted so that it could be plotted on a log-scale – the op-amp had an offset of about 12 mV.

Note that these detectors have a negative output polarity. The only affect this has on our system, is that the slope will now go from positive to negative, instead of the other way around. If it is so desired, a positive going slope can be obtained by simply swapping the ports of the differential amplifier.

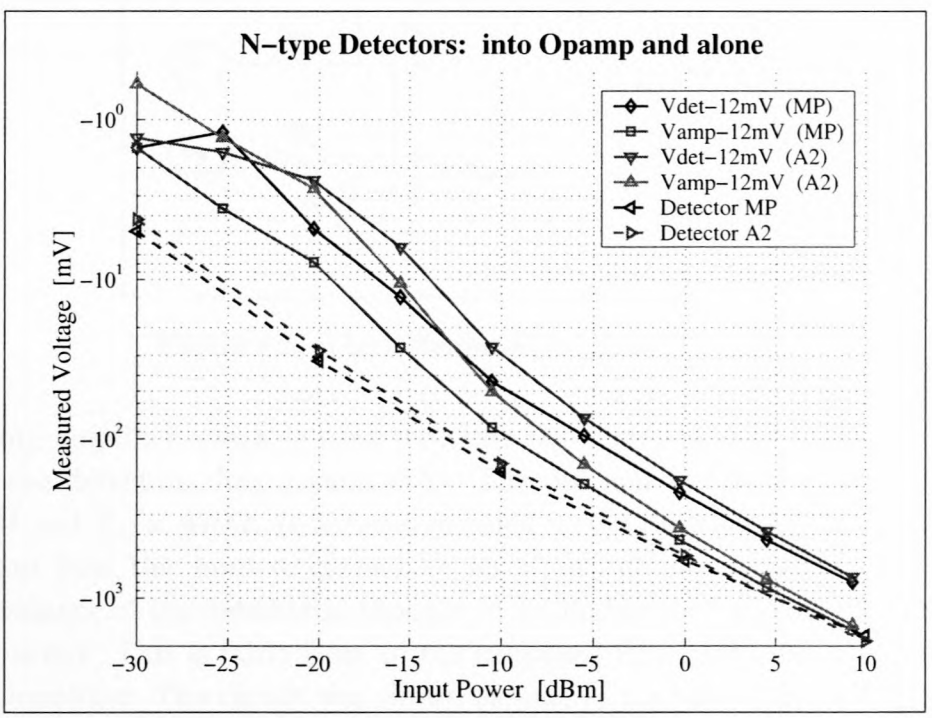

Figure 4.4: Measurements of the two detectors with N-type connectors.

4.3 Differential amplifier

The differential amplifier have to be fast enough to subtract signals with a frequency as high as the highest frequency of the baseband signal. A current-feedback amplifier from MAXIM was used for this purpose, though their application engineers advised me that it is not intended for such use. The reason for this is that the amplifier has very low input impedances. The circuit was built and tested and seem to work well enough.

The MAX4224 amplifier was implemented here, and has a SOT23-6 surface mount package. It works from a ±5.5 V dual power supply. The 3 dB bandwidth can be up to 600 MHz, depending on the resistor networks and signal powers. The minimum voltage gain for this device is 2 (6 dB). In the data sheets optimal values are given for the feedback resistor network for different gain values. The values were interpolated for a gain of ~10 dB, to give an $R_F = 330\Omega$ and $R_G = 200\Omega$. The circuit is shown in Figure 4.5.

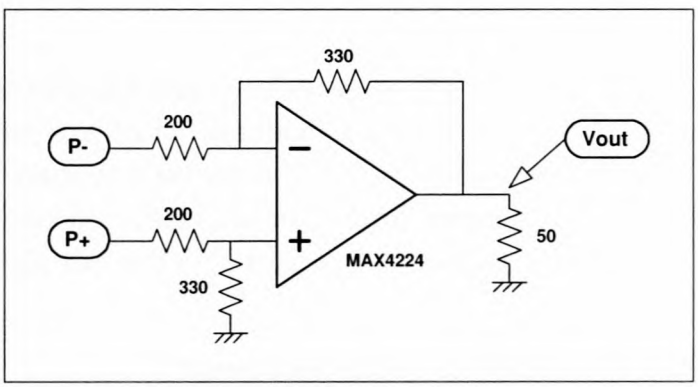

Figure 4.5: The differential amplifier circuit.

The buffering amplifier which is used with the 058 detector, and was used to test the loading of the detectors, has a gain of 2. The optimal feedback network is given by $R_F = 470\ \Omega$ and $R_G = 470\Omega$. It is recommended in the data sheets that a 75 Ω resistor should be put from the input to ground for an input line impedance of 75 Ω . Since the output impedance of the detector is thought to be higher than this, a 430 Ω resistor was put as instructed. This is fairly close to the supposed input impedance of 530 Ω for the differential amplifier. The circuit was shown as part of the test-setup in Figure 4.3 (a).

4.3.1 Measurements

The two amplifiers were measured in two ways: the gain was measured both as function of the frequency, and as a function of the input power. The measurement setup of the

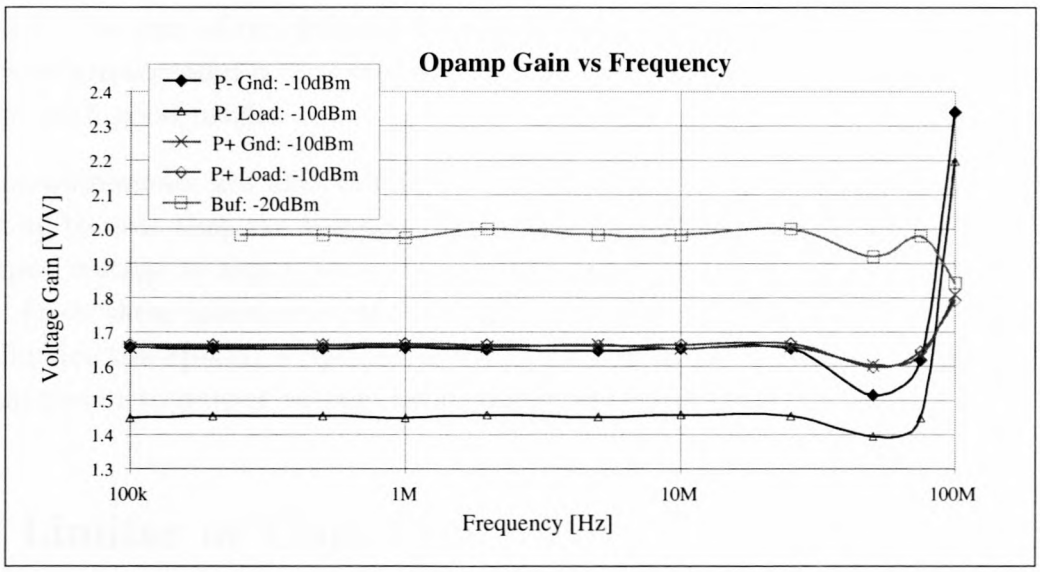

Figure 4.6: The Voltage gain of the op-amp as function of frequency.

differential amplifier had different configurations for the gain versus frequency measurements: the open port was either terminated with a 50 Ω load, or it was grounded. The measurements were made at several power levels, and compared well. The voltage gains at -10 dBm are shown in Figure 4.6, where 'P- Gnd' indicates that the port on the inverting side is grounded, while the non-inverting gain (Vo/V+) is measured.

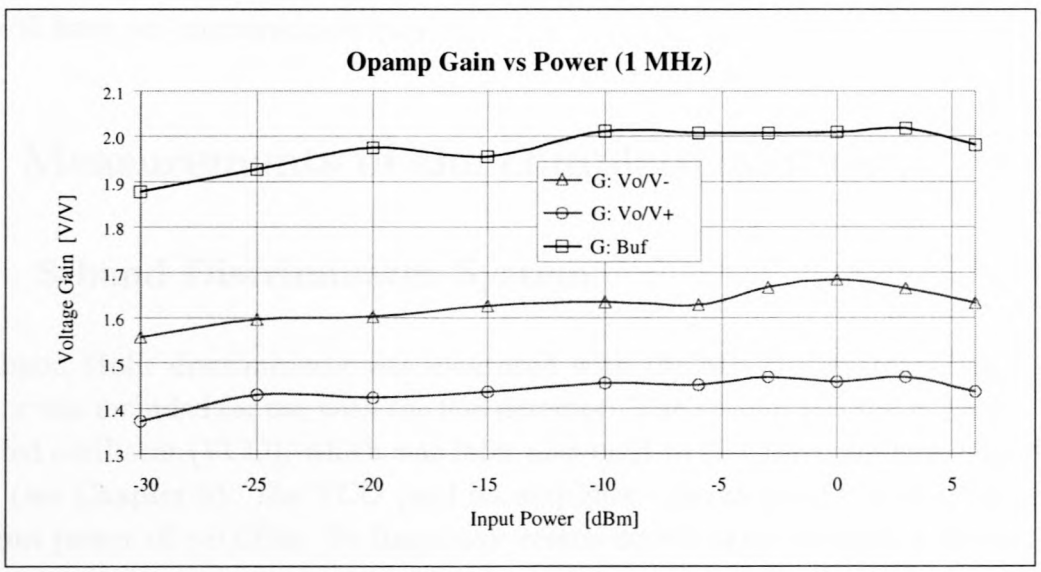

Figure 4.7: The Voltage gain of the Op-amp as function of power.

The output/input voltage ratio was also measured as a function of the input power, at a frequency of 1 MHz. For the differential amplifier, the other input port was terminated with a 50 Ω load. The voltage gains for the three sets of measurements are shown in

Figure 4.7. The gain of the differential amplifier is certainly not 10 dB – the interpolation is somehow unsuccessful in this sophisticated device. The amplifier is still functional, and was used with good results.

These measurements are also tabulated in Appendix B.3 in Tables B.1 and B.2. It is interesting to note that the voltages drop when connected to the inverting port, though the output voltage to input power ratio is the same for the inverting and non-inverting inputs. From these measurements it is concluded that the loading of the inverting port may influence the op-amp's operation, while the non-inverting will not. For equal loads, the input power to output voltage ratios ought to be the same.

4.4 Limiter or Gain Control

It is possible to have a direct translation of the frequency of the input signal, to a dc voltage value for the output signal. To achieve this, it is necessary that the input power be constant – the peak amplitude must be stable over time and frequency. Any amplitude variations of the input will result in errors in the presumed output to the system.

There exist many methods of employing such a system, but it was not included in this research. It is also possible to have a reference of the input amplitude at a post-processing stage. The output waveform can then be scaled according to the input power, and the result will have an improved accuracy.

4.5 Measurements of the complete systems

4.5.1 S-band Discriminator System

The S-band Mohr discriminator was measured with the MICA detectors. The buffering amplifier was included for use with the 058 detector. The system was tested with a voltage controlled oscillator (VCO), which was later also used to test the complete demodulation system (see Chapter 5). The VCO (and its amplifier – developed by Anton Snyman) has an output power of ~9 dBm. Its frequency versus dc-voltage is plotted in Figure 4.8.

The test setup is shown in Figure 4.9, and the measurements in Figure 4.10. A photograph of the system is shown in Figure C.2. It was measured twice, with the detectors swapping ports. The op-amp circuits was constructed so that the buffer amplifier's output was always connected to the inverting input of the differential amplifier.

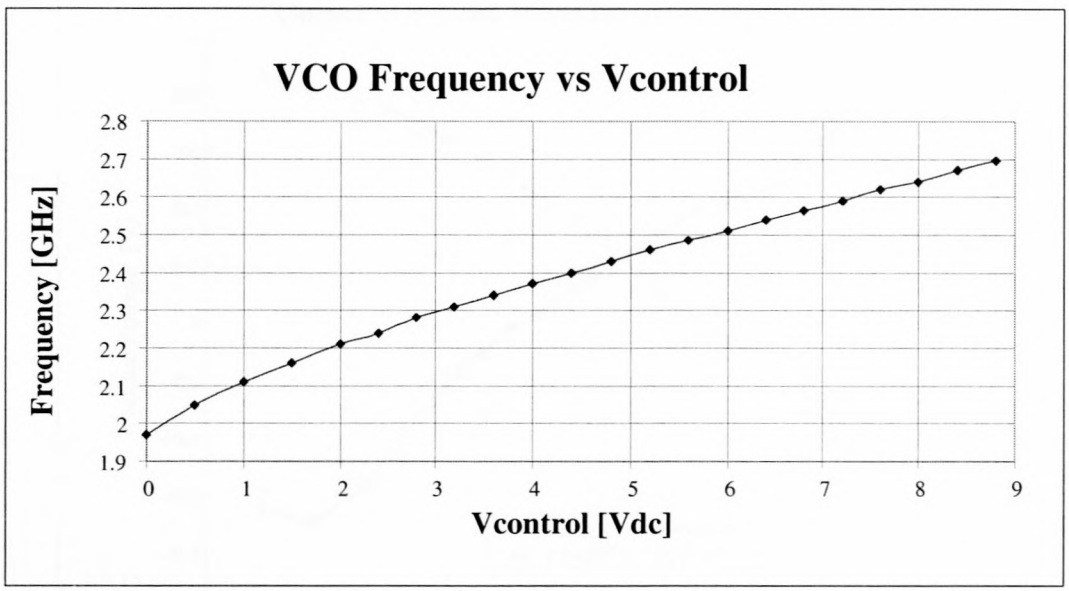

Figure 4.8: The Frequency vs dc-voltage characteristics of the VCO.

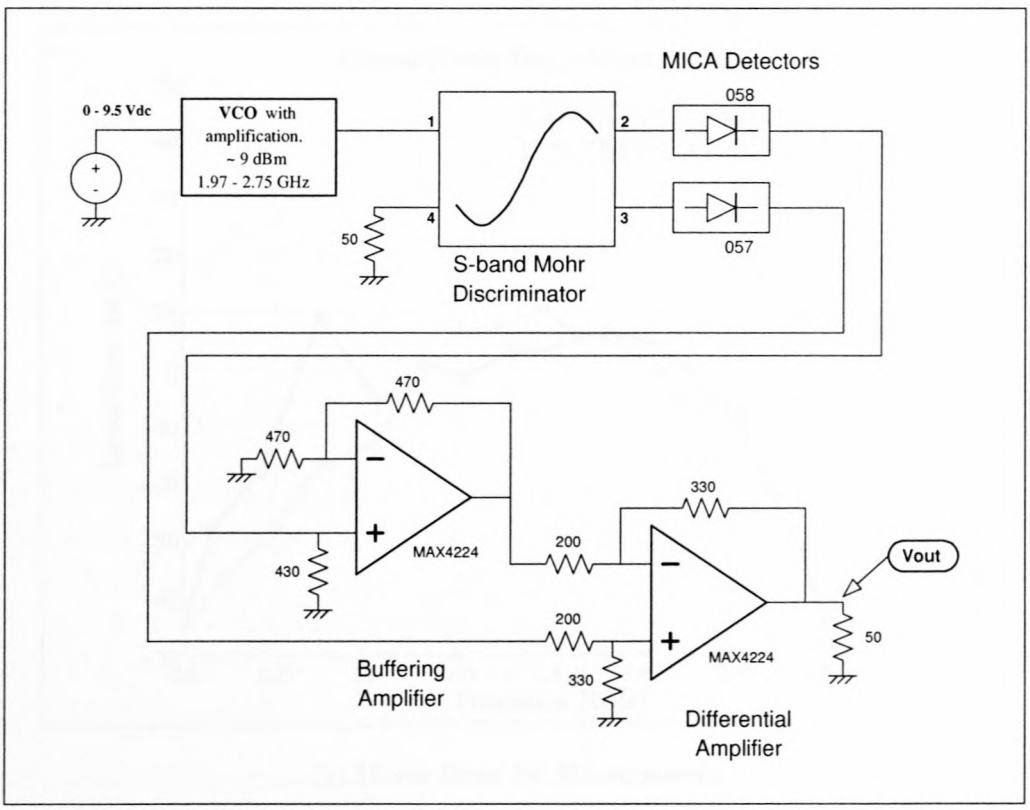

Figure 4.9: Setup of the S-band Mohr Discriminator System.

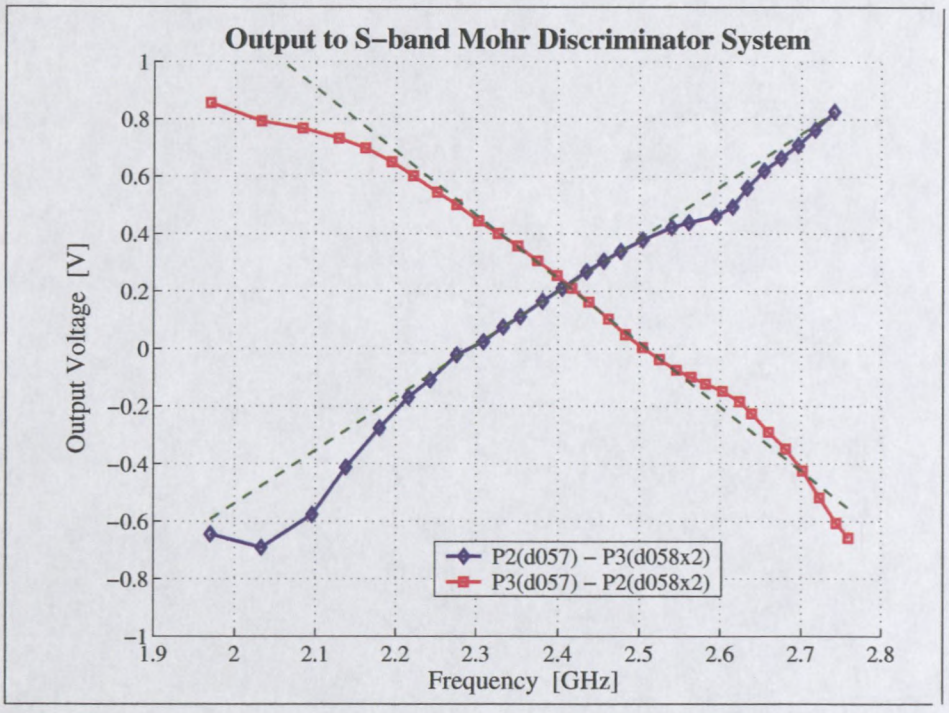

(a) Output Voltage vs Frequency

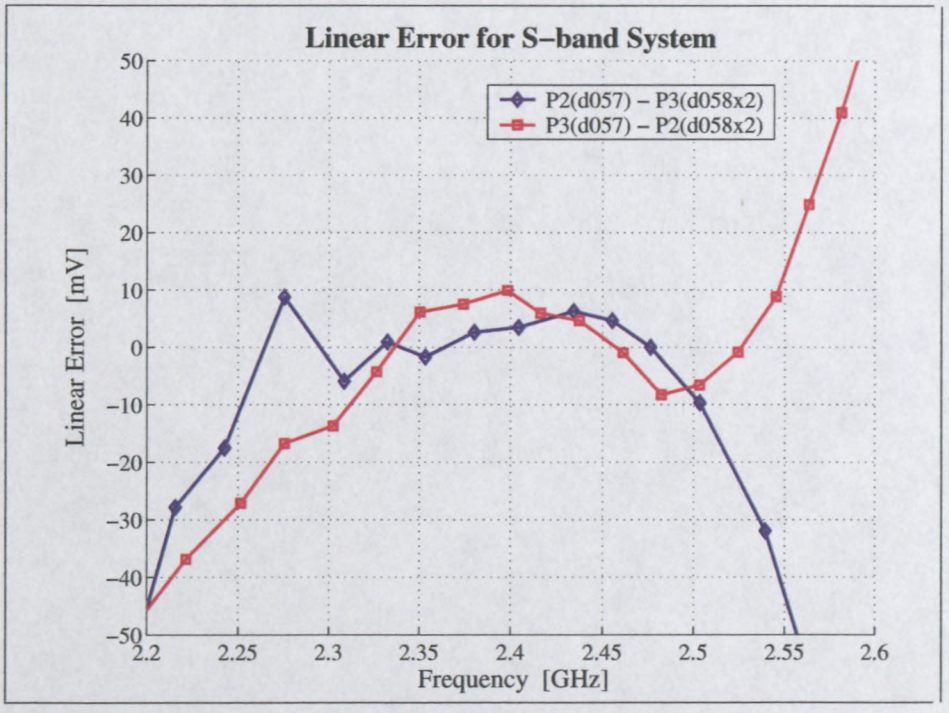

(b) Linear Error for Measurements

Figure 4.10: Measurements of the S-band Mohr Discriminator System.

A linear fit was done between 2.3 and 2.5 GHz for both measurements (8.3% bandwidth). From these fits a sensitivity was calculated of 0.18 V/100MHz for the positive-going, and 0.22 V/100MHz for the negative-going slopes. The linear error are within ±10 mV, which is very good considering the sensitivity. Notice that there exist a dc-offset of ~0.22 V in the output characteristics. The measurements are satisfactory, and this system could be used if highly accurate frequency measurements are not required. It will be used to test a communication system (Chapter 5).

4.5.2 X-band Discriminator System

The N-type connectors of the detectors are too wide for direct connection with the discriminator. Semi-rigid 50 Ω coax was used (with the necessary conversions) to connect these two stages. When measured on the Network Analyzer with these coax (not calibrated out), the system had an extra loss of around 1.5 dB.

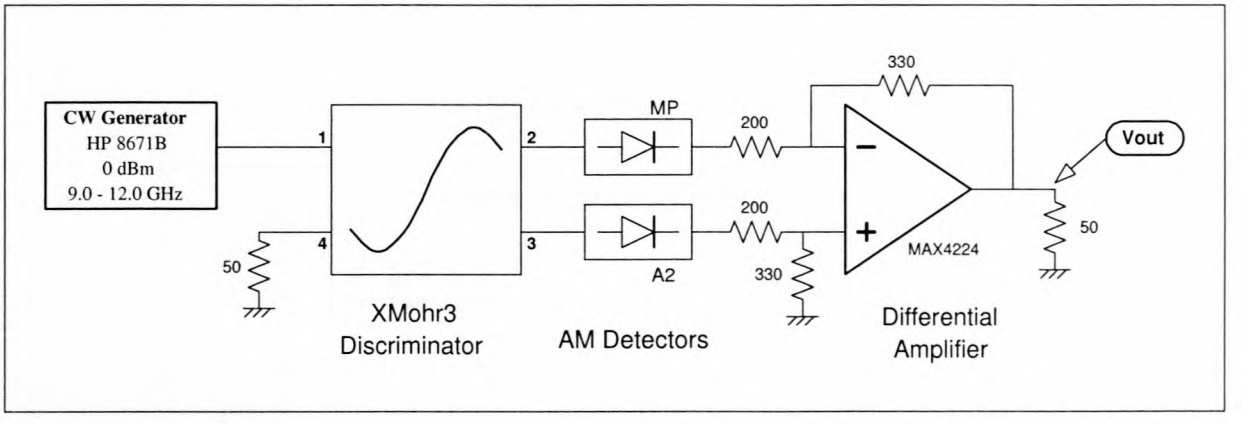

Figure 4.11: The X-band Discriminator System setup.

A diagram of the setup is shown in Figure 4.11, and a photograph thereof in Figure C.4. The measurements were repeated with both port 1 and port 4 as input. When measuring with port 4 as input, the detectors at ports 2 and 3 swapped places (they stayed connected with the differential amplifier as shown). The power level of the CW generator was set to 0 dBm. The loss of the system was measured by replacing the detector circuitry with a load and the Spectrum Analyzer, at the ends of the semi-rigid coax. With port 4 as input, two signals was measured: at 9.5 GHz at port 3 a signal of -4.2 dBm, and at 11.3 GHz at port 2 a signal strength of -4.3 dBm was measured.

The two functions to be measured is

$$Vo1 = -(|S31|_{A2} - |S21|_{MP}) \text{ and}$$
$$Vo4 = -(|S24|_{A2} - |S34|_{MP}).$$

The minus sign is because of the negative polarity of the detectors.

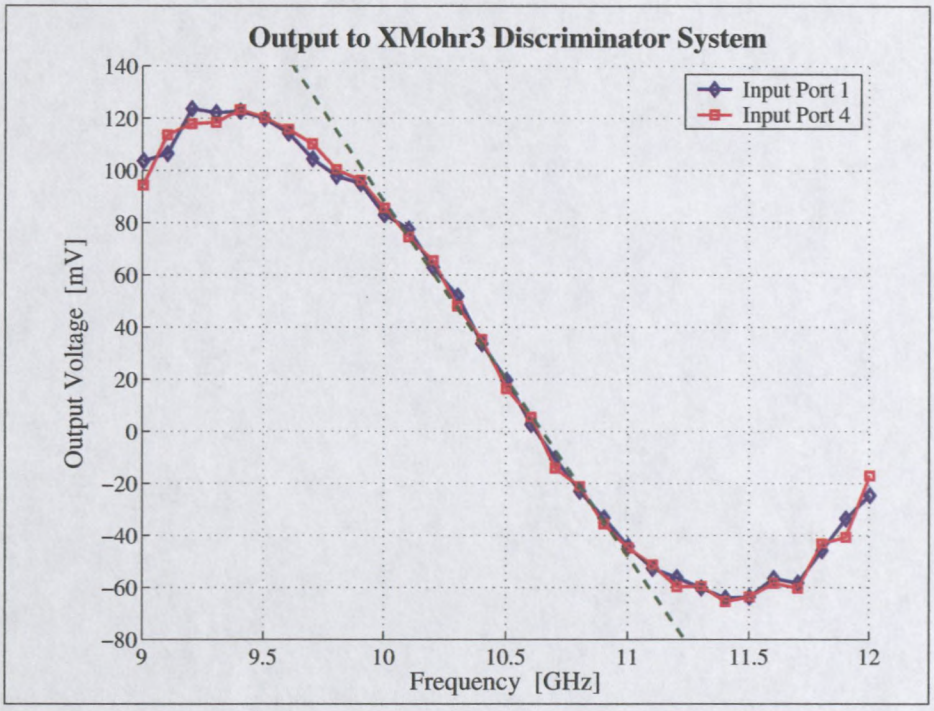

(a) Output Voltage vs Frequency

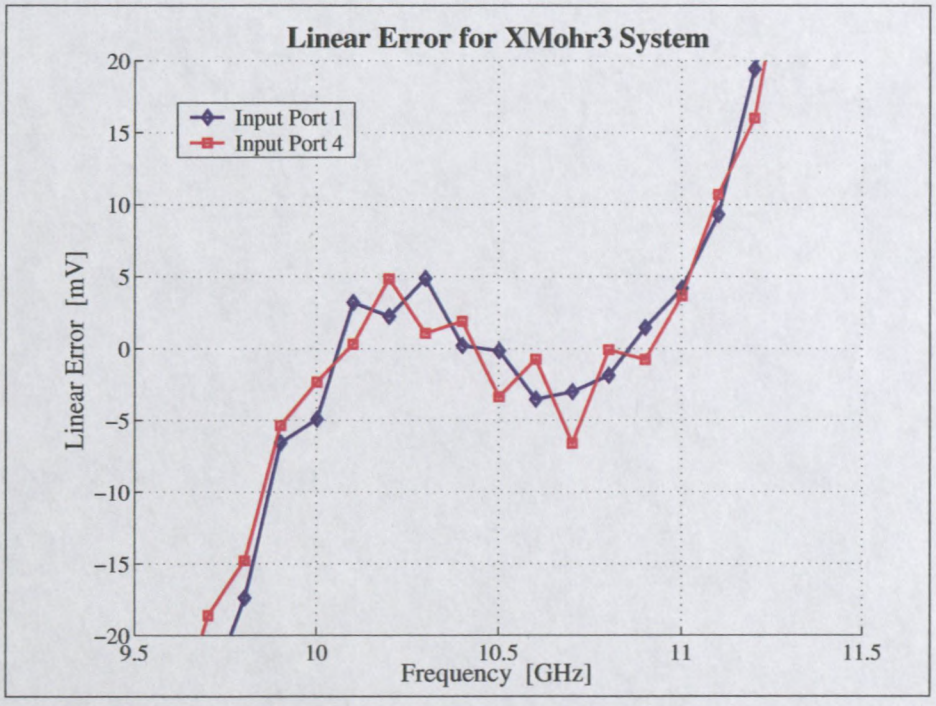

(b) Linear Error for Measurements

Figure 4.12: Measurements of the X-band Mohr Discriminator System.

The measurements are very good. The output voltages and linearized error functions are shown in Figure 4.12. The linear fit was done between 10 and 11 GHz, and has maximum errors of ±5 mV in this range. The detectors slightly degraded the linearity. Considering that the output voltage had ~5 mVp-p noise on it, these errors seem permissible. The S-curve of the discriminator is clearly visible, with a 20 mV dc-offset in the output voltage. The sensitivity was calculated to be ~13 mV/100MHz.

4.6 Conclusion

The topology of the discriminator system was shown, and aspects concerning the components thereof were discussed. Recommendations were made for the choice of detectors to be used. Linear detectors were used in the S- and X-band systems. These detectors were measured with a large load, and an equivalent load to the input impedance of the differential amplifier, to determine their response in the system.

A differential amplifier was built with a current-feedback amplifier, and measured with reasonable success. It does have a dc-offset and a possible non-symmetrical output, but it is believed that it does function as intended.

The complete systems were tested, and transfer functions plotted for the output voltage versus input frequency. The S-band system had a reasonable linearity over a small part of the S-curve. The detectors failed to do their job properly, and greatly reduced the system's bandwidth. The system had a sensitivity of around 0.2 V/100MHz.

The X-band system yielded much better results. The detector degraded the linearity, but it was still within ±4%. Due to the high losses in the system, the sensitivity was lower than expected. It was calculated to be ~13 mV/100MHz over the 1 GHz bandwidth of the system.

The discriminator systems were implemented with success, and can be used for numerous applications. It will be tested in the following chapter in the application of direct FM demodulation.

Chapter 5

Direct Demodulation System

In this chapter it will be shown how the S-band discriminator was implemented in a basic direct FM modulation/demodulation system. This was developed for a proposed 'Microwave Data Link'. The complete communication system will include many other modules such as amplifiers and filters. A block diagram of such a system is shown in Figure 5.1.

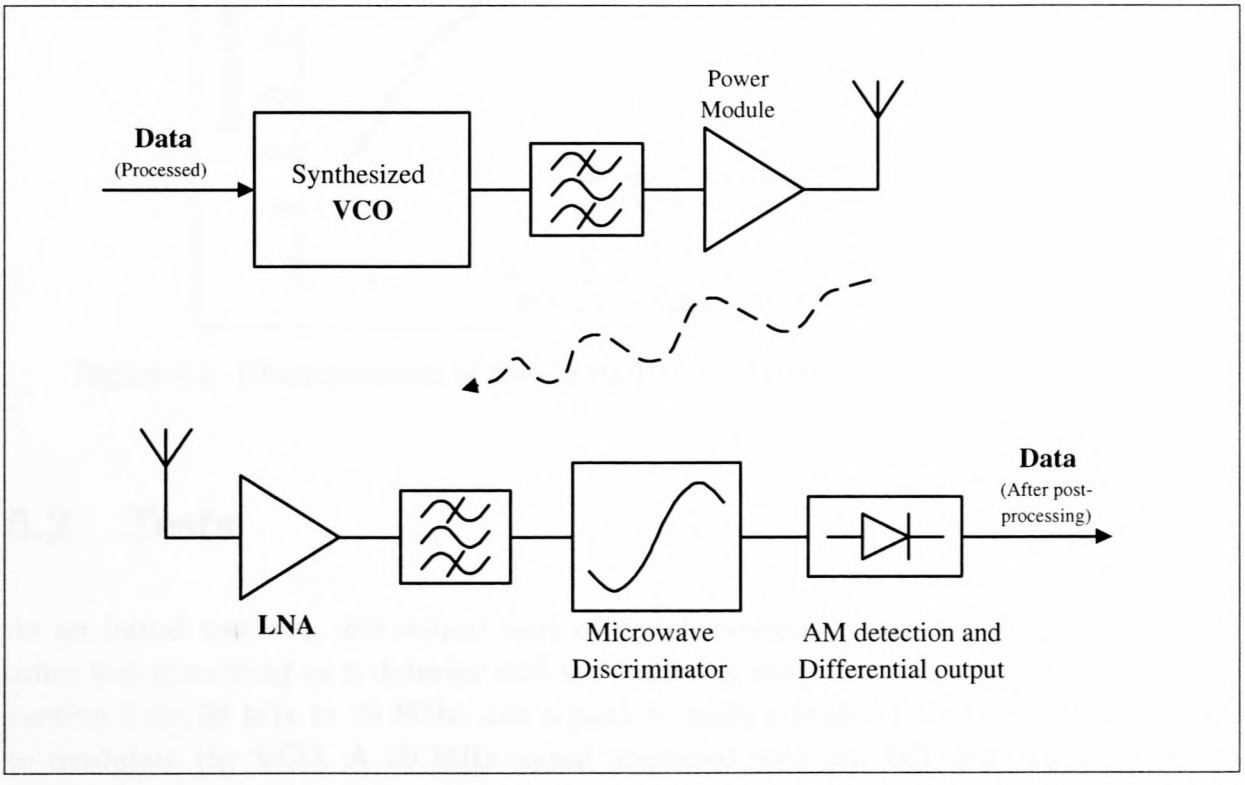

Figure 5.1: A direct FM modulation/demodulation system.

5.1 Topology and system characteristics

The setup of Figure 4.9 was used to test the communication system. A signal generator was used in the place of the dc-supply to modulate the VCO. The measurements discussed in Section 4.5.1, are shown in Figure 5.2 in a different form. It depicts the transfer function of the communication system, where the output voltage of the discriminator is plotted versus the control voltage of the VCO. For simplicity, the measured configurations will be referred to as setup 1 (P2(d057)-P3(d058×2)) and setup 2 (P3(d057)-P2(d058×2)). A photograph of the measurement setup is shown in Figure C.3.

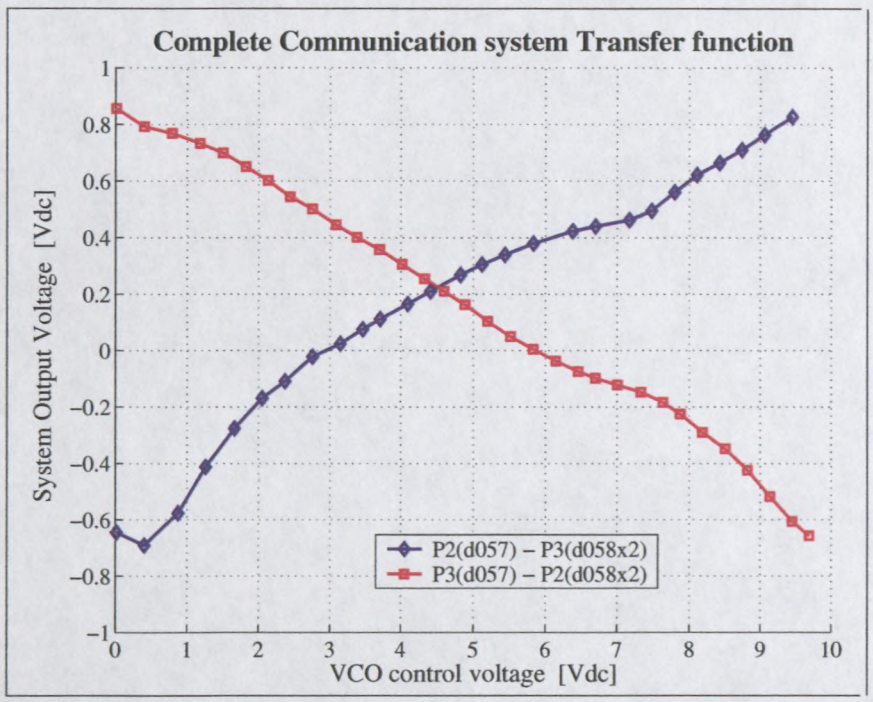

Figure 5.2: Characteristics of the direct FM modulation/demodulation system.

5.2 Tests

As an initial test run, one output port of the discriminator was terminated, while the other was connected to a detector and the buffering amplifier. Signals with frequencies varying from 50 kHz to 20 MHz, and a peak-to-peak voltage of about 7.9 V, were used to modulate the VCO. A 20 MHz signal measured with the 057 detector is shown in Figures 5.3 (a) and (b). Signals measured with the 058 detector, did not look as promising (see Figures 5.3 (c) and (d)). (All the screen-plots in the aforementioned figures have the same setup. In all the plots, those to follow as well, the top trace is measured at the input to the VCO, and the bottom trace is measured at the output of the differential amplifier.)

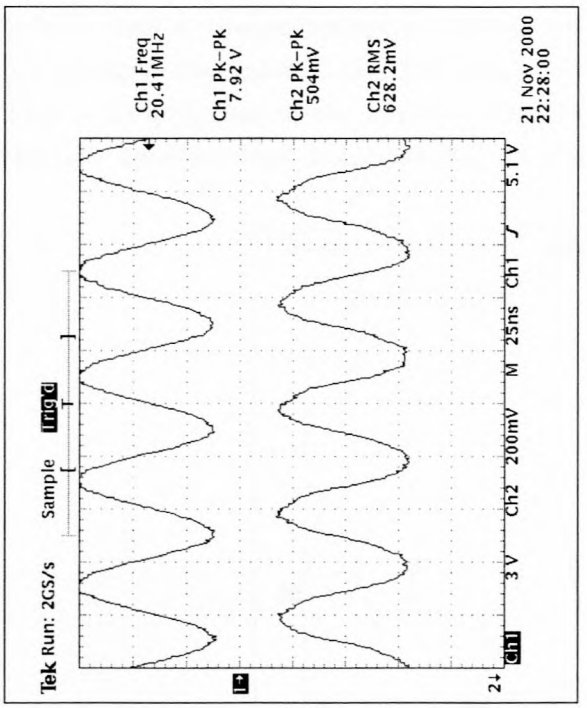

(a) d057 on P3 at 20 MHz

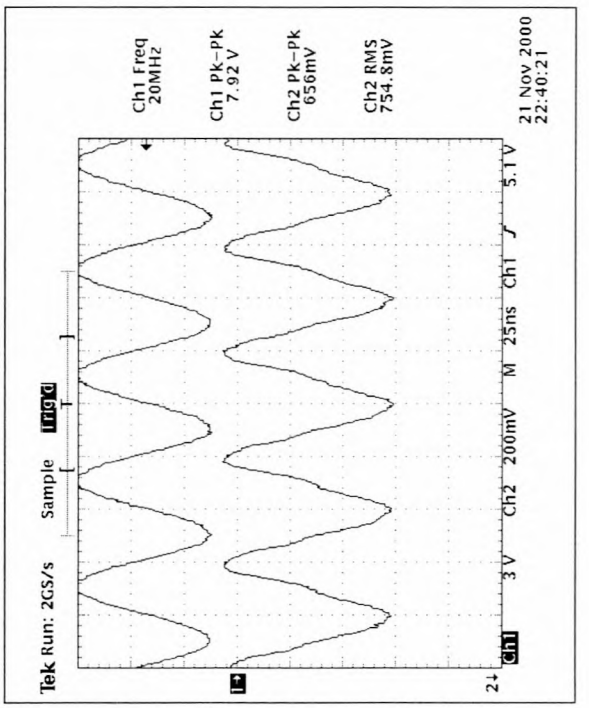

(b) d057 on P2 at 20 MHz

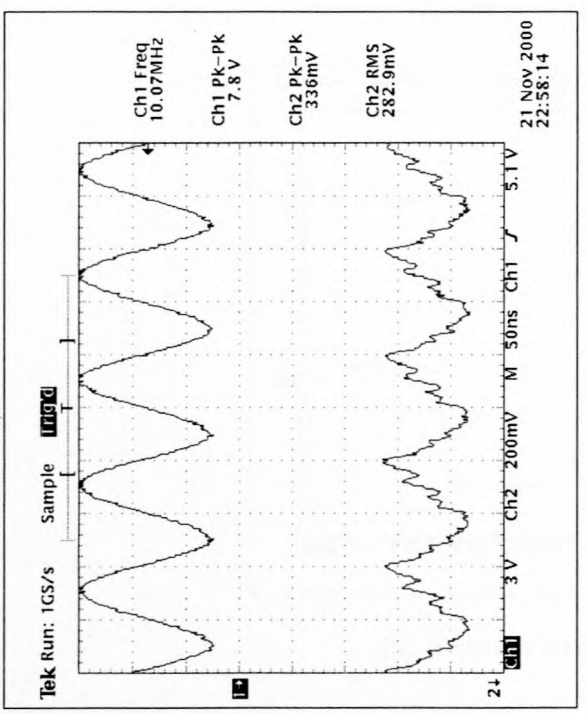

(c) d058 on P2 at 10 MHz

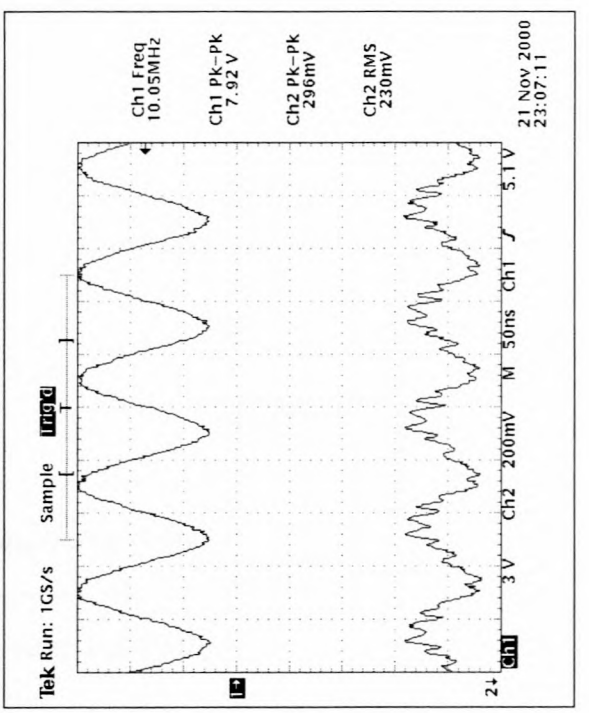

(d) d058 on P3 at 10 MHz

Figure 5.3: Measurements of signals going through the paths in the discriminator system.

As an example of how the system operate, the response to a single-frequency signal at 1 MHz and a square wave at 2 MHz, are plotted in Figure 5.4. The output signals are not always this smooth, and the input should be positioned correctly for a good response. This is largely due to the curves in the system's transfer function, but also the fact that the 058 detector was damaged and does not perform very well.

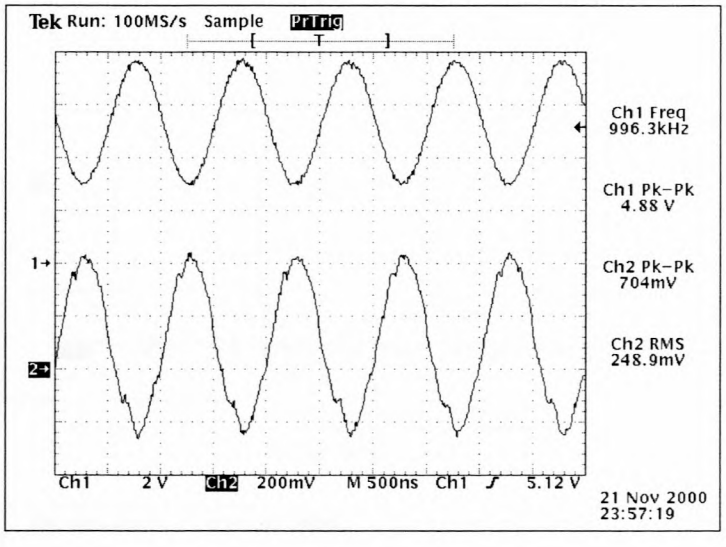

(a) A sinusoid on setup 2 at 1 MHz

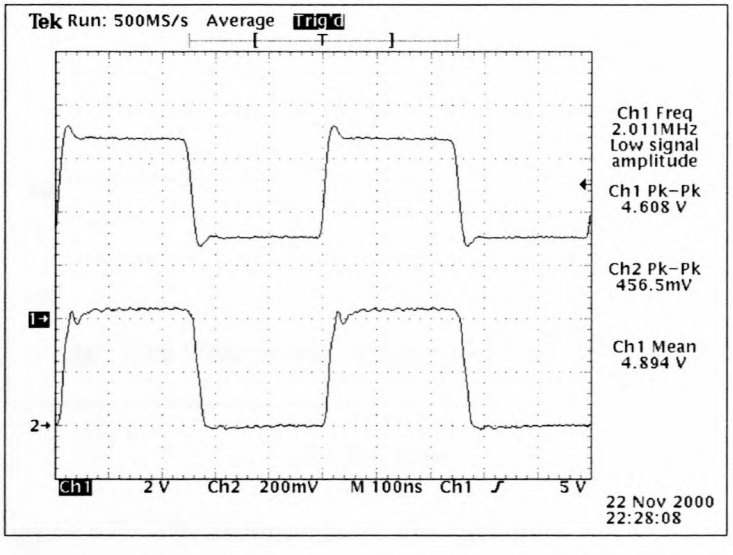

(b) A square wave on setup 1 at 2 MHz

Figure 5.4: Measurements of signals transmitted through the communication system.

The rise- and fall-times of the system was also tested (see Figure 5.5). The signal which was used to test these times with, are quite slow (>20 ns from a low to a high), and it

seems as though the output follows the input to our system very well. A system delay of about 10 ns was measured in both cases.

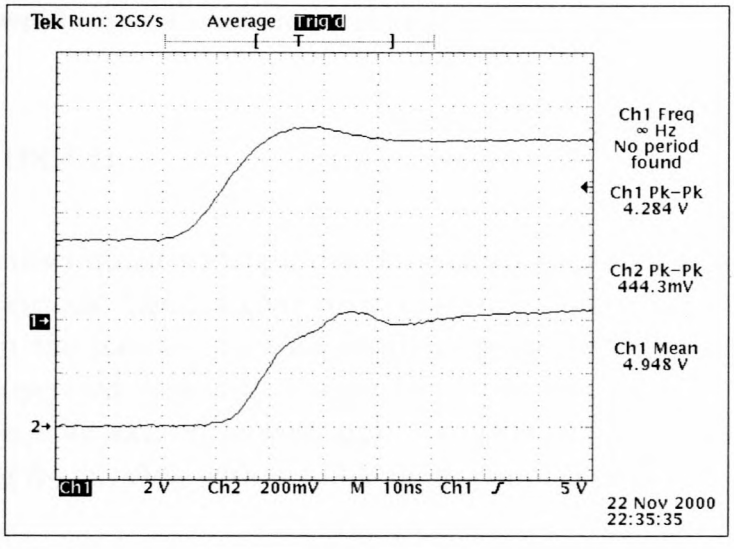

(a) Rise time

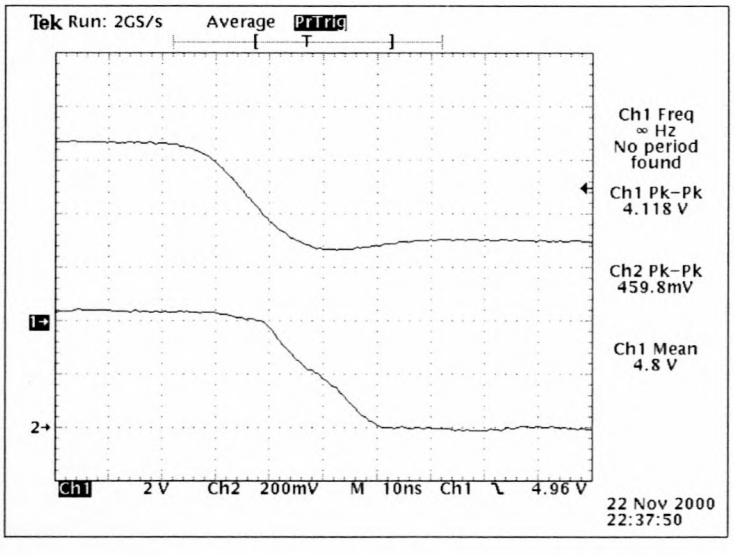

(b) Fall time

Figure 5.5: Measurements of the system's performance.

Digital communication possible

The square wave input shown in Figure 5.4 (b), has peak levels of 3 V and 7 V, which correspond to frequencies of 2.3 GHz and 2.6 GHz. The output waveform has voltage levels of 0 V and 0.45 V. It is clear that digital communication can be made possible with such a system. This example is the simplest form of FSK.

This application can be expanded with more bits in the digital signal at a higher frequency. There was not enough time in this research to develop a higher frequency test signal, with possibly more than two levels, but with the measured characteristics, it looks possible that this system will be able to handle much higher frequencies.

5.3 Conclusion

The S-band Mohr discriminator system was successfully employed as a direct demodulator of wide-band FM signals. The complete communication system has a fairly linear transfer function. Though the initial tests with single detectors were not very promising, the complete system operated very well. Except for the 10 ns time delay of the system, the output follows the input extremely well, and this system should be able to handle much higher modulating frequencies, with possible digital applications.

Conclusion

This was an introduction to the world of microwave frequency discriminators. Numerous techniques were discussed from articles, dating back as far as 1946. The techniques discussed here range from high-Q narrow-band discriminators, to super wide-band discriminators. They can be implemented in various applications.

The Mohr technique was implemented in the development of two discriminators at S- and X-band. These discriminators worked very well, with highly linear S-curves, and wide to medium bandwidths. Discriminator systems were developed to test the discriminators. These systems worked well, despite problems with the detectors at S-band, and extra losses in the X-band system.

The S-band discriminator system was employed as a direct FM demodulator. The complete modulation/demodulation system worked fairly well. It could not be tested to its extreme, but it is believed that it is able of handling much higher data rates as that imposed on it.

The knowledge gained through this thesis should serve as a foundation for future research at this university, since there are still many unexplored facets of these devices and their applications.

Bibliography

[1] P. H. Young, *Electronic Communication Techniques*, pp. 360–374. New York: Macmillan Publishing Company, third ed., 1994.

[2] J. G. Proakis and M. Salehi, *Communication Systems Engineering*, pp. 343–351. New Jersey: Prentice Hall International, 1994.

[3] R. E. Ziemer and W. H. Tranter, *Principles of Communications*, pp. 185–191,214–215. New York: John Wiley & Sons, Inc., fourth ed., 1995.

[4] S. N. Van Voorhis, *Microwave Receivers*, pp. 28–29,35–38. New York: McGraw-Hill Book Company, Inc., first ed., 1948.

[5] Z. Kuan-Jie and L. Fu-Hua, "Direct Microwave Modulation and Demodulation," *MTT-S International Microwave Symposium Digest*, pp. 547–549, 1983.

[6] J. A. Hall, R. D. Pering, and D. J. Mellor, "2.6 GHz Satellite TV Broadcast Receiver," *G-MTT International Microwave Symposium Digest of Technical Papers*, pp. 196–197, 1973.

[7] B. Glance and W. W. Snell, Jr., "A Discriminator-Stabilized Microstrip Oscillator (Short Papers)," *IEEE Transactions on Microwave Theory and Techniques*, vol. 24, pp. 648–650, Oct 1976.

[8] S. J. Fiedziuszko, "High Q Dielectric Resonator Frequency Discriminator," *MTT-S International Microwave Symposium Digest*, pp. 175–176, 1987.

[9] R. V. Pound, "Electronic frequency stabilization of microwave oscillators," *Review of Scientific Instruments*, vol. 17, pp. 490–505, Nov 1946.

[10] R. V. Pound, "Frequency Stabilization of Microwave Oscillators," *Proceedings of the IRE*, vol. 35, pp. 1405–1415, Dec 1947.

[11] W. R. Day, Jr., "Dielectric Resonators as Microstrip Circuit Elements," *G-MTT International Microwave Symposium Digest of Technical Papers*, pp. 24–28, 1970.

[12] A. G. Mann, "Active Stabilization of Crystal Oscillator FM Noise at UHF Using a Dielectric Resonator," *IEEE Transactions on Microwave Theory and Techniques (Short Papers)*, vol. 33, pp. 51–53, Jan 1985.

[13] S. Andersson, "Frequency-Discriminator-Stabilized Oscillators with Common Resonators," *Microwave and Optical Technology Letters*, vol. 21, pp. 417–423, June 1999.

[14] M. J. Bianchini, J. B. Cole, R. DiBiase, Z. Galani, R. W. Laton, and R. C. Waterman, Jr., "A Single-Resonator GaAs FET Oscillator with Noise Degeneration," *MTT-S International Microwave Symposium Digest*, pp. 270–273, 1984.

[15] Z. Galani, M. J. Bianchini, R. C. Waterman, Jr., R. DiBiase, R. W. Laton, and J. B. Cole, "Analysis and Design of a Single-Resonator GaAs FET Oscillator with Noise Degeneration," *IEEE Transactions on Microwave Theory and Techniques*, vol. 32, pp. 1556–1565, Dec 1984.

[16] J. Ruan, "Steady-state quasi-steady-state and transient-state analysis of delay line discriminators for FM noise measurement," *MTT-S International Microwave Symposium Digest*, pp. 289–290, 1987.

[17] J. R. Ashley, C. B. Searles, and F. M. Palka, "The Measurement of Oscillator Noise at Microwave Frequencies," *IEEE Transactions on Microwave Theory and Techniques*, vol. 16, pp. 753–760, Sept 1968. (Special Issue on Noise).

[18] J. R. Ashley, T. A. Barley, and G. J. Rast, Jr., "The Measurement of Noise in Microwave Transmitters," *IEEE Transactions on Microwave Theory and Techniques*, vol. 25, pp. 294–318, April 1977. (Special Issue on Low-Noise Technology).

[19] R. S. Brozovich, "A Unified Analysis of Transmission Line Discriminators for FM Noise Measurements," *MTT-S International Microwave Symposium Digest*, pp. 369–371, 1983.

[20] R. S. Brozovich and J. R. Ashley, "An Analysis of the AC Bandwidth of Transmission Line Discriminators for FM Noise Measurement," *MTT-S International Microwave Symposium Digest*, pp. 513–514, 1984.

[21] K. Watanabe and I. Takao, "Microwave Oscillator Noise Measuring System Employing a YIG Discriminator," *IEEE Transactions on Microwave Theory and Techniques (Short Papers)*, vol. 22, pp. 444–446, Apr 1974.

[22] H. Barth, "MM-Wave Frequency Discriminator Aids Reduction of Oscillator Chirp," *MTT-S International Microwave Symposium Digest*, pp. 133–135, 1983.

[23] N. E. Goddard, "Instantaneous Frequency-Measuring Receivers," *IEEE Transactions on Microwave Theory and Techniques (Letters)*, vol. 20, pp. 292–293, Apr 1972.

[24] R. G. Ranson and S. G. Gibbons, "A Rapid Channel Detection System for EW Receivers," *MTT-S International Microwave Symposium Digest*, vol. II, pp. 961–963, 1990.

[25] C. Sinclair, "A Coplanar Waveguide 6–18 GHz Instantaneous Frequency Measurement Unit for Electronic Warfare Systems," *MTT-S International Microwave Symposium Digest*, vol. III, pp. 1767–1770, 1994.

[26] N. D. Geldenhuys, "Mikrostrook Filter Optimering." Skripsie, November 1998. pp. 13–18.

[27] R. J. Mohr, "Broadband Microwave Discriminator," *IEEE Transactions on Microwave Theory and Techniques (Correspondence)*, vol. 11, pp. 263–264, July 1963.

[28] M. L. Sisodia and O. P. Gandhi, "Octave Bandwidth L- and S-band Stripline Discriminators," *IEEE Transactions on Microwave Theory and Techniques (Correspondence)*, vol. 15, pp. 271–272, April 1967.

[29] S. R. Mishra and R. P. Wadhwa, "Development of an X-band Waveguide Frequency Discriminator," *IEEE Transactions on Microwave Theory and Techniques (Correspondence)*, vol. 18, pp. 660–661, Sep 1970.

[30] L. I. Reber, "Improved performance in phase discriminators," *Microwaves*, pp. 48–52, May 1971.

[31] H. F. Lenzing, "An L-Band, High Baud-Rate DCPSK Detector/AFC Discriminator in Microstrip," *G-MTT International Microwave Symposium Digest of Technical Papers*, pp. 201–203, 1972.

[32] U. H. Gysel and J. P. Watjen, "Wide-Band Frequency Discriminator with High Linearity," *MTT-S International Microwave Symposium Digest*, pp. 373–376, 1977.

[33] S. J. Robinson, "Broadband Microwave Discriminator (Comments)," *IEEE Transactions on Microwave Theory and Techniques*, vol. 12, pp. 255–256, March 1964.

[34] H. G. Cho and C. W. Lee, "Microwave Transmission Line Frequency Discriminators," *MTT-S International Microwave Symposium Digest*, pp. 279–282, 1986.

[35] C. W. Lee and W. Y. Seo, "Super wide-band FM line discriminator," *Proceedings of the IEEE*, vol. 51, pp. 1675–1676, Nov 1963.

[36] C. W. Lee, "An analysis of a super wide-band FM line discriminator," *Proceedings of the IEEE*, vol. 52, pp. 1034–1038, Sep 1964.

[37] C. O. Risch, J. P. Singh, F. J. Rosenbaum, and R. O. Gregory, "A Low-Cost Multiple-Channel 12 GHz Receiver for Satellite Television Broadcasting," *IEEE Transactions on Microwave Theory and Techniques*, vol. 23, pp. 348–353, Apr 1975. Special Issue on Microwave Communications.

[38] M. D. Bonfield, M. J. Bonomi, and E. G. Jaasma, "An Integrated Microwave FM Discriminator," *MTT International Microwave Symposium Digest and Technical Program*, pp. 139–146, 1968.

[39] W. Y. Seo, "Microwave Discriminator for above 10 GHz," *Proceedings of the IEEE (Correspondence)*, vol. 53, p. 179, Feb 1965.

[40] R. M. Vaillancourt, "Errors in a Magic-Tee Phase Changer," *IRE Transactions on Microwave Theory and Techniques*, vol. 5, pp. 204–207, July 1957.

[41] T. Sieverding and F. Arndt, "Modal Analysis of the Magic Tee," *Microwave and Guided Wave Letters*, vol. 3, pp. 150–152, May 1993.

[42] J. Nigrin, N. A. Mansour, and W. A. G. Voss, "Single Hybrid Tee Frequency Discriminator," *IEEE Transactions on Microwave Theory and Techniques (Letters)*, vol. 23, pp. 776–778, Sept 1975.

[43] P. Z. Peebles, Jr. and A. H. Green, Jr., "A Microwave Discriminator at 35 GHz," *Proceedings of the IEEE*, vol. 68, pp. 286–288, Feb 1980.

[44] T. P. Chattopadhyay and B. N. Biswas, "Improved X-Band FM Discriminator," *IEEE Transactions on Microwave Theory and Techniques*, vol. 34, pp. 442–446, April 1986.

[45] T. P. Chattopadhyay, "An Injection-Locked Hybrid Microwave Discriminator," *Proceedings of the IEEE*, vol. 74, pp. 746–748, May 1986.

[46] T. P. Chattopadhyay, "Practical Aspects of the Injection-Locked Hybrid Discriminator," *IEEE Transactions on Microwave Theory and Techniques*, vol. 35, pp. 195–200, Febr 1987.

[47] T. P. Chattopadhyay and M. Bhattacharya, "A Novel Microwave Limiter-Discriminator: Design and Analysis," *IEEE Microwave and Guided Wave Letters*, vol. 2, pp. 108–110, March 1992.

[48] B. N. Biswas, S. Chatterjee, S. Sarkar, A. K. Bhattacharya, and S. K. Ray, "Bias-Tuned Injection-Locked Discriminators," *IEEE Transactions on Microwave Theory and Techniques*, vol. 35, pp. 812–818, Sept 1987.

[49] B. N. Biswas, A. P. Sinha, P. Lahiri, and D. Mondal, "Unconditionally Stable Tracking Discriminator at 35 GHz," *IEEE Transactions on Microwave Theory and Techniques*, vol. 41, pp. 388–394, March 1993.

[50] R. Knöchel, K. Schünemann, and B. Schiek, "The Measurement of Noise in Microwave Transmitters (Comments)," *IEEE Transactions on Microwave Theory and Techniques*, vol. 27, pp. 84–85, Jan 1979.

[51] J. R. Ashley, T. A. Barley, and G. J. Rast, Jr., "Discriminator Theory (Comments)," *IEEE Transactions on Microwave Theory and Techniques*, vol. 31, pp. 605–606, July 1983.

[52] K. E. Schmegner, "A Single Chip Monolithic Integrated S-Band Frequency Discriminator," *MTT-S International Microwave Symposium Digest*, pp. 1333–1336, 1995.

[53] H. Gruchala and A. Rutkowski, "Frequency Detector with Power Combiner Dividers," *IEEE Microwave and Guided Wave Letters*, vol. 8, pp. 179–181, May 1998.

[54] P. Chiu, "A Practical UHF Multidiscriminator Unit," *IEEE Transactions on Microwave Theory and Techniques (Correspondence)*, vol. 11, pp. 88–89, Jan 1963.

[55] A. Podell, "A high directivity microstrip coupler technique," *G-MTT International Microwave Symposium Digest of Technical Papers*, pp. 33–36, 1970.

[56] J. Lange, "Interdigitated Stripline Quadrature Hybrid," *IEEE Transactions on Microwave Theory and Techniques (Correspondence)*, vol. 17, pp. 1150–1151, Dec 1969.

[57] J. Reed and G. J. Wheeler, "A Method of Analysis of Symmetrical Four-Port Networks," *IRE Transactions on Microwave Theory and Techniques*, vol. 4, pp. 246–252, Oct 1956.

[58] B. Mayer and R. Knöchel, "Branchline-Couplers with Improved Design Flexibility and Broad Bandwidth," *MTT-S International Microwave Symposium Digest*, pp. 391–394, 1990.

[59] R. K. Hoffmann, *Handbook of Microwave Integrated Circuits*, pp. 290–298. Norwood: Artech House, 1987.

[60] Program: MicroSim PSpice. MicroSim Corporation. Evaluation Version 8.0 – July 1997.

[61] Program: Microwave Office 2000. Applied Wave Research, Inc.

[62] Program: ZSyn. University of Stellenbosch.

[63] Program: Libra for Windows. EEsof Inc. USA, © 1983–1988.

Appendix A

Listings of Libra circuit files

In this appendix two of the circuit files used in Libra will be listed. They are d46c.ckt, which compare the microstrip and stripline S-band Mohr discriminator circuits, and discr3g.ckt, which compares two configurations which implemented the stub-type discriminator with a divider.

A.1 S-band Mohr discriminator

d46c.ckt – In microstrip and stripline substrates.

```
! MICROWAVE TRANSMISSION LINE FREQUENCY DISCRIMINATOR
! DISCRIMINATOR USING 2 3DB HYBRID COUPLERS AND
! EMPLOYING UNEVEN-LENGTH TRANSMISSION LINES
! ** CENTER-FREQUENCY AT 2.45GHZ
! ** COMPARING MICROSTRIP WITH STRIPLINE
!
! AUTHOR : NICO GELDENHUYS
! DATE   : 2000/05/31
! RECONSTRUCTED : 2000/09/15
!

DIM
   FREQ  GHZ
   RES  OH
   COND  /OH
   IND  NH
   CAP  PF
   LNG  MM
   TIME  NS
   ANG  DEG
   VOL  V
   CUR  MA
   PWR  DBM
```

```
VAR
!MICROSTRIP PARAMETERS
!
  W50  = 1.80  !1.79
  W35  = 3.00
  W120 = 0.35  !0.25
!IDEAL LENGTHS
  L59  = 19.09
  L39  = 18.70
  L129 = 20.12
!OPTIMIZED HYBRID LENGTHS
  L39M = 18.15  !18.15
  L39V = 19.50  !19.52
  L39B = 19.85  !19.84
!PATH A
  LA3  = 6.2
  LM3  = 6.50
!PATH B
  LBA3 = 5.90
  LBB3 = 18.95
  LBC3 = 6.00
  LBD3 = 48.6
!
!STRIPLINE PARAMETERS
!
  W50S  = 1.85  !1.86
  W35S  = 3.20  !3.19
  W120S = 0.30  !0.18
!IDEAL LENGTH
  L9    = 17.5
!OPTIMIZED HYBRID LENGTHS
  L9M = 18.30
  L9V = 17.20
  L9B = 16.95
!PATH A
  LAS = 6.00
  LMS = 5.50
!PATH B
  LBA = 5.05
  LBB = 17.85
  LBC = 5.00
  LBD = 45.5
!BEND EQUIVALENT LENGTH
  LC = 1.0
!IDEAL TOTAL LENGTHS
!STRIPLINE:
!  LA  = 17.5
!  LB  = 105   !N=5 => 6*LA
!MICROSTRIP:
!  LA2 = 19.09
!  LB2 = 114.54
!

CKT
!THREE-ARM BRANCHLINE HYBRID #1
   MSUB   ER=3.20 H=0.762 T=0.03 RHO=0 RGH=0
   TAND   TAND=0.005
!
   MLIN   5  6  W=W35  L=L39V
   MLIN   9 10  W=W35  L=L39V
   MLIN   7  8  W=W35  L=L39B
   MLIN  11 12  W=W35  L=L39B
   MLIN  17 18  W=W35  L=L39M
   MLIN  13 14  W=W120 L=L39M
   MLIN  15 16  W=W120 L=L39M
!
   MTEE2  1  5 13  W1=W50  W2=W35  W3=W120
   MTEE2  4  9 14  W1=W50  W2=W35  W3=W120
   MTEE   6  7 17  W1=W35  W2=W35  W3=W35
   MTEE  10 11 18  W1=W35  W2=W35  W3=W35
   MTEE2  2 15  8  W1=W50  W2=W120 W3=W35
   MTEE2  3 16 12  W1=W50  W2=W120 W3=W35
!
   DEF4P  1 2 3 4 TABLH1
!
!THREE-ARM BRANCHLINE HYBRID #2
   SSUB   ER=3.05 B=3.048 T=0.03 RHO=0
   TAND   TAND=0.005
!
   SLIN  5  6  W=W35S  L=L9V
   SLIN  9 10  W=W35S  L=L9V
   SLIN  7  8  W=W35S  L=L9B
   SLIN 11 12  W=W35S  L=L9B
   SLIN 17 18  W=W35S  L=L9M
   SLIN 13 14  W=W120S L=L9M
   SLIN 15 16  W=W120S L=L9M
!
   STEE  1  5 13  W1=W50S  W2=W35S  W3=W120S
   STEE  4  9 14  W1=W50S  W2=W35S  W3=W120S
   STEE  6  7 17  W1=W35S  W2=W35S  W3=W35S
   STEE 10 11 18  W1=W35S  W2=W35S  W3=W35S
   STEE  2 15  8  W1=W50S  W2=W120S W3=W35S
   STEE  3 16 12  W1=W50S  W2=W120S W3=W35S
!
   DEF4P  1 2 3 4 TABLH2
!
!MOHR'S DISCRIMINATOR #1
   MSUB   ER=3.20 H=0.762 T=0.03 RHO=0 RGH=0
   TAND   TAND=0.005
!
   TABLH1  1 5 6 4
   TABLH1  2 7 8 3
   RES     4 0 R=50
!
   MLIN    5  9  W=W50  L=LA3
   MBEND3  9 10  W=W50
   MLIN   10 11  W=W50  L=LM3
   MBEND3 11 12  W=W50
   MLIN   12  7  W=W50  L=LA3
!
   MLIN    6 13  W=W50  L=LBA3
   MBEND3 13 14  W=W50
   MLIN   14 15  W=W50  L=LBB3
   MBEND3 15 16  W=W50
   MLIN   16 17  W=W50  L=LBC3
   MBEND3 17 18  W=W50
   MLIN   18 19  W=W50  L=LBD3
   MBEND3 19 20  W=W50
   MLIN   20 21  W=W50  L=LBC3
   MBEND3 21 22  W=W50
   MLIN   22 23  W=W50  L=LBB3
   MBEND3 23 24  W=W50
   MLIN   24  8  W=W50  L=LBA3
!
   DEF3P  1 2 3 MOHR1
!
!MOHR'S DISCRIMINATOR #2
   SSUB   ER=3.05 B=3.048 T=0.03 RHO=0
   TAND   TAND=0.005
!
   TABLH2  1 5 6 4
   TABLH2  2 7 8 3
```

```
   RES     4 0 R=50
!
!   SLIN  5 7  W^W50S L^LA
!   SLIN  6 8  W^W50S L^LB
!
   SLIN    5  9  W^W50S L^LAS
   SLIN    9 10  W^W50S L^LC
   SLIN   10 11  W^W50S L^LMS
   SLIN   11 12  W^W50S L^LC
   SLIN   12  7  W^W50S L^LAS
!
   SLIN    6 13  W^W50S L^LBA
   SLIN   13 14  W^W50S L^LC
   SLIN   14 15  W^W50S L^LBB
   SLIN   15 16  W^W50S L^LC
   SLIN   16 17  W^W50S L^LBC
   SLIN   17 18  W^W50S L^LC
   SLIN   18 19  W^W50S L^LBD
   SLIN   19 20  W^W50S L^LC
   SLIN   20 21  W^W50S L^LBC
   SLIN   21 22  W^W50S L^LC
   SLIN   22 23  W^W50S L^LBB
   SLIN   23 24  W^W50S L^LC
   SLIN   24  8  W^W50S L^LBA
!
   DEF3P  1 2 3 MOHR2
!

FREQ
  SWEEP 0.4 4.5 0.01
!  SWEEP 0.5 9.5 0.02

GRID
  FREQ 0.4 4.5 0.41
!  FREQ 0.5 9.5 0.45
  GR1 -40 0 5
  GR2 -40 0 5
  GR3 -40 0 5
  GR4 -40 0 5
!  FREQ 1.65 3.25 0.08
  GR5 0 1 0.05
  GR6 -10 10 1
  GR7 -1 1 0.1

OUTVAR
  OUT1 = MOHR1 S21
  OUT2 = MOHR1 S31
  OUT12 = MOHR2 S21
  OUT22 = MOHR2 S31
  M_OUT11 = MOHR1 MAG[S21]
  M_OUT21 = MOHR1 MAG[S31]
  M_OUT12 = MOHR2 MAG[S21]
  M_OUT22 = MOHR2 MAG[S31]

OUTEQN
  RATIO = OUT1/OUT2
  RATIO2 = OUT12/OUT22
  DIV1 = M_OUT11-M_OUT21
  DIV2 = M_OUT12-M_OUT22

OUT
  MOHR1 DB[S11] GR1
  MOHR1 DB[S22] GR1
  MOHR1 DB[S33] GR1
!
  MOHR2 DB[S11] GR2
  MOHR2 DB[S22] GR2
  MOHR2 DB[S33] GR2
!
  MOHR1 DB[S32] GR3
  MOHR2 DB[S32] GR3
!
  MOHR1 DB[S21] GR4
  MOHR1 DB[S31] GR4
  MOHR2 DB[S21] GR4
  MOHR2 DB[S31] GR4
!
  MOHR1 MAG[S21] GR5
  MOHR1 MAG[S31] GR5
  MOHR2 MAG[S21] GR5
  MOHR2 MAG[S31] GR5
!
  OUTEQN DB[RATIO] GR6
  OUTEQN DB[RATIO2] GR6
!
  OUTEQN RE[DIV1] GR7
  OUTEQN RE[DIV2] GR7

OPT
  RANGE 2.0 2.9
  MOHR2 DB[S23] < -18
  MOHR2 DB[S22] < -18
  MOHR2 DB[S33] < -18
  MOHR2 DB[S11] < -18
```

A.2 Discriminator using 3 dB binary power divider and stubs.

discr3g.ckt – Two configurations in microstrip. (These would have been built as well, but there were problems with the substrate, and it was abandoned.)

```
! MICROWAVE TRANSMISSION LINE FREQUENCY DISCRIMINATOR
! WIDEBAND DISCRIMINATOR USING 3DB BINARY POWER DIVIDER
! CENTER-FREQUENCY AT 2.45GHZ
!
! AUTHOR : NICO GELDENHUYS
! DATE   : 2000/06/07       RECONSTRUCTED : 2000/09/15
!

DIM
   FREQ  GHZ
   RES  OH
   COND  /OH
   IND  NH
   CAP  PF
   LNG  MM
   TIME  NS
   ANG  DEG
   VOL  V
   CUR  MA
   PWR  DBM

CKT
!DISCRIMINATOR #1
   MSUB   ER=3.2 H=0.762 T=0.03 RHO=0 RGH=0
   TAND   TAND=0.005
!
   MLIN    1 20  W=1.79  L=3.5
   MTEE2  21 22 20  W1=0.97 W2=0.97 W3=1.79
!WILKINSON DIVIDER
   MLIN   21 3   W=0.97  L=2.00
   MLIN   22 4   W=0.97  L=2.00
   MBEND3  3 5   W=0.97
   MBEND3  4 6   W=0.97
   MLIN    5 7   W=0.97  L=17.0  !15.62  !16.52
   MLIN    6 8   W=0.97  L=17.0  !15.62  !16.52
!CROSSES AND ISOLATING RESISTOR
   MCROS2  7  9 10 11  W1=0.97 W2=1.79 W3=1.79 W4=1.79
   MCROS2  8 12 13 14  W1=0.97 W2=1.79 W3=1.79 W4=1.79
   MLIN   11 15  W=1.79 L=1.75
   MLIN   12 16  W=1.79 L=1.75
   RES    15 16  R=100
!STUBS
   MLSC    9     W=1.79  L=10.5  !8.66  !9.55
   MLOC   14     W=1.79  L=10.5  !8.66  !9.55
!OUTPUT
   MLIN   10 17  W=1.79  L=5
   MLIN   13 18  W=1.79  L=5
!
   DEF3P  1 17 18  DIV1
!
!
!DISCRIMINATOR #2
   MSUB   ER=3.2 H=0.762 T=0.03 RHO=0 RGH=0
   TAND   TAND=0.005
!
   MLIN    1 20   W=1.79  L=3.90
```

```
   MTEE2  21 22 20  W1=0.97 W2=0.97 W3=1.79
!WILKINSON DIVIDER
   MLIN   21 3   W=0.97  L=2.0
   MLIN   22 4   W=0.97  L=2.0
   MBEND2  3 5   W=0.97
   MBEND2  4 6   W=0.97
   MLIN    5 7   W=0.97  L=17.0  !15.62  !16.52
   MLIN    6 8   W=0.97  L=17.0  !15.62  !16.52
!CROSSES AND ISOLATING RESISTOR
   MCROS2  7 11 10  9  W1=0.97 W2=1.79 W3=1.79 W4=1.79
   MCROS2  8 14 13 12  W1=0.97 W2=1.79 W3=1.79 W4=1.79
   MLIN   11 15  W=1.79 L=1.75
   MLIN   12 16  W=1.79 L=1.75
   RES    15 16  R=100
!STUBS
   MLIN    9 19  W=1.79  L=10.25  !8.66  !9.55
   MLOC   14     W=1.79  L=10.25  !8.66  !9.55
   MLIN   19 0   W=20.0  L=4.00
!OUTPUT
   MLIN   10 17  W=1.79  L=5
   MLIN   13 18  W=1.79  L=5
!
   DEF3P  1 17 18  DIV2

FREQ
  SWEEP 0.4 4.5 0.01

GRID
  FREQ 0.4 4.5 0.41
  GR1 -25 0 5
  GR2 -40 0 5
  GR3 -40 0 5
  FREQ 1.65 3.25 0.08
  GR4 -1.5 1.5 0.3

OUTVAR
  OUT1 = DIV1 S21
  OUT2 = DIV1 S31
  OUT12 = DIV2 S21
  OUT22 = DIV2 S31

OUTEQN
  RATIO = OUT1/OUT2
  RATIO2 = OUT12/OUT22

OUT
  DIV1 DB[S11] SCN
  DIV1 DB[S22] GR1
  DIV1 DB[S33] GR1
!
  DIV2 DB[S11] SCN
  DIV2 DB[S22] GR1
  DIV2 DB[S33] GR1
!
  DIV1 DB[S23] GR2
  DIV2 DB[S23] GR2
!
  DIV1 DB[S21] GR3
  DIV1 DB[S31] GR3
  DIV2 DB[S21] GR3
  DIV2 DB[S31] GR3
!
  OUTEQN DB[RATIO] GR4
  OUTEQN DB[RATIO2] GR4
  OUTEQN MAG[RATIO] GR4
  OUTEQN MAG[RATIO2] GR4
```

Appendix B

Measurements and Simulations

B.1 EM-simulation of the ring-structure in XMohr3

The current distribution in the copper, and the electric field distribution over the dielectric, are shown with a cool-to-hot colour scheme in Figure B.1. The edges of the structure have perfect conductors which is grounded. They cause some extra electric fields around the ports and on the outside edges of the ring. Their are also some electric fields coupling from the left- and right-hand sides of the ring. The analysis with this structure yielded similar results to the previous analysis. It was then assumed that the coupling across the ring will not greatly effect the performance of the hybrids.

B.2 XMohr1 and XMohr2 measurements

The devices were measured with consecutive two-port measurements, from which selected curves will be shown here. The S_{11} and S_{33} reflection coefficients, the isolation and the transmission coefficients of both discriminators are shown in Figure B.2. The devices were not well matched, and the transmission coefficients seem to have a ripple in their response.

B.3 Op-amp Measurements

The op-amp measurements are discussed in Section 4.3.1. The tabulated values given here, shows that the op-amp has equal power to output voltage transfers from the two input ports, though the input voltages differ at the inverting (V-) and non-inverting (V+) ports.

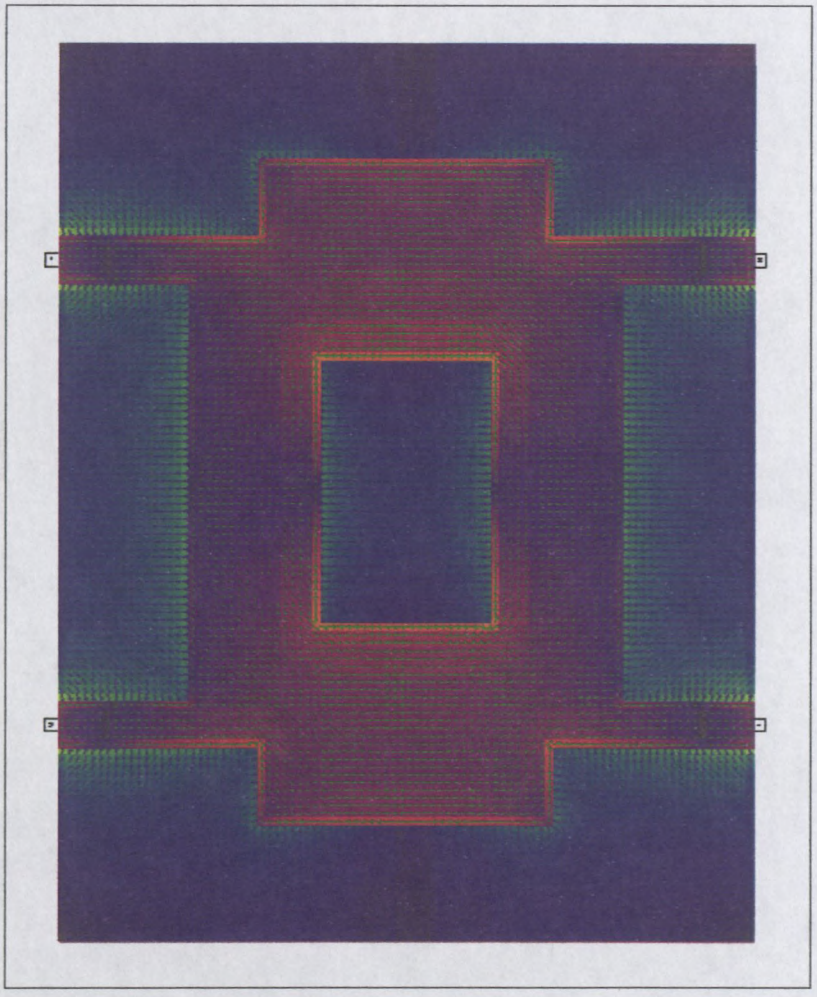

Figure B.1: Result of the EM-simulation of the ring-structure of the stripline X-band Mohr discriminator.

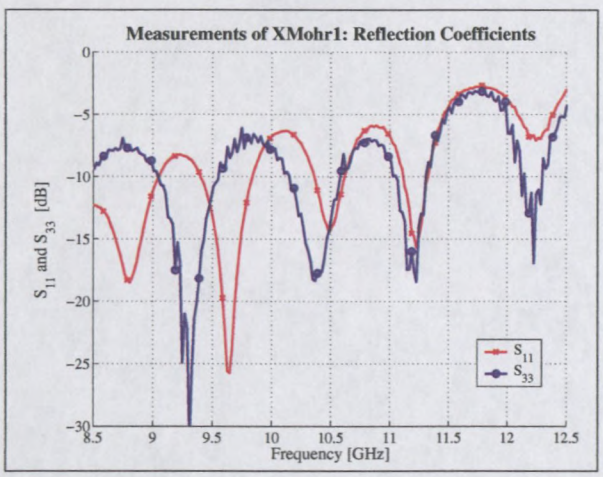

(a) XMohr1 Reflection Coefficients

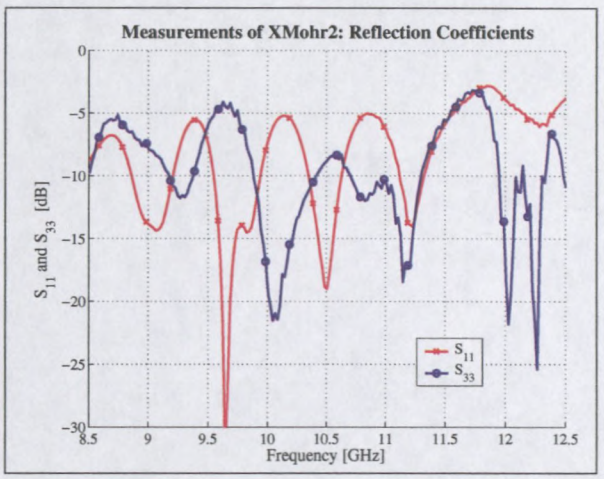

(b) XMohr2 Reflection Coefficients

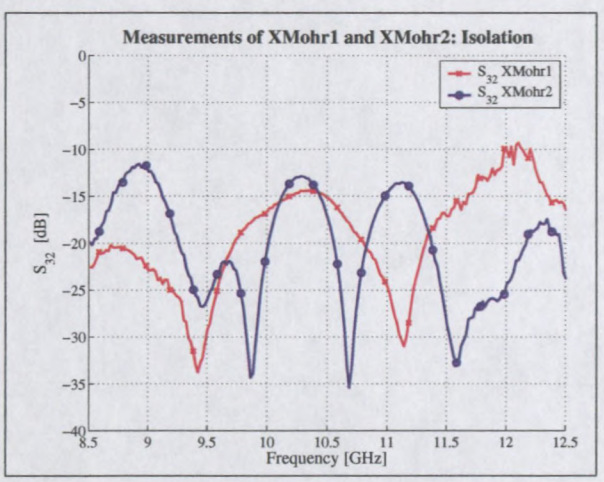

(c) Isolation

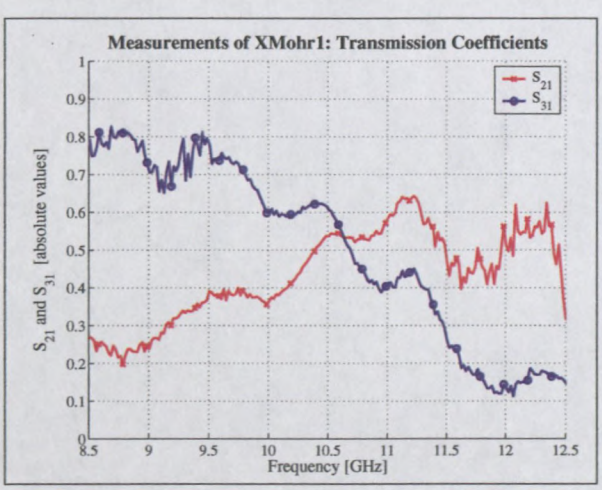

(d) XMohr1 Transmission Coefficients

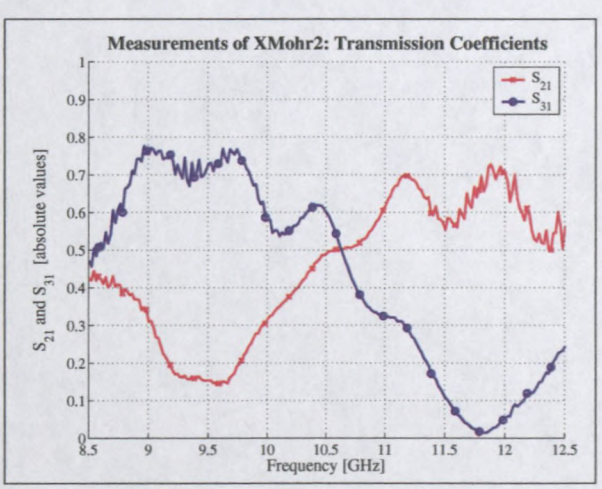

(e) XMohr2 Transmission Coefficients

Figure B.2: Measurements of the XMohr1 and XMohr2 X-band Mohr Discriminators.

Table B.1: Differential op-amp measurements of Gain vs Frequency.

Frequency	V+ in (V- grounded)			V+ in (V- loaded)		
	Vin	Vout	Gain	Vin	Vout	Gain
100k	531	878	1.653	544	788	1.449
200k	534	882	1.652	537	781	1.454
500k	533	880	1.651	534	776	1.453
1M	532	880	1.654	536	777	1.450
2M	533	878	1.647	533	776	1.456
5M	532	876	1.647	533	774	1.452
10M	540	892	1.652	543	791	1.457
25M	555	917	1.652	562	817	1.454
50M	604	915	1.515	596	831	1.394
75M	668	1080	1.617	668	968	1.449
100M	543	1270	2.339	521	1144	2.196
	V- in (V+ grounded)			V- in (V+ loaded)		
100k	470	778	1.655	467	776	1.662
200k	472	782	1.657	468	778	1.662
500k	470	780	1.660	469	780	1.663
1M	469	778	1.659	465	775	1.667
2M	468	776	1.658	465	773	1.662
5M	465	773	1.662	463	769	1.661
10M	475	785	1.653	471	783	1.662
25M	488	809	1.658	485	808	1.666
50M	558	894	1.602	555	887	1.598
75M	613	1000	1.631	609	1000	1.642
100M	625	1130	1.808	636	1140	1.792

The voltages are peak-to-peak values in mV, and the gain is the ratio Vout/Vin.
The input power level is at -10 dBm.

Table B.2: Op-amp measurements of Voltage Gain vs Power characteristics.

Pin	V- in (V+ loaded)			V+ in (V- loaded)			Buffer amp		
	Vin	Vout	Gain	Vin	Vout	Gain	Vin	Vout	Gain
-30	36	56	1.556	40.2	55.1	1.371	39.5	74.2	1.878
-25	59.6	95.1	1.596	66.7	95.4	1.430	65.2	125.7	1.928
-20	103	165	1.602	116	165	1.422	114	225.1	1.975
-15	182	296	1.626	206	296	1.437	202.2	395.5	1.956
-10	325	531	1.634	365	531	1.455	356	716	2.011
-6	509	829	1.629	582	845	1.452	565	1134	2.007
-3	713	1188	1.666	811	1190	1.467	795	1596	2.008
0	1010	1700	1.683	1160	1690	1.457	1136	2283	2.010
3	1430	2380	1.664	1620	2380	1.469	1591	3210	2.018
6	2040	3330	1.632	2320	3330	1.435	2270	4500	1.982

The voltages are peak-to-peak values in mV, and the gain is the ratio Vout/Vin.

Appendix C

Photos of the Discriminator Systems

The op-amp circuit used with the S-band system is shown in Figure C.1. On the left is the differential amplifier, and on the right the buffering amplifier. It is slightly modified for the X-band system. The S-band discriminator with the MICA detectors and the VCO present, is shown in Figure C.2. The complete direct modulation/demodulation system is shown in Figure C.3. The spectrum of the FM signal is monitored on the spectrum analyzer with a 'probe-antenna' lying over the VCO. The traces on the 400 MHz oscilloscope is: the input to the VCO at the top, and the output from the discriminator system at the bottom. The WaveTek signal generator used to test this system, is in the middle. The 2.0-18.0 GHz CW generator used for testing the detectors and the X-band system, is underneath the 22 GHz spectrum analyzer.

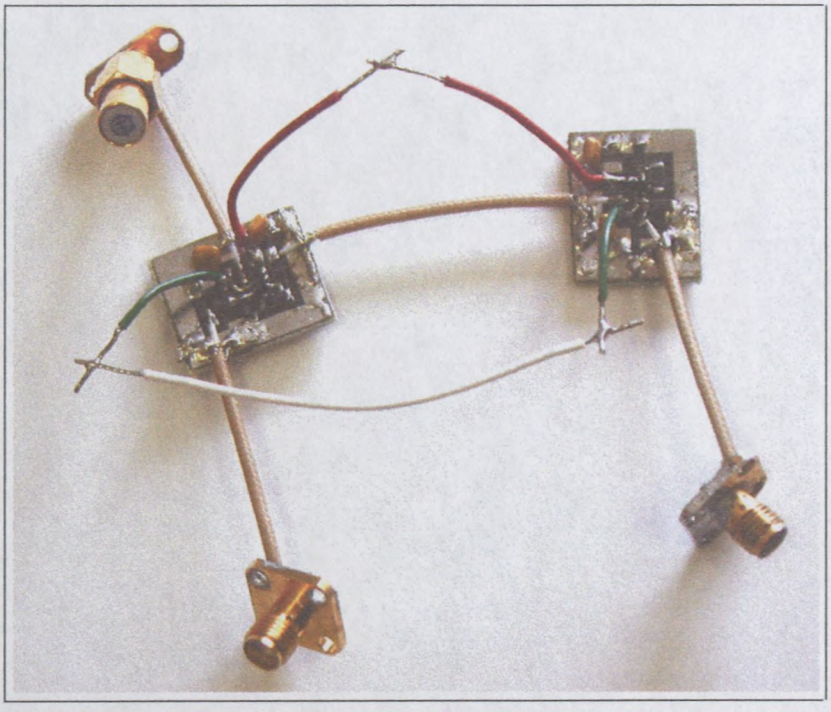

Figure C.1: Photo of the Op-amp circuit used. On the left is the differential amplifier, and on the right the buffering amplifier.

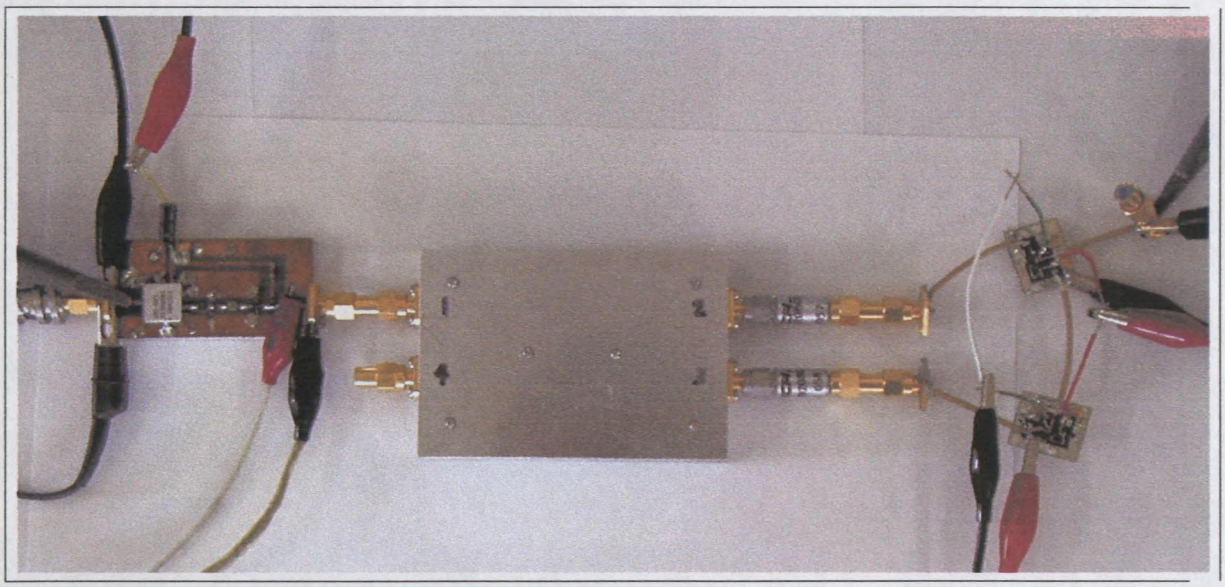

Figure C.2: Photo of the S-band Mohr Discriminator System, with the VCO on the left.

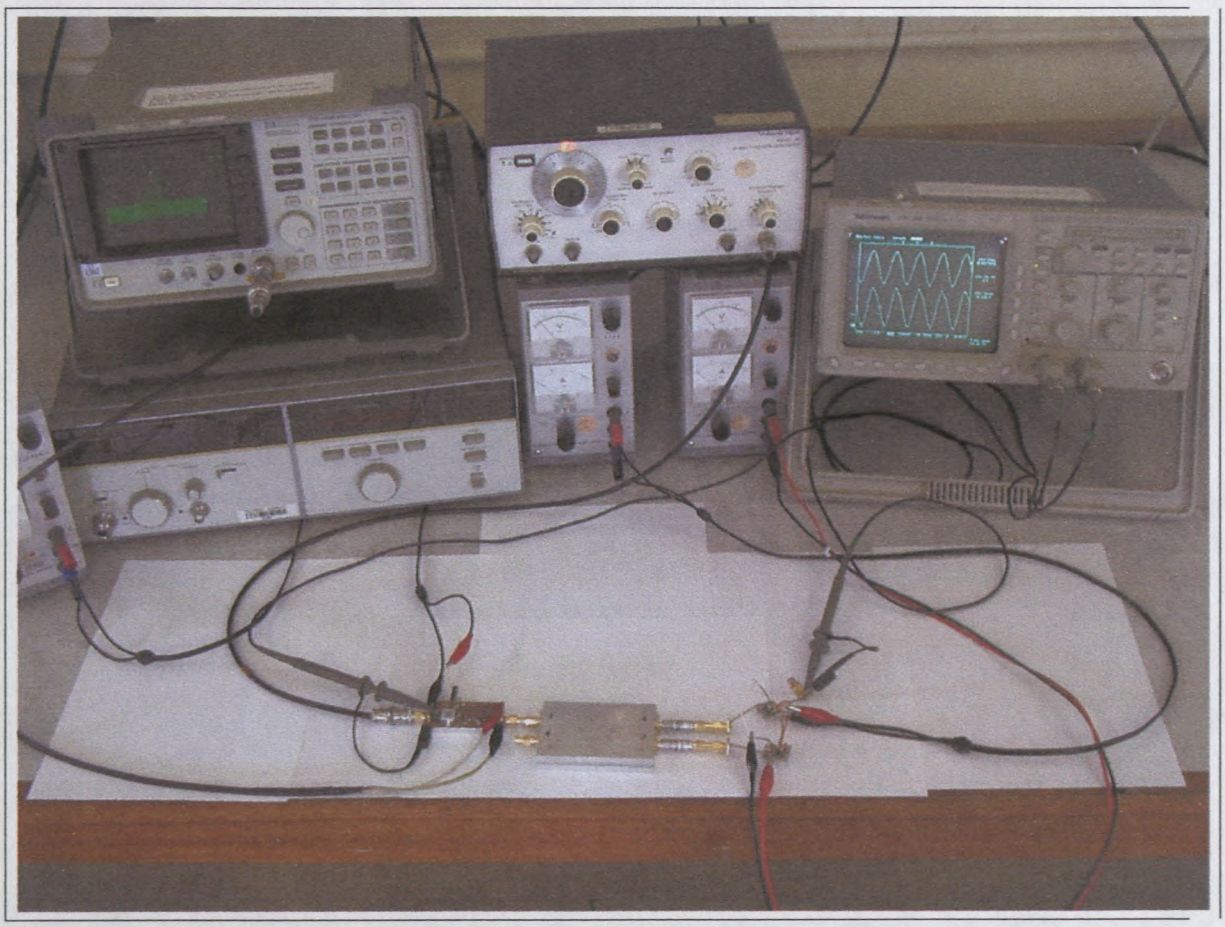

Figure C.3: Photo of the test setup for the Direct Modulation/Demodulation system.

The X-band discriminator system is shown in Figure C.4. Here port 4 is used as input, and port 1 is terminated. The internal structure is reflected by the drawing on the device. Ports 2 and 3 are connected with the N-type MI detectors through two semi-rigid coaxial cables, and numerous conversions. The op-amp circuit is modified to consist only of the differential amplifier.

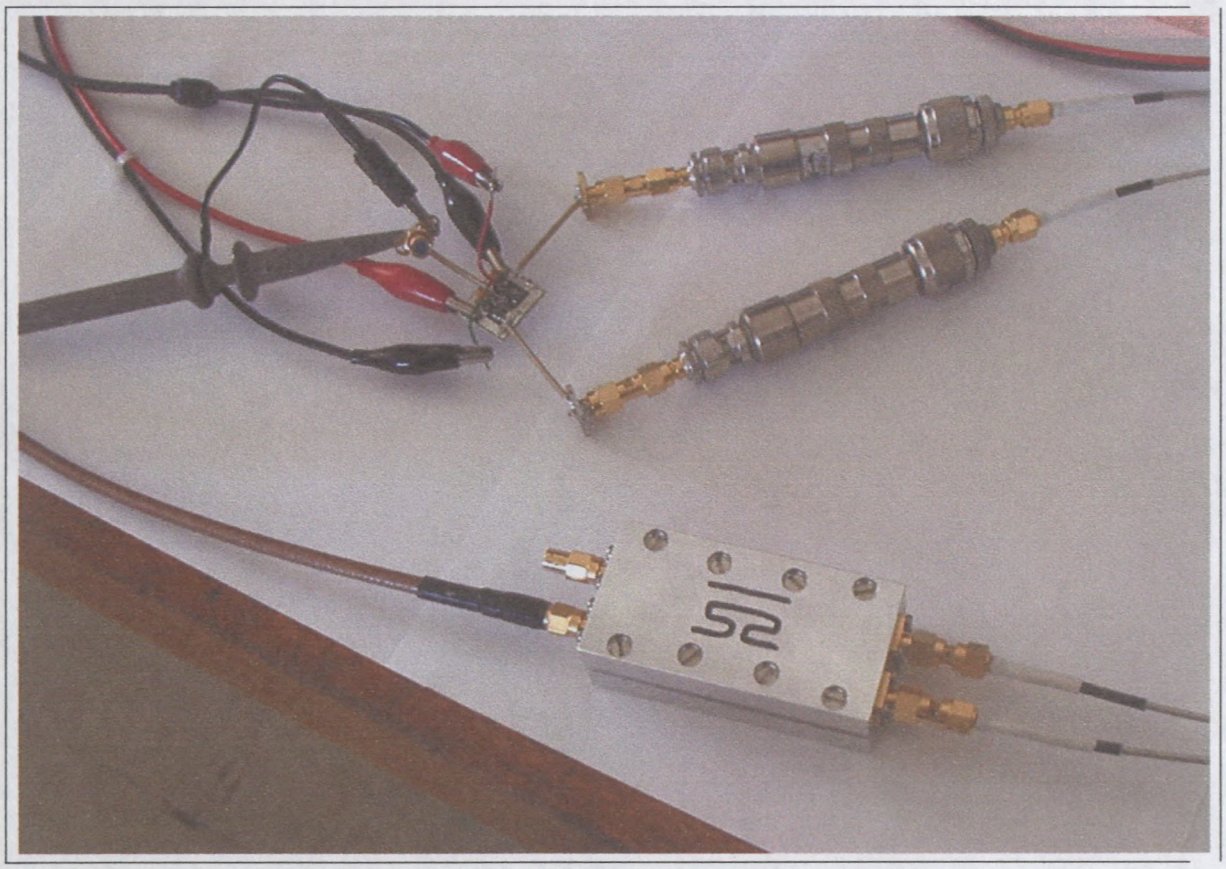

Figure C.4: Photo of the X-band Mohr Discriminator System.


geldenhuys_microwave_2001